EXPLORATION ON ATYPICAL KINETICS OF UGT1A1 AND UGT1A4

A DISSERTATION
SUBMITTED TO THE FACULTY OF THE GRADUATE SCHOOL
OF THE UNIVERSITY OF MINNESOTA
BY

JIN ZHOU

IN PARTIAL FULFILLMENT OF THE REQUIREMENTS
FOR THE DEGREE OF
DOCTOR OF PHILOSOPHY

Dr. Rory P. Remmel, Adviser
Dr. Timothy S. Tracy, Co-adviser

August 2010

Acknowledgements

I wish to express my sincere appreciation and gratitude to Dr. Rory Remmel and Dr. Timothy Tracy for their guidance over the years of my graudate training. Dr. Remmel and Dr. Tracy both have contributed tremendously to my scientific and personal life.

I also wish to thank the members of the examining committee: Dr. Stephen Hecht, Dr. Shana Sturla, and Dr. Chengguo Xing for their assistance and constructive suggestions.

I would like to thank everyone who has helped me over the past few years, particularly various members in Drug Design Center, Dr. Peter Villalta in Cancer Center, the faculty and staff of the Department of Medicinal Chemistry, and the members of the Drug Metabolism journal club.

Finally, I would like to thank Bristol-Myers Squibb and NIH for their financial support of this project.

THIS THESIS IS DEDICATED TO

MY LOVING HUSBAND AND PARENTS

Abstract

Atypical (non-Michaelis-Menten) kinetics confound straightforward in vitro-in vivo extrapolations on clearance and inhibition potentials of new chemical entities. However, unlike cytochrome P450s, studies on atypical kinetics of uridine 5'-diphospho-glucuronosyltransferases (UGTs) are much less prevalent. With the use of model substrates, the atypical kinetics of two important glucuronidation enzymes, UGT1A1 and UGT1A4, were explored.

In Chapter 2 (Part I), two positional isomers dihydrotestosterone (DHT) and trans-androsterone (t-AND) were used as probe substrates and their glucuronidation kinetics with recombinant UGT1A4 were evaluated alone and in the presence of a UGT1A4 substrate (tamoxifen (TAM) or lamotrigine (LTG)). Interestingly, co-incubation with TAM, a high affinity UGT1A4 substrate, resulted in a concentration-dependent activation/ inhibition effect on DHT and t-AND glucuronidation. The glucuronidation kinetics of TAM and the interactions of DHT or t-AND on TAM glucuronudation were then evaluated. TAM displayed substrate inhibition kinetics, however, the substrate inhibition kinetic profile of TAM became more hyperbolic, as DHT or t-AND concentration was increased. Kinetic analysis with two-site kinetic models demonstrated that these atypical interactions can be explained by the existence of multiple aglycone substrate binding sites in UGT1A4. In this chapter, the glucuronidation kinetics of DHT, t-AND and TAM with two UGT1A4 variants (UGT1A4 P24T and UGT1A4 L48V) (Part II) and the interactions of ethinylestradiol and estradiol-3-sulfate on UGT1A4-catalyzed LTG glucuronidation (Part III) were also described.

In Chapter 3, a robust bilirubin glucuronidation assay with recombinant UGT1A1 was established (Part I). With this assay, the correlation between UGT1A1-catalyzed bilirubin glucuronidation and estradiol-3-glucuronidation was studied in the presence model UGT1A1 substrates or inhibitors. Through this evaluation, we found estradiol-3-glucuronidation is a reasonable surrogate *in vitro* predictor for interactions with bilirubin even though they displayed different kinetic profiles. However, atypical interactions by some effectors were observed with estradiol-3-glucuronidation but not with bilirubin glucuronidation. The atypical interactions of daidzein and SN-38 on ethinylestradiol-3-glucuronidation were also analyzed with multi-site kinetic models.

In conclusion, through kinetic studies with prototype substrates, we found evidence to support the existence of multiple aglycone substrate binding sites in UGT1A1 and UGT1A4. Thus, multiple probe substrates may be needed to evaluate drug-drug interactions involving UGT1A1/UGT1A4-catalyzed metabolism.

Table of Contents

ABSTRACT iii

TABLE OF CONTENTS v

LIST OF TABLES xi

LIST OF FIGURES xii

NON-STANDARD ABBREVIATIONS xvi

CHAPTER 1- INTRODUCTION 1

I. Glucuronidation and UDP Glucuronosyltransferases 1

Overview 1

Nomenclature of UGTs 2

Tissue Distribution of UGTs 5

Topology of UGTs 7

Molecular Regulation of UGTs 8

Substrate Specificities of UGTs 11

UGT-Mediated Drug Interactions 13

Assessment of UGT-mediated Drug Interactions 14

In Vitro Glucuronidation Assay Conditions 15

II. Atypical Kinetics 18

Overview 18

Types of Atypical Kinetics 19

Mechanistic Aspects of Atypical Kinetics for CYPs 21

Kinetic Models for Atypical Kinetics 24

Impact of Atypical Kinetics 29

III. Hypotheses and Aims 33

CHAPTER 2 - KINETIC ANALYSIS ON UGT1A4-CATALYZED GLUCURONIDATION 34

Part I: Glucuronidation of Dihydrotestosterone and Trans-Androsterone by Recombinant UGT1A4: Evidence for Multiple UGT1A4 Aglycone Binding Sites 34

Background 34

Materials and Methods 38

Materials 38

Culture Procedures for HEK293 Cells 39

Synthesis of Tamoxifen-N- Glucuronide 41

Incubations to Characterize Glucuronidation Kinetics in the Absence of Modifiers 44

Incubations to Characterize Interactions between UGT1A4 Substrates 45

Chromatographic Analysis of Glucuronides 46

Estimation of Non-specific Protein Binding 55

Data Analysis 55

Results 62

Non-Specific Binding of DHT, t-AND, TAM and LTG 62

Kinetics of DHT and t-AND Glucuronidation 62

Effect of TAM on DHT and t-AND Glucuronidation 67

Kinetics of TAM Glucuronidation 71

Effect of LTG on DHT and t-AND Glucuronidation 72

Effects of TAM on LTG glucuronidation 75

Effects of DHT and t-AND on TAM glucuronidation 76

Discussion 78

Part II: Function Analysis of UGT1A4.2 and UGT1A4.3 in Comparison with UGT1A4.1 on Dihydrotestosterone, Trans-Androsterone, and Tomoxifen Glucuronidation 85

Background 85

Materials and Methods 89

Materials 89

Incubation Conditions 89

Quantification of Glucuronides 89

Western Blot Analysis 89

Data Analysis 90

Results 91

Western Blot Analysis of UGT1A4 Protein with Anti-UGT1A Antibody 91

Kinetic Profiles of DHT, t-AND and TAM Glucuronidation with UGT1A4.1, UGT1A4.2 and UGT1A4.3 92

Kinetic Parameters for DHT, t-AND and TAM Glucuronidation with UGT1A4.1, UGT1A4.2 or UGT1A4.3 94

Effect of 10 µM TAM on DHT glucuronidation with UGT1A4.1, UGT1A4.2 or UGT1A4.3 95

Discussion 97

Part III: Effects of Ethinyl Estradiol and Estradiol Sulfate on UGT1A4-Catalyzed Lamotrigine-N2-glucuronidation 115

Background 101

Materials and Methods 102

Results and Discussion 104

Effect of Ethinylestradiol on LTG Glucuronidation 104

Effect of Estradiol-3- Sulfate Conjugate on LTG Glucuronidation 106

CHAPTER 3: KINETIC ANALYSIS ON UGT1A1-CATALYZED GLUCURONIDATION 109

Part I: Bilirubin Glucuronidation Revisited: Proper Assay Conditions to Estimate Enzyme Kinetics with Recombinant UGT1A1 109

Background 109

Materials and Methods 113

Materials 113

Incubation Conditions 113

Quantification of Bilirubin Monoglucuronides and Diglucuronide 114

Data Analysis 118

Results and Discussion 119

Effects of Protein Concentration 121

Effects of Incubation Time 122

Effects of Bilirubin Concentration (1.25-80 μM) on Total Glucuronide Formation Rate 123

Kinetic Profiles for Total Bilirubin Glucuronide Formation 125

Effects of Bilirubin Concentration on the Proportions of BMGs or BDG 128

Part II: Correlation between Bilirubin Glucuronidation and Estradiol-3-Gluronidation in the Presence of Model UGT1A1 Substrates/Inhibitors 130

Background 130

Materials and Methods 133

Materials 133

Incubation Conditions to Characterize Kinetic Profiles 134

Interaction Studies 134

Quantification of Estradiol-3-Glucuronide and Bilirubin Glucuronides 135

Data Analysis 139

Results 143

Kinetics of Bilirubin Glucuronidation and Estradiol-3-Glucuronidation 143

Interaction between Bilirubin and Estradiol glucuronidation 144

Effects of 16 model UGT1A1 Substrates or Inhibitors on Bilirubin and Estradiol Glucuronidation 145

Kinetics of Estradiol-3-glucuronidation in the Presence of Daidzein 150

Kinetics of Estradiol-3-glucuronidation in the Presence of SN-38 152

Discussion 155

Future Directions 164

References 162

Appendix 1: Equations 190

Appendix 2: Derivation of Rate Equations for Formation of Bilirubin Mono-glucuronide, Di-glucuronide and Total Glucuronide Based on a Sequential reaction Model in Figure 3.7 192

List of Tables

Table 1.1. Expression of UGTs in Various Human Tissues 6

Table 1.2. Transcriptional receptors and their targeted UGT isoforms 10

Table 1.3. Isoform-selective substrates of some drug-metabolizing UGTs expressed in liver 12

Table 2.1. Kinetic parameters for the glucuronidation of DHT, t-AND, TAM and LTG by recombinant UGT1A4 64

Table 2.2. Kinetic parameters obtained by fitting various two-site models to kinetic data 65

Table 2.3. Kinetic parameters for DHT glucuronidation in the presence or absence of TAM 70

Table 2.4. Kinetic parameters for DHT, t-AND and TAM glucuronidation with UGT1A4.1, UGT1A4.2 or UGT1A4.3 94

Table 3.1. Effects of 16 UGT1A1 substrates/inhibitors on bilirubin glucuronidation and estradiol-3-glucuronidation 148

Table 3.2. Kinetic parameters obtained by using multiple-site models to explain the effect of daidzein or SN-38 on estradiol-3-glucuronidation 154

List of Figures

Figure 1.1. The Arrangements of UGT Genes 4

Figure 1.2. Michaelis-Menten kinetic model and Michaelis-Menten equation 18

Figure 1.3. Kinetic profiles for Michaelis-Menten (hyperbolic), sigmoidal, biphasic, and substrate inhibition kinetics in substrate concentration verus velocity plots and Eadie-Hofstee plots (insects) 20

Figure 1.4. A generic two-site model for homotropic cooperativity 26

Figure 1.5. A two-site model for heterotropic interactions 28

Figure 1.6. Clearance plots for a compound exhibited sigmoidal kinetics (solid line) or Michaelis-Menten kinetics (dashed line) 30

Figure 2.1. Structures of DHT, t-AND, TAM and LTG 36

Figure 2.2. Hypothesized orientations for DHT and t-AND to bind to the UGT1A4 active site 37

Figure 2.3. ^{1}H-NMR spectrum of tamoxifen-N-glucuronide 43

Figure 2.4. Chromatograms of trans-androsterone glucuronide, dihydrotesosterone glucuronide and testosterone glucuronide with a capilliary LC-MS/MS method 48

Figure 2.5. Chromatograms of trans-androsterone glucuronide, dihydrotesosterone glucuronide and testosterone glucuronide with LC-MS 50

Figure 2.6. Chromatograms of tamoxifen-N-glucuronide and internal standard lamotrigine-N2-glucuronide with LC-MS 53

Figure 2.7. Chromatograms of lamotrigine-N2-glucuronide and internal standard morphine-3-glucuronide with LC-MS 54

Figure 2.8. A two-site kinetic model for substrate inhibition kinetics (Equation 2.7) 59

Figure 2.9. A two-site kinetic model to explain the effect of TAM on DHT glucuronidation (Equation 2.8) 59

Figure 2.10. A two-site kinetic model to explain the effect of DHT on TAM glucuronidation (Equation 2.9) 60

Figure 2.11. Two-site kinetic models to explain the effect of t-AND on TAM glucuronidation (Equation 2.10 and 2.11) 61

Figure 2.12. Kinetic plots (Rate versus [S]) for DHT (A) and t-AND (B) glucuronidation by recombinant UGT1A4 66

Figure 2.13. Rate percentage of control versus [S] plots for the effect of TAM on DHT glucuronidation (A) and for the effect of TAM on t-AND glucuronidation (B) 68

Figure 2.14. Kinetic modeling for the effect of TAM on DHT glucuronidation 69

Figure 2.15. Kinetic plots (Rate versus [S]) for TAM glucuronidation by recombinant UGT1A4 71

Figure 2.16. Kinetic plots (Rate versus [S]) for LTG glucuronidation by recombinant UGT1A4 73

Figure 2.17. Rate percentage of control versus [S] plots for the effect of LTG on DHT glucuronidation (A) and for the effect of LTG on t-AND glucuronidation (B) 74

Figure 2.18. Dixon plots for inhibition of DHT glucuronidation by LTG (A) and for inhibition of t-AND glucuronidation by LTG (B) 74

Figure 2.19. Rate percentage of control versus [S] plots (A) and Dixon plot for the effect of TAM on LTG glucuronidation 75

Figure 2.20. Kinetic plots (Rate versus [S]) for TAM glucuronidation by recombinant UGT1A4 in the presence of 250 µM of DHT (A) or 250µM of t-AND (B) 77

Figure 2.21. Kinetic modeling for effect of DHT (A) and t-AND (B) on TAM glucuronidation 77

Figure 2.22. Western blot analysis of UGT1A4 protein with anti-UGT1A antibody 91

Figure 2.23. Rate versus [S] plots for DHT, t-AND and TAM glucuronidation with UGT1A4.1, UGT1A4.2 and UGT1A4.3 92

Figure 2.24. Effect of 10 μM TAM on DHT glucuronidation with UGT1A4.1, UGT1A4.2 and UGT1A4.3 96

Figure 2.25. A mixed partial inhibition model 103

Figure 2.26 Rate percentage of control versus [S] plots for the effect of ethinylestradiol on LTG glucuronidation 105

Figure 2.27. A Dixon plot of lamotrigine-N2-glucuronidation in the presence of different concentrations of ethinylestradiol (inhibitor) 106

Figure 2.28. Rate percentage of control versus [S] plots for the effect of estradiol sulfate conjugate on LTG glucuronidation 107

Figure 3.1. Chromatograms for bilirubin glucuronidation in the presence (A) or absence (B) of UDPGA 117

Figure 3.2. Effects of protein concentration on BDG (A and B), BMG (C and D), and total glucuronide (E and F) formation 121

Figure 3.3. Effects of incubation time on BDG (A and B), BMG (C and D), and total glucuronide (E and F) formation 122

Figure 3.4. Effects of bilirubin concentration (1.25-80 μM) on total glucuronide formation rate 123

Figure 3.5. Substrate-concentration versus rate plots for total bilirubin glucuronide formation 125

Figure 3.6. Effects of bilirubin concentration on the proportions of BMGs or BDG 128

Figure 3.7. Kinetic scheme for bilirubin glucuronidation 129

Figure 3.8. Chromatograms of estradiol-3-glucuronide and trans-androsterone glucuronide with a LC-MS method 137

Figure 3.9. Chromatograms of estradiol-3-glucuronide and trans-androsterone glucuronide with a capilliary LC-MS/MS method 138

Figure 3.10. Multiple-site kinetic models for interactions of daidzein or SN-38 on estradiol-3-glucuronidation 142

Figure 3.11. Kinetic plots (Rate versus [S]) for estradiol-3-glucuronidation 143

Figure 3.12. Interactions between estradiol and bilirubin (rate percentage of control versus [modifier] plots) 144

Figure 3.13. Structures of 16 model modifiers (14 UGT1A1 substrates and 2 UGT1A1 inhibitors) 147

Figure 3.14. Comparison of IC_{50}s for bilirubin glucuronidation and IC_{50}s for estradiol-3-glucuronidation 149

Figure 3.15. Effect of daidzein on estradiol-3-glucuronidation 151

Figure 3.16. Effect of SN-38 on estradiol-3-glucuronidation 153

NON-STANDARD ABBREVIATIONS

AICc: Second-Order Akaike Information Criterion

BDG: Bilirubin di-glucuronide

BMG: Bilirubin mono-glucuronide

DHT: Dihydrotestosterone

LTG: Lamotrigine

TAM: Tamoxifen

t-AND: trans- androsterone (epiandrosterone)

UDPGA: uridine diphosphate glucuronic acid

UGT: uridine 5'-diphospho-glucuronosyltransferases

CHAPTER 1 – INTRODUCTION

I. Glucuronidation and UDP Glucuronosyltransferases

- **Overview**

The uridine 5'-diphospho-glucuronosyltransferases (UGTs) are a superfamily of enzymes that catalyze the transfer of various glycosyl groups (such as glucose, glucuronic acid, xylose, galatose, etc.) to lipophilic acceptor molecules (aglycones) (Remmel et al., 2008). The aglycone acceptors have diverse chemical structures; however, they all contain functional groups such as alcohols, carboxylic acids, thiols, amino groups, or acidic carbon atoms, to which the glucuronosyl groups may be attached (Remmel et al., 2008). The most common sugar donor used by mammalian UGTs is UDP-glucuronic acid (UDPGA) and the process of UGTs catalyzing the conjugation of glucuronic acid to aglycones is termed as glucuronidation (Remmel et al., 2008). Glucuronidation largely increases the water-solubility of the aglycones, facilitating their elimination (Remmel et al., 2008). Many important endogenous chemicals such as bilirubin, steroid hormones, thyroid hormones, retinoic acid, and biogenic amines are substrates of UGTs (Remmel et al., 2008). Glucuronidation plays very important roles in the homeostasis of these endogenous chemicals and may participate in regulating the function of some nuclear receptors (Zhou et al., 2005). In addition, glucuronidation represents an important elimination pathway for a wide variety of xenobiotics. Many therapeutic agents and their metabolites, carcinogens, and

environmental pollutants are substrates of UGTs. Except for a few cases such as morphine-6-glucuronidation (Oelberg et al., 1984; Bock, 1992; Lotsch and Geisslinger, 2001), glucuronidation usually leads to inactivation of the aglycone substrates. In addition, formation of acyl glucuronides may result in covalent binding to proteins either by direct displacement or via Schiff base formation followed by an Amadori rearrangement (Bailey and Dickinson, 2003).

- **Nomenclature of UGTs**

The human UGT superfamily contains four families: UGT1, UGT2, UGT3, and UGT8, among which UGT1 and UGT2 are the ones that use UDPGA as a sugar donor (Mackenzie et al., 2005). The human UGT1 family consists of nine functional proteins (UGT1A1, UGT1A3, UGT1A4, UGT1A5, UGT1A6, UGT1A7, UGT1A8, UGT1A8, UGT1A9, and UGT1A10) and four pseudogenes (UGT1A2P, UGT1A11P, UGT1A12P and UGT1A13P) (Mackenzie et al., 2005). Members in UGT1 family are all encoded by a large gene locus at chromosome 2q37. Each mRNA transcript is formed by splicing four common exons (exon 2-5), located at the downstream of this locus, with a viable first exon (exon 1) upstream (Figure1.1 A) (Gong et al., 2001; Mackenzie et al., 2005). Thus, members in human UGT1 family have the identical C-terminuses but variable N-terminuses.

The human UGT2 family is located on chromosome 4q13. It has two subfamilies: UGT2A and UGT2B (Mackenzie et al., 2005). The arrangement of UGT2 members along chromosome 4q13 is shown in Figure1.1 B. The UGT2A subfamily contains three members: UGT2A1, UGT2A2 and UGT2A3 (Mackenzie et al., 2005). Similar to the members in UGT1 family, UGT2A1 and UGT2A2 are

both composed of a unique first exon and a set of shared exons downstream (exon 2-6) (Mackenzie et al., 2005). UGT2A3, on the other hand, has a set of unique exons (Mackenzie et al., 2005). The UGT2B family contains seven functional proteins (UGT2B4, UGT2B7, UGT2B10, UGT2B11, UGT2B15, UGT2B17 and UGT2B28) and five pseudogenes (UGT2B24P, UGT2B25P, UGT2B26P, UGT2B27P, UGT2B29P) (Mackenzie et al., 2005). They each are encoded by six exons unique from other members (Mackenzie et al., 2005). Similar to UGT1A members, UGT2B members have variable N-terminuses but highly conserved C-terminuses. Although UDPGA is the preferred sugar donor for UGT1 and UGT2 enzymes, other sugar donors may also be used. For instance, UDP xylose and UDP glucose were both documented as sugar donors for UGT1A1 (Senafi et al., 1994) and UDP glucose was documented as sugar donor for UGT2B7 (Mackenzie et al., 2003a; Tang et al., 2003).

Figure 1.1. The arrangements of UGT genes

A: The UGT1A gene complex contains 13 variable first exons and 4 shared exons (exon 2, 3, 4, and 5), and is located on chromosome 2q37; B: UGT2 genes have unique sets of exons and are located on chromosome 4q13. Figures are adapted from (Mackenzie et al., 2005).

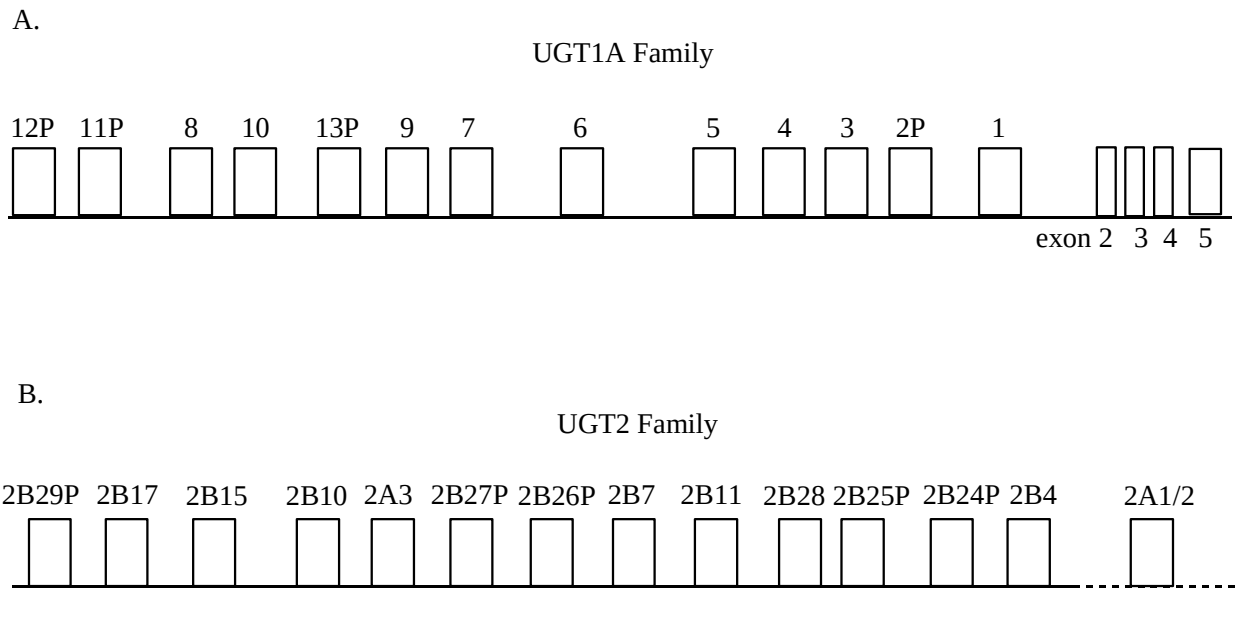

- **Tissue Distribution of UGTs**

UGTs are widely distributed in various tissues, including liver, small intestine, colon, kidney, esophagus, brain, prostate, placenta, testes, bladder etc. (Ohno and Nakajin, 2009). Due to lack of isoform-specific antibodies, the expression and localization of UGTs were mostly evaluated at mRNA level with reverse transcription-polymerase chain reaction (RT-PCR) or Northern blotting (Strassburg et al., 1997; Beaulieu et al., 1998; Strassburg et al., 1998; Levesque et al., 1999; Strassburg et al., 2000; Tukey and Strassburg, 2001; Turgeon et al., 2001; Nakamura et al., 2008). Recently, Ohno and Nakajin reported an extensive study on the expression of 15 catalytically active UGTs in various human tissues with RT-PCR (Table 1.1) (Ohno and Nakajin, 2009). The authors found UGTs are predominantly expressed in liver, intestine, colon, and kidney. Liver, as the major organ for glucuronidation has the highest level of total UGT mRNAs. Multiple UGTs, including UGT1A1, UGT1A3, UGT1A4, UGT1A5, UGT1A6, UGT1A7, UGT1A9, UGT2B4, UGT2B7, UGT2B10, UGT2B15 and UGT2B17 were detected in liver with UGT2B4 as the most abundant isoform, followed by UGT2B15. Interestingly, although UGT1A8 and UGT1A10 are highly expressed in intestine, colon and kidney, they are not present in liver. Also the mRNA level of UGT1A7 in liver is extremely low compared to extrahepatic tissues such as esophagus and cervix. Table 1.1 summarizes the expression of the 15 UGTs in various tissues. Although some UGTs are present in different tissues, the expression level in specific tissue varies significantly between different

.individuals and may not be the same in case of disease or induction by drugs or environmental compounds (Trubetskoy et al., 2008).

Table 1.1. Expression of UGTs in various human tissues (Ohno and Nakajin, 2009)

UGTs	Tissues
UGT1A1	Liver > Small intestine > Colon > Stomach
UGT1A3	Liver > Small intestine
UGT1A4	Liver
UGT1A5	Small Intestine > Colon >Kidney, Esophagus, Trachea, Prostate, Placenta > Lung, Bladder, Cervix, Thymus, Liver > Brain, Testes
UGT1A6	Kidney > Liver > Stomach > Adrenal > Trachea, Bladder, Small Intestine
UGT1A7	Esophagus > Cervix >Trachea > Kidney, Colon, Small intestine > liver
UGT1A8	Colon, Small Intestine, Adrenal > Trachea, Bladder, Breast
UGT1A9	Kidney > Liver >Adrenal > Colon, Small Intestine > Esophagus, Bladder
UGT1A10	Small intestine, Colon> Stomach, Esophagus > Adrenal, Trachea
UGT2B4	Liver >> heart > Esophagus, Prostate, Kidney > Trachea > Thymus > Testes
UGT2B7	Liver, Kidney > Small intestine, Colon
UGT2B10	Liver
UGT2B11	Not detected
UGT2B15	Liver >> Stomach, Thymus > Small intestine, Colon, Prostate > Trachea > Testes
UGT2B17	Colon > Small intestine > Liver > Stomach, Breast , Cervix > Thymus, Lung, Spleen, Ovary > Adipose, Kidney, Trachea > Testes, Brain

- **Topology of UGTs**

Human UGTs are integral membrane proteins, with the majority of the protein, including the substrate binding sites (both aglycone and UDPGA), on the lumenal side of the endoplasmic reticulum membrane (Radominska-Pandya et al., 1999). Originally, UGTs were synthesized as precursor proteins with about 530 residues. Each precursor has a signal peptide at the N-terminal end, which facilitates the integration of the precursor into the ER membrane and is cleaved subsequently upon the insertion of precursor into the ER membrane (Radominska-Pandya et al., 1999). The mature UGTs contain about 505 residues and are divided into two domains by the ER membrane. The lumenal domain contains about 95% of the protein, whereas, the cytoplasmic domain consists of only 20 residues or so (Radominska-Pandya et al., 1999). The lumenal domain and the cytoplasmic domain are connected through a highly conserved hydrophobic polypeptide with about 17 residues embedded in the ER lipid bilayer (Radominska-Pandya et al., 1999). Because the C-terminal ends of UGTs are highly conserved and the N-terminal ends are variable, the C-terminal ends of the proteins are predicted to interact with the common cofactor UDPGA, whereas, the aglycone substrate binding sites are thought to be located in the N-terminal ends of the proteins (Radominska-Pandya et al., 1999). Although an apo crystal structure of UDPGA binding domain of human UGT2B7 has recently been determined (Miley et al., 2007), the three-dimensional structures of the aglycone binding sites of UGTs are unknown. Indirect methods such as site-directed mutagenesis (Senay et al., 1997), chemical modification (Battaglia et al., 1994)

and photoaffinity labeling (Senay et al., 1999) were used to identify the residues crucial for enzyme activity and to provide insight into the interactions between aglycone substrates and UGTs. In addition, accumulating evidence suggests that UGTs may exist as homodimers, heterodimers or tetramers (Peters et al., 1984; Ikushiro et al., 1997; Ghosh et al., 2001; Kurkela et al., 2003; Fujiwara et al., 2007; Operana and Tukey, 2007). Oligomerization may affect the enzyme activity (Ghosh et al., 2001; Fujiwara et al., 2007), which may be a challenge on prediction of *in vivo* clearance from *in vitro* systems (Bock and Kohle, 2009).

- **Molecular Regulation of UGTs**

Similar to other drug metabolism enzymes, UGTs are subjected to molecular regulation. Several transcription factors including hepatocyte nuclear factor 1 (HNF1), CAAT-enhancer binding protein, Cdx2, octamer transcription factor 1, and pre-β cell homeobox transcription factor 2 have been identified as regulators for constitutive expression of UGTs in various tissues (Bernard et al., 1999; Ishii et al., 2000; Gregory and Mackenzie, 2002; Toide et al., 2002; Mackenzie et al., 2003b). As illustrated above, UGTs are differentially expressed in a wide range of tissues. The tissue-specific expression may be in part due to the presence of specific transcription factors in different tissues and the relative locations of transcription factor–binding sites in UGT genes (Mackenzie et al., 2003b). For instance, an HNF1α response element has been shown to be important for specific gene expression in liver (Lichtsteiner et al., 1987). For several UGT2B isoforms which are highly expressed in liver, a putative HNF1α binding site was found in the promoter region at relatively similar locations, whereas, for

extrahepatic UGT1A8 and UGT1A10, the consensus sequence was not present at the same location (Mackenzie et al., 2003b). In addition, many xenobiotics and endogenous chemicals may also change the expression level of UGTs through various nuclear or cytosolic receptors such as constitutive androstane receptor (CAR), aryl hydrocarbon receptor (AhR), pregnane X receptor (PXR), PPAR-alpha, etc (Mackenzie et al., 2003b). This type of regulation is also isoform specific (Zhou et al., 2005) and may have important roles in drug-drug interactions. Table 1.2 lists the reported transcriptional receptors along with their targeted UGT isoforms.

Table 1.2. Transcriptional receptors and their targeted UGT isoforms [modified from (Zhou et al., 2005)]

UGT Isoforms	Transcriptional Receptors
UGT1A1	Pregnane X receptor (PXR), Constitutive androstane receptor (CAR), Aryl hydrocarbon receptor (AhR), Glucocorticoid receptor (GR), Peroxisome proliferator-activated receptor α (PPARα), Nuclear factor like 2(Nrf2)
UGT1A3	Pregnane X receptor (PXR) , Peroxisome proliferator-activated receptor α (PPARα)
UGT1A4	Pregnane X receptor (PXR), Peroxisome proliferator-activated receptor α (PPARα)
UGT1A6	Pregnane X receptor (PXR), Aryl hydrocarbon receptor (AhR)
UGT1A9	Pregnane X receptor (PXR), Peroxisome proliferator-activated receptor α (PPARα), Peroxisome proliferator-activated receptor γ (PPAR γ)
UGT2B4	Farnesoid X receptor (FXR), Peroxisome proliferator-activated receptor α (PPARα)
UGT2B7	Farnesoid X receptor (FXR), PXR
UGT2B1 2B15 or 2B17	Constitutive androstane receptor (CAR)

- **Substrate Specificities of UGTs**

The substrate specificities of UGTs are complex. Most UGTs are able to catalyze the glucuronidation of several, sometimes many, compounds with significantly-varied structures. A large amount of research effort has been put forth to find out the relationship between chemical structures and UGT activity. For instance, Yin et al. have shown that compounds with high lipophilicity tend to have high glucuronidation rates (Yin et al., 1994); Jackson et al. demonstrated small phenols were more rapidly glucuronidated than bulky phenols by kidney UGT2B12 (Jackson et al., 1988). However, the detailed structure-activity relationship for UGTs is not fully understood (Lin and Wong, 2002).

UGTs are well-known for their strikingly overlapping substrate specificities. Many compounds can be glucuronidated by multiple UGTs. For instance, 4-nitrophenol is glucuronidated by UGT1A1, UGT1A3, UGT1A4, UGT1A6, UGT1A7, UGT1A8, UGT1A9, UGT1A10, UGT2B4 and UGT2B15 (King et al., 2000). The following generalizations with regards to UGT substrate specificity are widely accepted: 1. All UGTs are capable of catalyzing O-glucuronidation; 2.carboxylic acid glucuronidation are mainly catalyzed by UGT1A3, UGT1A9 and UGT2B7; 3. UGT1A4, UGT1A3 and UGT2B10 are important for N-glucuronidation and they are the only UGTs capable of forming quandary ammonium glucuronides; 4. UGT2B4 and UGT2B7 are the main enzymes for opioid glucuronidation; 5. Steroids are glucuronidated by both UGT1A and UGT2 members.(Kiang et al., 2005; Remmel et al., 2008; Zhou et al., 2010a)

Although, UGT substrate specificities are highly overlapping, there are still some substrates that are relatively specific for certain UGT isoforms. For instance, bilirubin is highly specific for UGT1A1. Isoform-specific substrates have important applications in reaction phenotyping (determining which UGT isoform catalyzes the reaction) and drug-drug interaction studies (Court, 2005). Table 1.3 lists isoform-specific substrates for several important liver-expressing UGTs.

Table 1.3. Isoform-selective substrates of some drug-metabolizing UGTs expressed in liver (Court, 2005; Miners et al., 2010)

UGT	Substrates
1A1	Bilirubin, β-estradiol (3-glucuronidation), Etoposide, SN-38
1A3	R-lorazepam
1A4	1'-hydroxymidazolam, Trifluoperazine, hecogenin, lamotrigine
1A6	Deferiprone, Serotonin
1A9	Mycophenolic acid (7-glucuronidation), Phenylbutazone, Propofol, Sulfinpyrazone
2B4	Codeine
2B7	Denopamine, Epirubincin,6α-hydroxyprogesterone, 21-Hydroxyprogesterone, Morphine (3- and 6- glucuronidation), Zidovudine
2B15	S-oxazepam, S-lorazepam, E-4-OH-tamoxifen, 5-OH-rofecoxib
2B17	Dihydrotestosterone (also a substrate of UGT1A4)

- **UGT-Mediated Drug Interactions**

UGT-mediated drug interactions are usually less of a concern, compared to CYP-mediated drug interactions because changes in AUCs due to UGT-mediated drug interactions are generally less than 3-fold (Lin and Wong, 2002; Williams et al., 2004; Kiang et al., 2005; Remmel et al., 2008). Several reasons may be involved for the small magnitudes of UGT-mediated drug interactions: 1) UGT substrates usually have higher K_ms; 2) Multiple UGTs catalyze one reaction, thus compensatory pathways are available if the function of one UGT is impaired; 3) the therapeutic concentrations of UGT inhibitors are often well below the K_is of the inhibitors, thus limiting the inhibition effect(Kiang et al., 2005). Nevertheless, clinically significant UGT-mediated drug interactions have also been reported. For instance, valproic acid inhibits lamotrigine glucuronidation, resulting in an increase in half-life and serum concentration of lamotrigine (Anderson et al., 1996), which may account for the increased risk of side effects when lamotrigine is co-administered with valproic acid. Zidovudine, an important nucleoside used in the treatment of AIDS, is primarily eliminated through glucuronidaton (Veal and Back, 1995). Coadministration with rifampicin (an inducer of UGTs) resulted in a 2-4 fold decrease in the AUC of zidovudine (n=4) (Gallicano et al., 1999). Atazanavir, an HIV protease inhibitor was reported to significantly increase bilirubin concentration by inhibiting UGT1A1 activity, which may exacerbate the hyperbilirubinemia condition in patients with Gilbert's syndrome (Lankisch et al., 2006). Thus, it is still important to assess UGT-mediated drug interactions for

new drug candidates, especially for those that are mainly metabolized through glucuronidation and those with narrow therapeutic indexes.

- **Assessment of UGT-mediated Drug Interactions**

Two questions need to be addressed in the assessment of UGT-mediated drug interactions for new chemical entities: 1) whether the new chemical entities are susceptible to UGT inhibition; 2) whether the new chemical entities are UGT inhibitors (Lin and Wong, 2002). To answer the first question, it is important to know whether the compound is mainly eliminated through glucuronidation and the contribution of individual UGT isoforms to the glucuronidation reaction. If multiple elimination pathways are involved or the glucuronidation reaction is catalyzed by multiple UGT isoforms with similar contributions, it is less likely that the compound is susceptible to inhibition of only one UGT isoform. However, unlike the situations with CYPs, there are substantial technical challenges in determining the relative contributions of different UGTs to one glucuronidation reaction since the relative protein levels of UGTs are unknown (Remmel et al., 2008). This problem may soon be overcome by recent developments in proteomics(Remmel et al., 2008). Fallon et al recently established a reproducible proteomic digestion method for UGT absolute quantification (Fallon et al., 2008). With the use of stable isotope-labeled peptides as internal standards and isotope dilution techniques, they quantitated UGT1A1 and UGT1A6 protein in human liver microsomes by LC-MS/MS. The results they obtained with this method were in high correlation with the results obtained by Western blot (Fallon et al., 2008).

To assess whether a new chemical entity is a potent UGT inhibitor, one may evaluate the effect of the compound on the glucuronidation reaction of an isoform-specific UGT probe substrate with human liver microsomes. However, due to the highly overlapping substrate specificities, the information on isoform-specific probe substrates of UGTs is generally lacking, compared to CYPs (Lin and Wong, 2002). Thus, currently the best method to characterize the inhibition potentials of new chemical entities on UGTs is to conduct studies with cloned, expressed enzymes (Remmel et al., 2008). Several heterologous expression systems have been employed for stable expression of human UGTs, including monkey kidney COS cells, Chinese hamster lung fibroblast (V79) cells, human embryoinic kidney cells (HEK293), *E. coli*, yeast, and baculovirus-infected insect cells (Radominska-Pandya et al., 2005). Because UGTs are trans-membrane proteins and studies have shown that the composition of the ER membrane may affect UGT activities, mammalian cell lines such as COS, V79, and HEK293 represent a better expression system. Unfortunately, most recombinant UGTs that are commercially available are expressed in insect cells (Supersomes®, BD Life Sciences). Kinetic determination with Supersomes® may not necessarily reflect the kinetics in human liver microsomes.

- **In Vitro Glucuronidation Assay Conditions**

Latency (increased activity in the presence of a membrane-disrupting agent) is an important characteristic of UGTs in intact microsomes (Fisher et al., 2001). This property of UGTs is likely due to the luminal localization of the active sites, whereby the microsome membrane imparts a diffusional barrier, preventing the

hydrophilic cofactor UDPGA from having free access to the active site (Fisher et al., 2001). Thus, a membrane-disrupting agent is needed for *in vitro* incubation assays. The most commonly used membrane-disrupting agent is alamethicin: a 20-amino acid peptide. Unlike detergents, alamethicin does not inhibit UGT or CYP activity and the optimal concentration is isoform independent. Fisher et al reported that the optimal concentration for elimination of the latency was 50 μg alamethicin per mg microsomal protein (Fisher et al., 2001).

UGT activity also depends on incubation pH, buffer type and ionic strength. To mimic the condition in vivo, pH 7.4 is usually selected, although for some UGTs, this condition is not optimal for enzyme activity. There is no consensus with regards to the optimal buffer type for *in vitro* glucuronidation assay; however Tris buffer and phosphate buffer are used most commonly. Divalent metal ions such as Mg^{2+} and Ca^{2+} were found to increase UGT activity, thus are usually added to *in vitro* incubation. In addition, 5-10 mM of the glucuronidase inhibitor saccharo-1, 4-lactone may be added to eliminate glucuronide hydrolysis by β-glucuronidase. (Fisher et al., 2001)

Recently, Rowland et al suggested that albumin or human intestinal fatty acid binding protein (IFABP) may need to be added to microsomal incubations of some enzymes (e.g. UGT2B7) to sequester the long-chain fatty acids present in the incubation, because fatty acids may be substrates for some UGT enzymes (Rowland et al., 2008; Rowland et al., 2009). However, potential non-specific binding of substrates to those additional proteins may cause problems in kinetic determinations. Further investigations are needed to evaluate whether albumin or

human intestinal fatty acid binding protein (IFABP) should be routinely added to in vitro incubations.

II. Atypical Kinetics

- **Overview**

For many years, the Michaelis-Menten kinetic model (Figure 1.2) has been used to describe the kinetics of drug metabolizing enzymes (Houston and Galetin, 2005). This model, which assumes the enzyme has one substrate binding site, gives a characteristic hyperbolic curve in substrate concentration versus velocity plots and a linear relationship in Eadie-Hofstee plots (Figure 1.3) (Houston and Galetin, 2005). In drug discovery and development settings, the Michaelis-Menten kinetic model is widely used to estimate in vivo clearance and the inhibition potentials of new chemical entities from in vitro kinetic data (Tracy, 2006). However, increasing numbers of reports, most notably with CYP3A4, indicated that the single-site Michaelis-Menten kinetic model may not always explain the kinetic features observed with drug metabolizing enzymes (Houston and Galetin, 2005). Atypical (non-Michaelis-Menten) kinetics confounds straightforward *in vitro-in vivo* extrapolations on both clearance and inhibition potentials of new chemical entities(Tracy, 2006). Thus it is important to address the problems associated with this kinetic phenomenon.

Figure 1.2. Michaelis-Menten kinetic model and Michaelis-Menten equation

$$S + E \underset{k_{-1}}{\overset{k_1}{\rightleftharpoons}} ES \xrightarrow{k_2} E + P$$

$$V_0 = \frac{V_{max}[S]}{K_m + [S]} \qquad V_{max} = k_2[E]_{tot} \qquad K_m = \frac{k_{-1} + k_2}{k_1}$$

- **Types of Atypical Kinetics**

In general, atypical kinetics are either caused by homotropic cooperativity or heterotropic cooperativity, depending on whether there is a second compound involved (Atkins, 2005). Both homotropic cooperativity and heterotropic cooperativity may be positive or negative in nature. Typically positive homotropic cooperativity results in a sigmoidal-shaped kinetic profile in substrate concentration versus velocity plots and this type of kinetics is termed as sigmoidal (auto-activation) kinetics (Figure 1.3). Negative homotropic cooperativity results in two types of kinetic profiles in substrate concentration versus velocity plots. One is characterized as a decrease in velocity at high substrate concentrations after an initial hyperbolic increase (substrate inhibition kinetics) and the other is characterized as a linear increase in velocity at high substrate concentrations and a hyperbolic phase at low substrate concentrations (biphasic kinetics). The three types of homotropic cooperativty also have their own unique and characteristic curvatures in Eadie-Hofstee plots as opposed to the linear relationship for Michaelis-Menten kinetics (Figure 1.3). Thus, the Eadie-Hofstee plot is usually used as a diagnostic tool to identify and discriminate different types of kinetics (Atkins, 2005).

<u>Figure 1.3.</u> Kinetic profiles for Michaelis-Menten (hyperbolic), sigmoidal, biphasic, and substrate inhibition kinetics in substrate concentration verus velocity plots and Eadie-Hofstee plots (insects)

This figure was obtained from (Atkins, 2005).

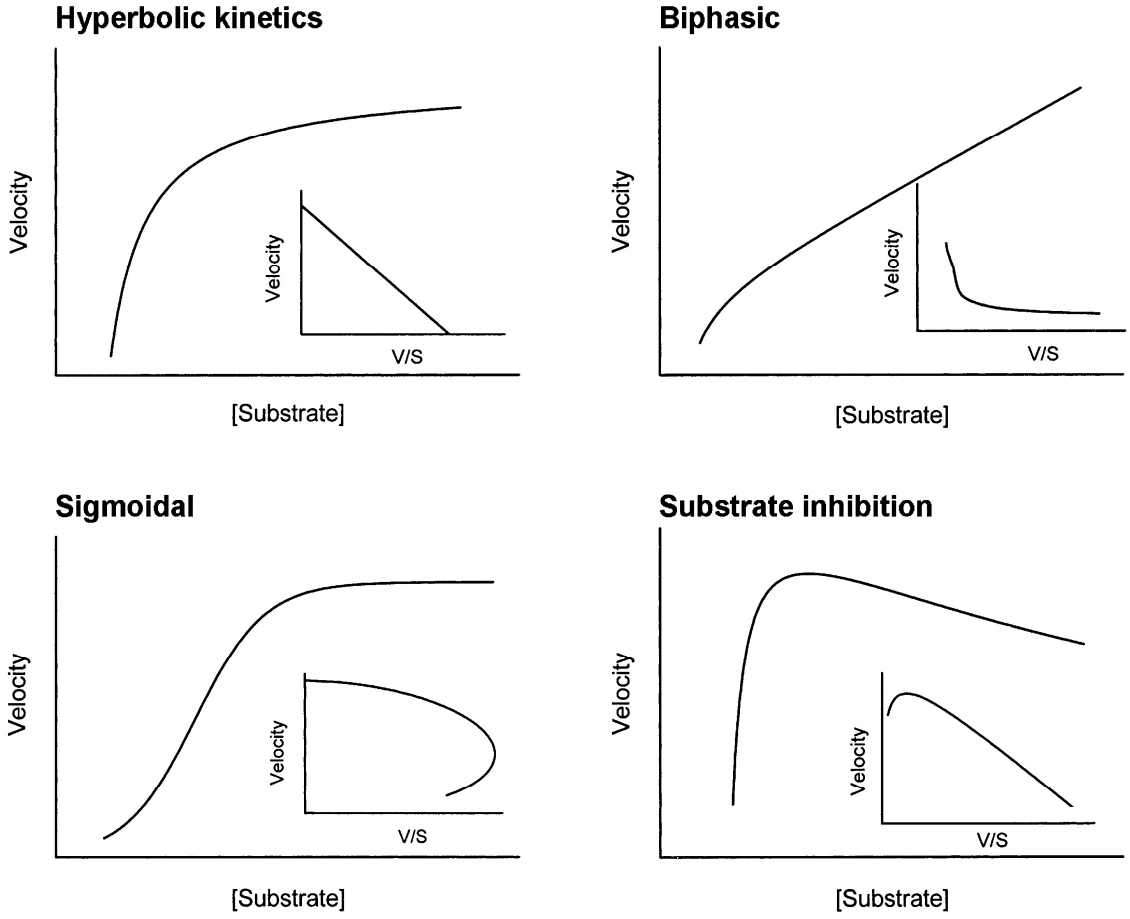

Due to the existence of an additional compound, heterotropic cooperativity is more complicated than homotropic cooperativity. In reviewing the literature, heterotropic cooperativity is exhibited as the following formats (Shou et al., 2001; Tracy, 2006).

- Activation: the presence of a second compound increases the metabolism of the substrate.
- Substrate-dependent inhibition: the inhibition effect of an effector on the enzyme depends on the substrate present (i. e. inhibition may be found on some reactions but not on other reactions catalyzed by the same enzyme).
- Partial inhibition: incomplete inhibition; inhibition never approaches 100% even at saturation inhibitor concentrations.
- Pathway differential effect: an effector activates the metabolism of a given substrate at one position but inhibits metabolism at a different position.

- **Mechanistic Aspects of Atypical Kinetics for CYPs**

Two main theories have been proposed to explain the atypical kinetics associated with CYPs. One theory which involves multiple protein conformations was mainly proposed by Koley and co-workers (Koley et al., 1995a; Koley et al., 1995b). They probed the interaction of α-naphthoflavone with benzo[a]pyrene metabolism(Koley et al., 1997a) and the interaction of quinidine with nefedipine metabolism(Koley et al., 1997b) through studying the kinetics of CO binding to

CYP3A4 with flash photolysis technique. Their results indicated that α-naphthoflavone, a substrate of CYP3A4, stimulated the reaction of beno[a]pyrene by selectively binding and activating an inactive conformer of CYP3A4, and thus increasing the total active conformers (Koley et al., 1997a); whereas quindine, which acted as a non-competitive inhibitor of nifedipine metabolism, inactivated a subset of CYP3A4 molecules and induced their binding to nifedipine (Koley et al., 1997b). This hypothesis, although is able to explain some of the atypical kinetics observed with CYP3A4 as mentioned above, is difficult to model with kinetic equations (Shou et al., 1999). In addition, evidence for this hypothesis is limited to the results obtained through the kinetic study of CO-binding to the enzyme.

A more widely accepted and intensively investigated hypothesis for atypical kinetics of CYPs involves multiple substrate /effector binding sites. It is hypothesized that enzymes displaying atypical kinetics have multiple substrate /effector binding sites and multiple molecules can simultaneously bind to the enzyme (Segel, 1993). Several multi-site kinetic models have been developed based on this hypothesis as discussed below. Since almost all types of atypical kinetic features observed with CYPs can be explained with multi-site kinetic models (Shou et al., 2001; Houston and Galetin, 2005), kinetic analysis with these models provided strong support for this hypothesis. However, this type of studies do not provide mechanistic information in terms of where those sites are located and how substrates and/or effectors interact with each other and the enzyme, especially given the complexity of the P450 cycle. Although some researchers speculated that the “effector” site(s) is an allosteric site separated

from the enzyme active site (Johnson et al., 1988; Schwab et al., 1988), accumulating evidence indicated that multiple molecules can simultaneously bind within or near the enzyme active site (Shou et al., 1994; Rock et al., 2003). For instance, Shou et al (Shou et al., 1994) studied the interactions between two CYP3A4 substrates: 7,8-benzoflavone and phenanthrene. They found that these two compounds affected the V_{max} of the other compound but did not affect the K_m. Their results provided the first evidence that two different molecules can simultaneously bind to the active site of a P450 since both compounds are substrates of the same enzyme and did not interfering the binding of each other (no changes in K_m). Several site-directed mutagenesis studies also suggested that the "effector" site(s) is located close to or within the enzyme active site (Harlow and Halpert, 1997; Harlow and Halpert, 1998; Domanski et al., 2000; He et al., 2003). For instance, Harlow and Halpert replaced two small residues in the active site of CYP3A4 with bulky residues and observed the disappearance of positive homotropic cooperativity of testosterone-6β-hydroxylation, and the overall activity on that reaction was increased compared to the wild type enzyme. The authors thought that the bulky residues not only prevented the binding of the second testosterone molecule to the enzyme active site (no positive homotropic cooperativity), but also mimicked its action by reducing the size of the active site (Harlow and Halpert, 1998). Evidence for multiple molecules simultaneously binding to the enzyme active site also comes from kinetic deuterium isotope effect experiment. Rock et al (Rock et al., 2003) studied the interactions of deuterated laurate on palmitate metabolism by $P450_{BM3}$ and observed isotope

effects on palmitate metabolite ratios, which could only occur if both laurate and palmitate occupy the active site simultaneously. Based on these findings, it is likely atypical kinetics are caused by changes in enzyme properties such as enzyme conformation upon the occupation of one of the binding sites. In addition, since the binding sites are located in the enzyme active site, it is likely that ligands may have access to the heme and can form products from all the binding sites. Due to the complexity of a P450 reaction, the mechanisms for atypical kinetics may not be limited to the changes in the oxidation reaction. Hutzler and co-workers clearly demonstrated that one mechanism for increased CYP2C9-catalyzed flurbiprofen metabolism by dapsone was by decreasing the branching reactions in the P450 cycle (Hutzler et al., 2003).

- **Kinetic Models for Atypical Kinetics**

Atypical kinetic data are typically analyzed in one the following approaches: 1) Forcing the kinetic data through a hyperbolic curve (Michaelis-Menten model) regardless of the observed kinetic profile; 2) Fitting empirical models such as Hill equation (Equation 1.1) and uncompetitive substrate inhibition model (Equation 1.2) to the kinetic data; 3) Employing multi-site kinetic models(Houston and Galetin, 2005). Clearly the first approach is not a good way to analyze atypical kinetic data because it would result in inaccurate estimation of kinetic parameters. The empirical kinetic models can accurately predict rates of product formation, representing a useful tool for preliminary data analysis. However, the information obtained through the second approach is rather limited since the kinetic parameters such as the n and S_{50} in the Hill equation do not have

physiological meanings. Based on the central hypothesis of atypical kinetics that the enzyme has multiple substrate/effector binding sites, multiple-site kinetic models not only can predict reaction rates accurately, but also provide information such as substrate/effector binding affinity, enzyme catalytic efficiency, and their changes upon simultaneous binding to the enzyme etc. Thus, the last approach represents the most informative and rational way to analyze kinetic data (Houston and Galetin, 2005).

Equation 1.1: $$V_0 = \frac{V_{max} \times [S]^n}{S_{50}{}^n + [S]^n}$$

Equation 1.2: $$V_0 = \frac{V_{max} \times [S]}{K_m + [S] \times (1 + \frac{[S]}{K_{si}})}$$

Figure 1.4 shows a generic multiple-site model for homotropic interactions (Houston and Galetin, 2005). In this model, the enzyme has two equivalent binding sites, which have the same dissociation constant (K_s) for the substrate and identical effective catalytic constant (k_p) for product formation. In this model the substrate not only can associate with free enzyme but also with substrate-enzyme complex, forming the S-E-S complex. The dissociation constant and the effective catalytic constant for the S-E-S complex are different from the S-E or E-S complex and are modeled with factors α and β respectively. This model is versatile in that it can explain all three types of homotropic cooperativity. Sigmoidal kinetics, a results of positive homotropic effect, can be modeled as an increase in substrate binding affinity upon the first substrate binding to the enzyme (α <1), or an increase in k_p for S-E-S complex compared with substrate-

enzyme complex (β>1). In contrast, negative cooperativity can be modeled by changes in α and β in opposite directions, namely α>1, for biphasic kinetics and β<1, for substrate inhibition kinetics(Houston and Galetin, 2005). Variations of this kinetic model (Figure 1.4) were also employed to explain homotropic cooperativity (Korzekwa et al., 1998; Shou et al., 1999; Lin et al., 2001; Khan et al., 2002). For instance, Shou et al proposed model that the enzyme has two kinetically distinct binding sites instead of two identical sites(Shou et al., 1999; Lin et al., 2001). Khan et al. proposed a model where the substrate sequentially binds to the two binding sites available in the enzyme (Khan et al., 2002).

Figure 1.4. A generic two-site model for homotropic cooperativity (Houston and Galetin, 2005)

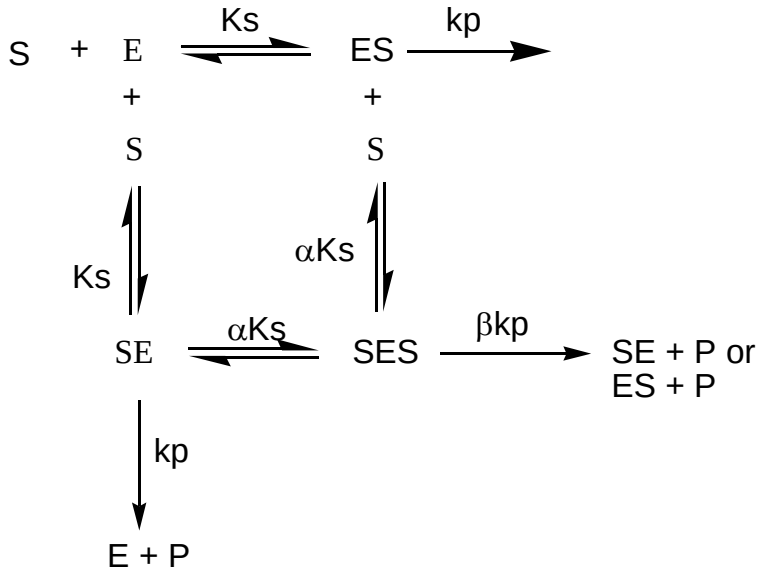

$$\frac{V_0}{V_{max}} = \frac{2\frac{[S]}{K_s} + \frac{\beta[S]^2}{\alpha[K_s]^2}}{1 + \frac{2[S]}{K_s} + \frac{[S]^2}{\alpha[K_s]^2}}$$

The kinetic models for heterotropic cooperativity are more complex due to the presence of an additional compound and the increased number of enzyme complexes. Several reviews described different multiple-site kinetic models for heterotropic cooperativty of CYPs (Korzekwa et al., 1998; Shou et al., 2001; Houston and Galetin, 2005). Figure 1.5 illustrated the simplest multiple-site kinetic model for heterotropic cooperativity (Houston and Galetin, 2005). In this model, the enzyme also has two equivalent binding sites. Both the effector and the substrate can bind to these two sites. Upon binding of one molecule (substrate or effectors), the enzyme catalytic efficiency and the binding affinity of the substrate/effector may be altered (Houston and Galetin, 2005).

Figure 1.5. A two-site model for heterotropic interactions (Houston and Galetin, 2005).

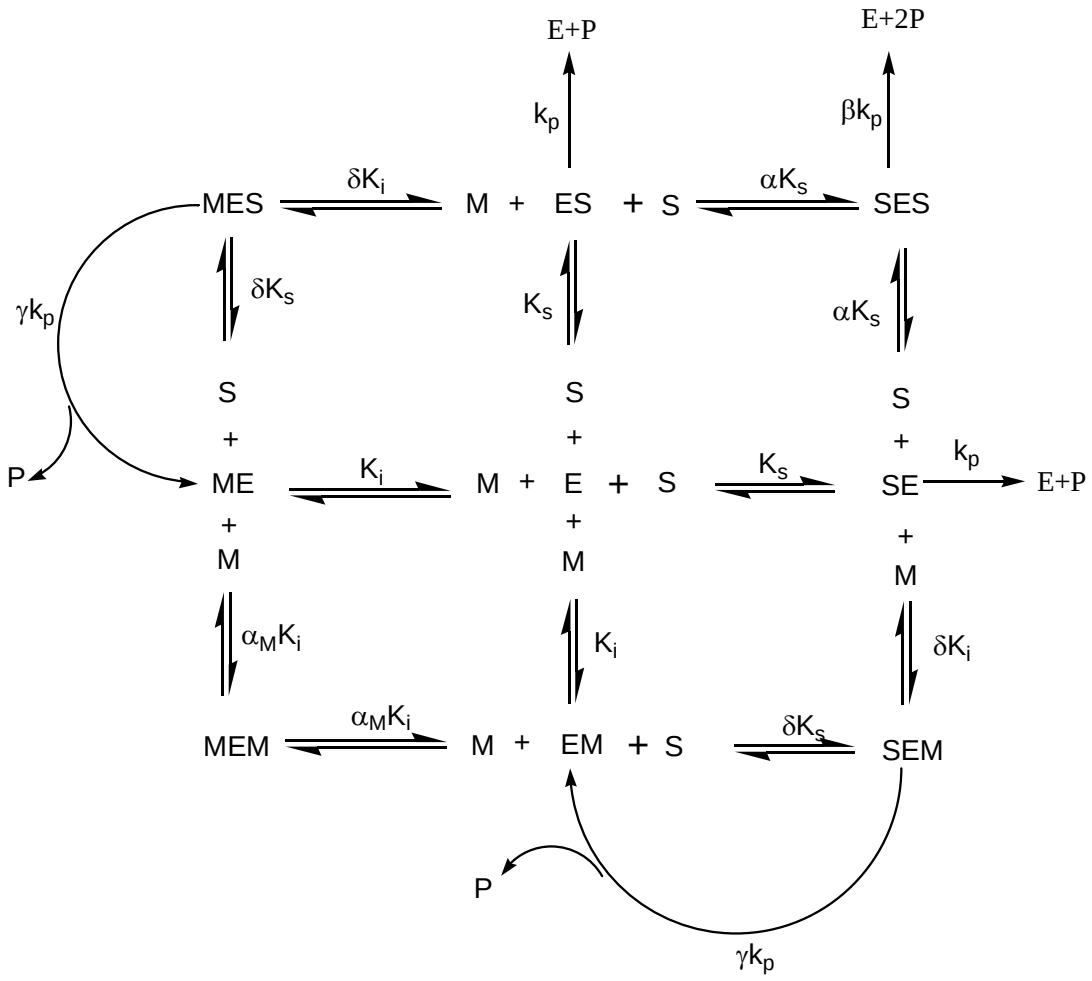

$$\frac{V_0}{V_{max}} = \frac{2\frac{[S]}{K_s} + \frac{\beta[S]^2}{\alpha[K_s]^2} + 2\frac{\gamma[S][I]}{\delta K_s K_i}}{1 + \frac{2[S]}{K_s} + \frac{[S]^2}{\alpha[K_s]^2} + \frac{2[S][I]}{\delta K_s K_i} + \frac{2[I]}{K_i} + \frac{[I]^2}{\alpha_i[K_i]^2}}$$

- **Impact of Atypical Kinetics**

Employment of *in vitro* kinetic data obtained from human liver microsomes or hepatocytes to predict *in vivo* clearance is a widely accepted procedure in drug discovery and development settings. The fundamental principle of this procedure is that the intrinsic clearance [CL_{int}, rate of metabolism divided by substrate concentration (Rate/[S])] obtained *in vitro* is essentially equivalent to the *in vivo* CL_{int}. Thus, one can scale up the *in vitro* CL_{int} to *in vivo* total clearance by applying estimates of *in vivo* enzyme amounts, blood flow, plasma protein binding etc. to models such as the well-stirred model or parallel tube model. Commonly in vitro CL_{int} is expressed with kinetic parameters of the one-site Michaelis-Menten model. Under therapeutic conditions, the free drug concentration at the site of metabolism is much lower than its K_m. Thus the equation for the rate of metabolism of drugs can be reduced to $V_0 = \frac{V_{max}[S]}{K_m}$ and the CL_{int} can be expressed as V_{max}/K_m by rearranging the equation. (Tracy, 2006) However, for drugs displaying sigmoidal kinetics, the CL_{int} is substrate-concentration dependent even at low substrate concentrations as shown in Figure 1.6 (Houston and Kenworthy, 2000). Thus *in vivo*, the compound would have non-linear pharmacokinetic properties and the prediction of *in vivo* clearance based on in vitro CL_{int} calculated as V_{max}/K_m would not be accurate. For substrate inhibition and biphasic kinetics, although at low substrate concentrations, the kinetic curves are both hyperbolic (same as the Michaelis-Menten kinetics) (Houston and Kenworthy, 2000), one must be cautious in

selecting the correct kinetic model to predict kinetic parameters for *in vitro* CL_{int} calculations. Forcing kinetic data through a hyperbolic curve would result in mis-estimation of K_m and V_{max}, and thus affect the estimation of *in vivo* clearance.

Figure 1.6. Clearance plots for a compound exhibited sigmoidal kinetics (solid line) or Michaelis-Menten kinetics (dashed line) (Houston and Kenworthy, 2000).

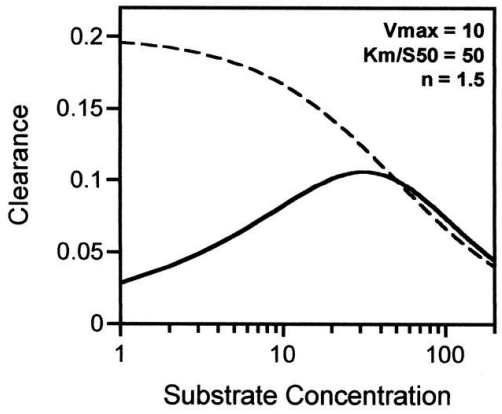

The use of in vitro kinetic studies to predict potential drug-drug interactions involving inhibition of drug metabolism enzymes is also a common practice in drug discovery and development settings. Generally, a substrate of the enzyme in question is used as a probe and the inhibition potentials of new chemical entities on the probe substrate can be extrapolated to other substrates of the same enzyme, based on the assumptions that all the substrates share only one binding site in the enzyme. Also based on this assumption, substrates of the same enzyme competitively inhibit the reactions of the other substrates, and thus are likely to affect the pharmacokinetics of the other substrates, causing drug-drug interactions *in vivo*. However, because of heterotropic cooperativity, the interactions between two substrates of the same enzyme may not necessarily be

competitive inhibition, and an inhibitor for the probe reaction may not always inhibit metabolism of other substrates catalyzed by the same enzyme (substrate-dependent effect). Thus atypical kinetics may profoundly affect the accuracy of predictions of drug-drug interactions since the fundamental premises of this practice may not be correct (Houston and Galetin, 2005). To increase the confidence for the predictions, employment of multiple probe substrates are suggested in *in vitro* drug-drug interaction studies (Kenworthy et al., 1999; Kumar et al., 2006).

In addition, in recent years great effort has been put forth to quantitatively predict the degree of in vivo interaction between two drugs based on in vitro kinetic data. Equations were developed to quantitatively predict the changes in AUC (area under curve of the plasma concentration-time plot) in the presence of an inhibitor. Assuming the substrate is eliminated by a single metabolizing pathway, the ratio of AUC in the absence of and presence of an inhibitor equals to $1+ [I] /K_i$. Interactions are regarded as low risk if the $[I]/K_i$ ratio is less than 0.1 and high risk if the ratio is bigger than 1. However, the accuracy of the prediction largely depends on the accuracy of the K_i obtained from in vitro kinetic studies. Employment of simple one-site inhibition models to compounds displaying heterotropic cooperativity may lead to inaccurate estimation of the Ki , thus inaccurate prediction of changes in AUC in the presence of an inhibitor.(Houston and Galetin, 2005) It is also very difficult to determine the free concentration of inhibitors at the active site in the liver. For UGTs this is even more problematic than for P450s since the enzyme active site is inside the lumen of the

endoplasmic reticulum and the product must be transported out of the ER and then be further transported into the blood or excreted into the bile.

III. Hypotheses and Aims

Frequently, different types of homotropic cooperativity were reported with UGT-catalyzed reactions. For instance, morphine-6-glucuronidation by UGT2B7 displayed biphasic kinetics(Ohno et al., 2008), estradiol-3-glucuronidation by UGT1A1 exhibited autoactivation(Williams et al., 2002), and substrate inhibition kinetics were observed with resveratrol glucuronidation by UGT1A9 (Iwuchukwu and Nagar, 2008). These kinetic observations indicated that UGTs may also have multiple substrate binding sites, similar to CYPs. However, the atypical kinetic features associated with heterotropic cooperativity are less prevalent for UGTs. This may be because very few studies systemically evaluated the interactions between UGT substrates. In searching for heterotropic cooperactivity to further support the hypothesis that UGTs have multiple aglycone substrate binding sites, we evaluated the interactions between prototype substrates of two glucuronidation enzymes: UGT1A1 or UGT1A4. In addition, multisite kinetic analysis represents a useful way to analyze atypical kinetic data for CYPs. Employment of this approach on atypical kinetics of UGTs is rare. Therefore, the other aim of the present study is to evaluate whether multisite kinetic models can also be used to explain the atypical kinetics observed with UGT1A1 and UGT1A4.

CHAPTER 2 - KINETIC ANALYSIS ON UGT1A4-CATALYZED GLUCURONIDATION

Part I: Glucuronidation of Dihydrotestosterone and Trans-Androsterone by Recombinant UGT1A4: Evidence for Multiple UGT1A4 Aglycone Binding Sites

Background

Human UGT1A4 is mainly expressed in liver. It is largely considered as the primary catalyst for N-glucuronidation due to its efficiency in catalyzing the glucuronidation of primary, secondary, tertiary and aromatic amines(Kiang et al., 2005). Approximately 20% of the top 200 prescribed drugs that are cleared to some degree through glucuronidation are metabolized by UGT1A4-catalyzed N-glucuronidation (Williams et al., 2004). Examples of drugs that have UGT1A4-catalyzed N-glucuronidation as an elimination pathway include imipramine, trifluoperazine, tamoxifen, lamotrigine and midazolam etc. UGT1A4-catalyzed-N-glucuronidation also plays important role in carcinogen elimination. For instance, UGT1A4 catalyzes the N-glucuronidation of benzidine, NNAL (4-(Methylnitrosamino)-1-(3-Pyridyl)-1-Butanol) and PhiP (2-Amino-1-methyl-6-phenylimidazo [4, 5-b] pyridine) etc. In addition to N-glucuronidation, UGT1A4 also catalyze O-glucuronidation. Many steroidal compounds such as dihydrotestosterone (DHT), trans-androsterone (t-AND) and hecogenin are UGT1A4 substrates (Green and Tephly, 1996).

Atypical kinetics of UGT1A4-catalyzed glucuronidation have been reported (Chouinard et al., 2006; Hashizume et al., 2008; Hyland et al., 2009). However, systematic kinetic studies to explore the existence of multiple aglycone binding sites in UGT1A4 have never been conducted. Dihydrotestosterone (DHT) and trans-androsterone (t-AND) (Figure 2.1) are two steroidal substrates of UGT1A4. Although the glucuronidation of DHT and t-AND by UGT1A4 has been clearly established (Green and Tephly, 1996), a detailed kinetic analysis of these processes has not been reported. These two compounds, based on a planar, rigid steroidal scaffold, differ only with respect to the position of the hydroxyl group (at position 3 or 17, the site of glucuronidation) and the location of the ketone group (position 17 or 3). Because of the rigid steroidal scaffold shared by these two compounds and the differing placement of substituents, we hypothesized that these two compounds may either occupy the same region of the active site but in opposite orientation or occupy two separate regions in UGT1A4 active site. Studies in our lab on the activities of two polymorphic UGT1A4 enzymes (UGT1A4.2 and UGT1A4.3) demonstrated that mutations of amino acids in exon 1 of UGT1A4 exhibited a differential effect on DHT and t-AND glucuronidation (as mentioned in Part II). Because it is generally accepted that aglycone substrate binding sites of UGT1A enzymes are within the exon 1-coded N-terminal ends of the proteins (Radominska-Pandya et al., 1999), such polymorphism effects may indicate the possibility of DHT and t-AND occupying two separate regions in UGT1A4, reinforcing the need to conduct systematic kinetic studies with these two compounds to explore the existence of multiple

aglycone binding sites in UGT1A4. To this end, a detailed characterization of the glucuronidation kinetics of these two compounds by HEK293-expressed UGT1A4 was conducted. Interactions of DHT or t-AND with another UGT1A4 substrate (tamoxifen (TAM) or lamotrigine (LTG), structures shown in Figure 2.1) were also evaluated.

Figure 2.1. Structures of DHT, t-AND, TAM and LTG

The glucuronidation sites of the compounds are illustrated with arrows.

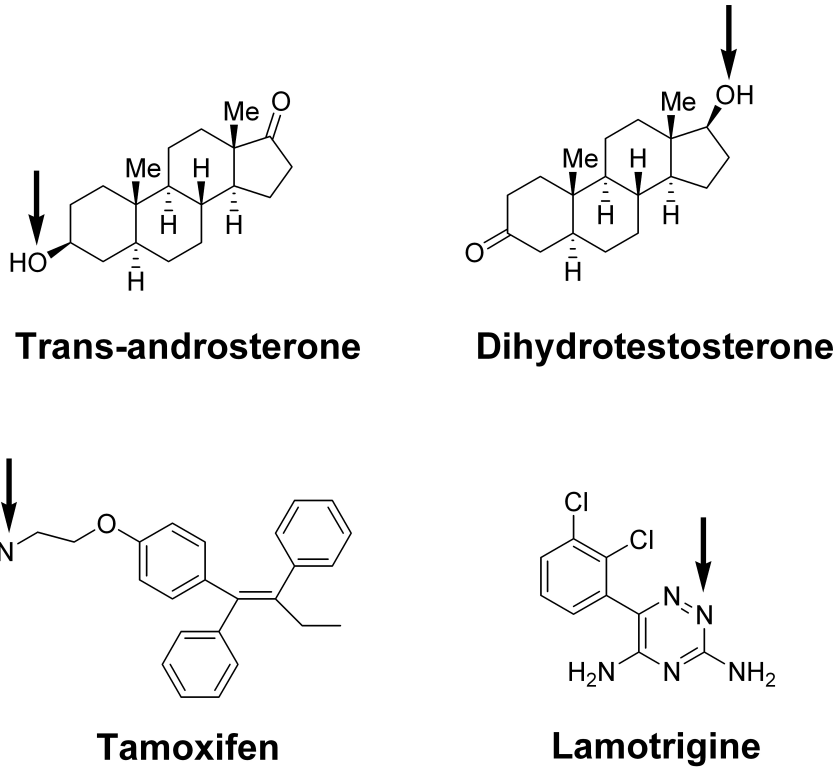

<u>Figure 2.2.</u> Hypothesized orientations for DHT and t-AND to bind to the UGT1A4 active site

The shapes for the enzyme active site and the distances between substrates are arbitrary.

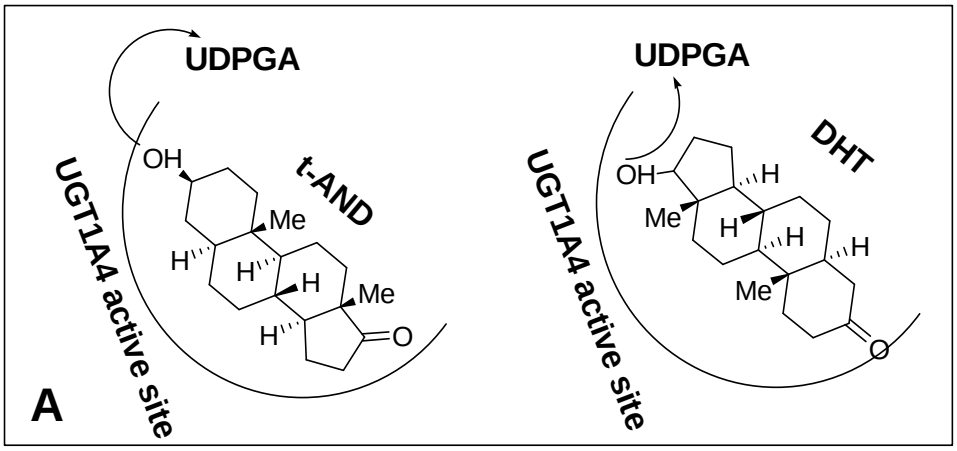

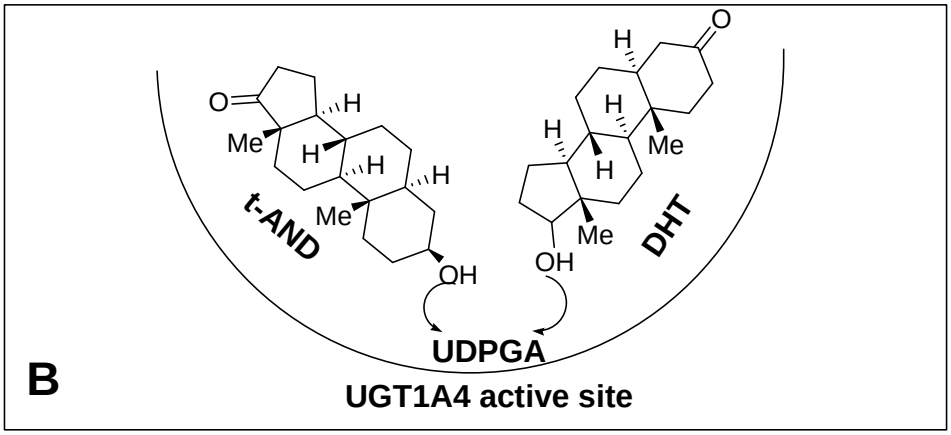

Materials and Methods

Materials. Tamoxifen citrate and tamoxifen were purchased from MP Biomedical LLC (Santa Ana, CA). Lamotrigine was purchased from Toronto Research Chemicals Inc (North York, ON, Canada). Dihydrotestosterone, dihydrotestosterone glucuronide, trans-androsterone (epiandrosterone), tran-androsterone glucuronide and testosterone glucuronide were purchased from Steraloids, Inc. (Newport, RI). Lamotrigine N_2- glucuronide was a gift from GlaxoSmithKline (Philadelphia, PA). Uridine-diphosphate glucuronic acid (UDPGA), Trizma base, Trizma HCl, D-saccharic acid 1,4-lactone, alamethicin, morphine-3-glucuronide, and acetobromo-α-D-glucuronic acid methyl ester were purchased from Sigma-Aldrich (St. Louis, MO). $MgCl_2$ was purchased from Mallinckrodt Corp. (Hazelwood, MO). All other chemicals employed in the glucuronidation incubations, as well as the HPLC solvents were of HPLC grade. Chemicals used in the synthesis of tamoxifen –N-glucuronide were ACS grade. Recombinant UGT1A4 was produced in HEK293 cells. Cell lysate was prepared by sonication of UGT1A4-HEK293 cells in 10 mM Tris Buffer (pH=7.4 at 37˚C) containing 0.25 M sucrose for three 30-second bursts, each separated by 1-minute cooling on ice and was added directly to the incubation as the enzyme source. The protein concentration in cell lysate was determined with the Pierce BCA™ protein assay kit (Thermo Fisher Scientific Inc., Rockford, IL).Cell culture procedures for HEK293 cells were as followed.

Culture procedures for HEK293 cells

HEK293 cells expressing UGT1A4 were gifts from Dr. Philip Lazarus (Pennsylvania State University, Hershey, PA) and Blank HEK293 cells were obtained from Dr. Williams Elmquist (University of Minnesota, Minneapolis, MN)

- **Preparation of media**

A. HEK 293 blank cell growth medium (medium for HEK 293 blank cells): Five ml Penicillin-Streptromycin solution (contains 10,000 units penicillin and 10 mg streptomycin per ml in 0.9% NaCl, Sigma-Aldrich, St. Louis, MO)and 50 ml Fetal bovine serum (FBS, Sigma-Aldrich, St. Louis, MO) were added to 445 ml sterile Dulbecco's Modified Eagle Medium (DMEM, Fisher Scientific, Pittsburg, PA).

B. Selection growth medium (medium for HEK293 cells expressing UGT1A4): To 500 ml blank cell growth medium, 175 mg geneticin (Invitrogen, Carlsbad, CA) were added.

All media were incubated at 37℃ with 95% air/5% CO2 and 98% humidity for 24 hour to test if media were sterile.

- **Seeding**

All standard laboratory procedures for aseptic cell culture were followed. Growth media were warmed up at 37ºC. After the media were warmed up, 18 ml growth media were added to a tissue culture flask (250mL 75cm^2, Fisher scientific, Pittsburg, PA). HEK293 cells were thawed at 37ºC and then added to

corresponding medium. Cell suspensions were then incubated at 37℃ with 95% air/5% CO2 and 98% humidity. Cells were checked for confluence every day.

- **Splitting**

After about 80% of confluence was reached, media were removed. Cells were then washed twice with 20ml Hanks' balanced salt solution (HBSS, Invitrogen, Carlsbad, CA). Five ml Trpsin-0.25%-EDTA (Invitrogen, Carlsbad, CA) were added to each flask and were incubated at the conditions mentioned above for 5-10 min. Fifteen ml of corresponding growth media were then added to each flask. The resulting cell suspensions were thoroughly mixed by pipetting up and down for at least 50 times. Four ml of each cell suspension was transferred to tissue culture flask which contains 16 ml corresponding medium. The resulting cell suspensions were then incubated at 37℃ with 95% air /5% CO_2 and 98% humidity. After about 80% of confluence was reached, media were removed. Cells were then washed twice with 20ml Hanks' balanced salt solution (HBSS, Invitrogen, Carlsbad, CA). Five ml Trpsin-0.25%-EDTA (Invitrogen, Carlsbad, CA) were added to each flask and were incubated at the conditions mentioned above for 5-10 min.

- **Homogenization**

Five ml blank growth medium (without geneticin) were added to each flask. The resulting suspensions were homogenized by pipetting up and down for at least 50 times and then were transferred to 50ml centrifuge tubes. The suspensions were centrifuged at 2500 rpm for 3 min at room temperature. The supernatant

was decanted and then 40 ml of HBSS were added to re-suspend the pellets. The centrifugation step was repeated. The HBSS was decanted and the pellets were used to prepare cell lysate with the procedures above.

Synthesis of Tamoxifen-N- glucuronide (Kaku et al., 2004). Fifty mg (0.134 mmol) of Tamoxifen and 80.2 mg (0.202 mmol) of acetobromo-α-D-glucuronic acid methyl ester were dissolved in 0.4ml anhydrous dichloromethane and stirred for 72 hr at room temperature under nitrogen protection. The organic solvent was then removed by rotary evaporation. The resulting residue was dissolved in 3 ml of methanol and 1.5 ml of 0.5 M of aqueous sodium carbonate was added to the methanolic solution. The resulting solution was stirred at room temperature for five hrs. Twenty-five ml of water were then added to the reaction mixture, which was extracted five times with equal volumes of ether to remove unreacted tamoxifen. The pH of the aqueous layer was adjusted to 5.0 with 1 mol/l of HCl. Water in the aqueous layer was then removed by lypholization. The resulting residue was re-dissolved with a small volume of 0.1% formic acid in MeOH and loaded onto a preparative HPLC column (Higgins Haisil HL C18 5µm 100 x 20mm). The tamoxifen glucuronide was eluted with a mobile phase, consisting of 0.1% of formic acid in water-0.1% formic acid in MeOH (4:6 v/v), at a flow rate of 22 ml/min and monitored by UV absorbance at 254nm. The tamoxifen-N-glucuronide eluted at 16.5 min and collected fractions were pooled. Evaporation of the combined eluate fractions yielded 9.8 mg of white powder (13.2%). ^{1}H-NMR (600MHz, dimethyl sulfoxide-d6)(Figure 2.3): δ 0.885 (t, 3H, *J* 7.2 Hz, CH_2CH_3), 2.409 (q, 2H, *J* 7.2 Hz, CH_2CH_3), 3.159-3.229(m, 7H, N-$(CH_3)_2$ and H-

4′), 3.329 (m, 1H, H-3′), 3.464 (d, 1H, *J* 8.4 Hz, H-5′), 3.589 (m, 1H, H-2′), 3.843-3.886 (m, 2H, N-C*H*$_2$CH$_2$-O), 4.391 (m, 2H, N-CH$_2$C*H*$_2$-O), 4.694 (d, 1H, *J* 7.2 Hz, H-1′),6.716 (d, 2H, *J* 8.4 Hz, ArH, *ortho* to NCH$_2$CH$_2$O–), 6.80 (d, 2H, *J* 9 Hz, ArH, *meta* to NCH$_2$CH$_2$O–), 7.157–7.433 (m, 10H, ArH). ESI-TOF-MS: 548.2649$[M]^+$ (error 0.18ppm).

Figure 2.3. ^{1}H-NMR spectrum of tamoxifen-N-glucuronide

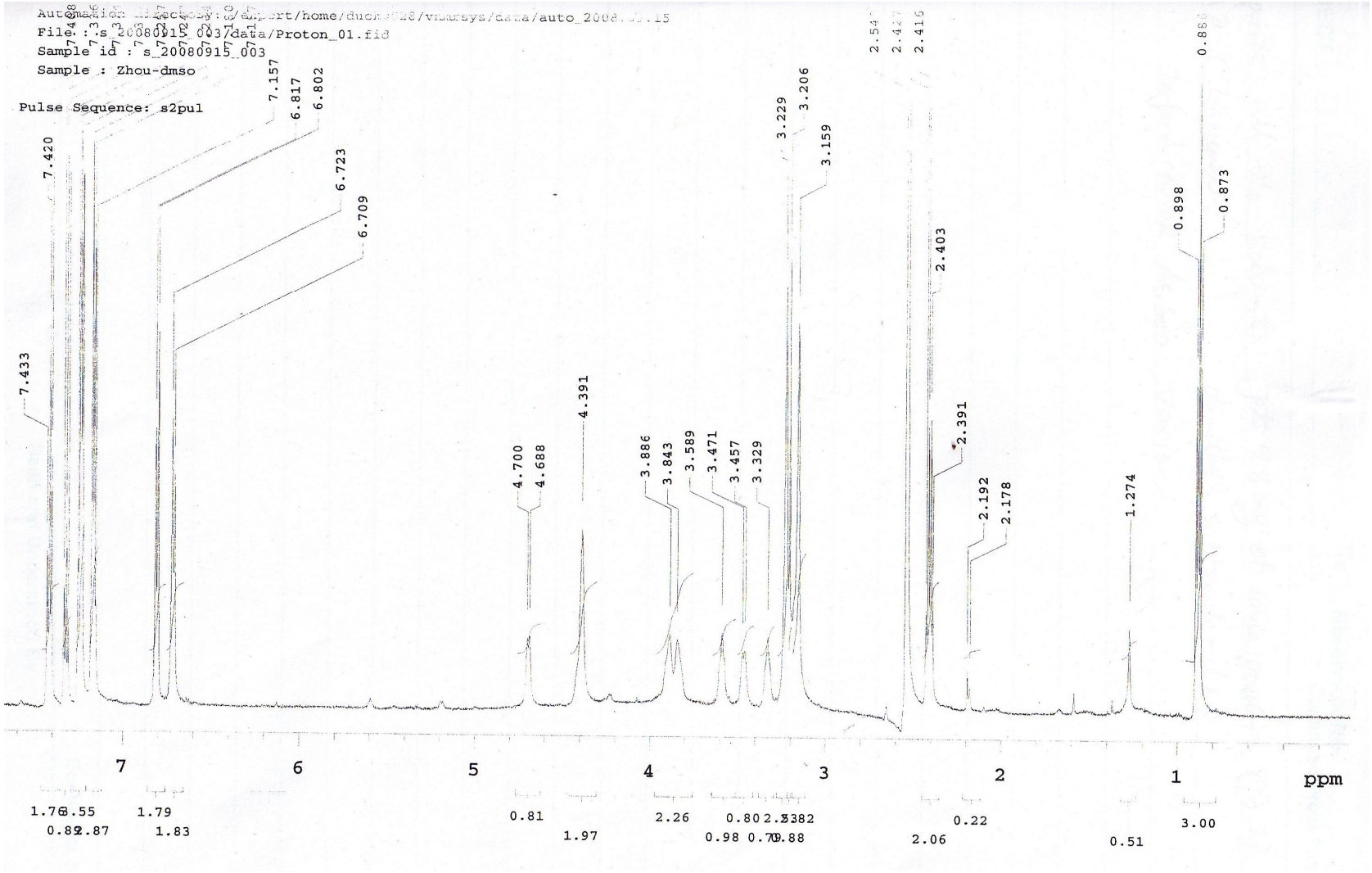

Incubations to Characterize Glucuronidation Kinetics in the Absence of Modifiers. Preliminary experiments were conducted to ensure that all kinetic determinations were carried out under linear conditions with respect to time and protein concentration. Incubation mixtures (200 µl final volume) contained UGT1A4-HEK293 cell lysate (0.25 mg/ml of protein for t-AND, DHT and LTG glucuronidation or 0.1mg/ml of protein for TAM glucuronidation), Tris-HCl buffer (0.1 M), $MgCl_2$ (5 mM), D-saccharic acid 1,4-lactone (5 mM), UDPGA (3 mM), alamethicin (50 µg/mg of protein) and DHT (3.9-250.0 µM), t-AND (2.8-202.2 µM), TAM (0.5-100 µM) or LTG (47.4-4969.8 µM). DHT, t-AND and TAM were initially dissolved in DMSO before addition to the incubation mixtures, whereas LTG was initially dissolved in 0.1 M acetic acid containing 4% of DMSO. The final organic solvent concentrations in all incubation mixtures were always less ≤2%. In each experiment, the organic concentration was constant irrespective of substrate concentration. The final pH of all incubation mixtures was 7.4 at 37˚C. Cell lysates were pre-incubated on ice with alamethicin for 30 minutes before reaction initiation. This step was followed by a 3-min preincubation at 37℃, after which the reaction was initiated by addition of UDPGA. After 30-min (DHT, t-AND and LTG) or 20-min (TAM) incubation in a shaking water bath, reactions were terminated by addition of 200 µl cold acetonitrile, followed by addition of internal standards (DHT and t-AND glucuronidation assay: 20 µl of 1.07 µg/ml testosterone glucuronid; TAM glucuronidation assay: 10 µl of 14.2 µg/ml lamotrigine glucuronide; LTG glucuronidation assay: 10 µl of 50 µg/ml morphine-3-glucuronide). Protein precipitate was removed by centrifugation at 13,000 X g

for 5 minutes and the reaction mixture was filtered through a 0.2 µ nylon spin filter (Grace Davison Discovery Science, Deerfield, IL) prior to injection onto the HPLC system.

Incubations to Characterize Interactions between UGT1A4 Substrates. The effect of TAM on DHT and t-AND glucuronidation was initially evaluated with three DHT or t-AND concentrations (approximately $0.5K_m$, K_m and $2K_m$) and six TAM concentrations (0, 1.25, 2.5, 5, 10, 20 µM). Because we observe a significant activation effect of TAM on DHT glucuronidation in this initial study, the effect of TAM on DHT glucuronidation was further evaluated with seven DHT concentrations (2.5-100 µM) in the absence or presence of five TAM concentrations (2.5-40 µM). The effect of LTG on DHT and t-AND glucuronidation was also evaluated with three DHT or t-AND concentrations (approximately $0.5K_m$, K_m and $2K_m$) and six LTG concentrations (0, 0.375, 0.75, 1.5, 3, 4.5 mM) and the effect of TAM on LTG glucuronidation was studied with three LTG concentrations (0.75, 1.5, 3 mM) and six TAM concentrations (0, 1.25, 2.5, 5, 10, 20 µM). The incubation conditions were as described above. In order to quantify dihydrotestosterone glucuronide by LC-MS, a liquid-liquid procedure was applied after reaction termination and protein precipitation. Fifty µl of 2.4 mol/l HCl solution were added to the incubation supernatants and the sample was extracted twice with 500 µl of ethyl acetate. The ethyl acetate extracts were then combined and dried under N_2 gas. Residues were reconstituted with 50 µl of water-acetonitrile (3:7 v/v) and 25 µl of the sample were injected onto the HPLC system for quantification. The recovery of the liquid-liquid extraction process was

100.2%±6.5% for dihydrotestosterone glucuronide and 96.9%±9.5% for internal standard testosterone glucuronide. To study the effect of DHT or t-AND on TAM glucuronidation, preliminary experiments were conducted at three concentrations of TAM (1.51, 7.57, 15.14 µM). Detailed kinetic studies on TAM (1.0-100 µM) glucuronidation were conducted in the presence of six DHT or t-AND concentrations (25 -250 µM). The incubation conditions were as previously described.

Chromatographic Analysis of Glucuronides. Two methods were developed to quantify trans-androsterone glucuronide and dihydrotestosterone glucuronide. To characterize the glucuronidation kinetics of DHT and t-AND in the absence of a modifier, trans-androsterone glucuronide and dihydrotestosterone glucuronide were quantified by an LC-MS/MS method with an Agilent 1100 series capilliary LC system coupled with a Thermo Finnigan TSQ quantum triple quadrupole mass spectrometer (Waltham, MA). Separation was carried out on a Thermo BetaBasic-18 column (150 x 0.5 mm, 3 µm, Waltham, MA). The mobile phase consisted of 10mM ammonium formate (A) and methanol (B) and was delivered at a flow rate of 12 µl/min. A linear gradient elution program, beginning with 50% of mobile phase B, then increasing mobile phase B linearly from 50% to 90% over one minute and holding at 90% of B for 9 min was employed. The column was then re-equilibrated at initial conditions for 10 minutes. Both tran-androsterone glucuronide and dihydrotestosterone glucuronide eluted at 7.10 min and the internal standard testosterone glucuronide eluted at 6.71 min. The mass spectrometer was equipped with an ESI interface operated in negative ion

mode. Quantification was accomplished in multiple reaction monitoring (MRM) mode by monitoring a transition pair of m/z 465→287 for trans-androsterone glucuronide and dihydrotestosterone glucuronide and 463→285 for the internal standard, testosterone glucuronide. Argon was used as the collision gas. The MS operating conditions were optimized as follows for transandrosterone glucuronide: spray voltage 4000V, sheath gas pressure 19mTorr, aux gas pressure 22mTorr, capillary temperature 355ºC, tube lens offset -95, collision pressure 2.2 mTorr, collision energy 46V; and as follows for dihydrotestosterone glucuronoide: spray voltage 3200V, sheath gas pressure 19mTorr, aux gas pressure 5mTorr, capillary temperature 355ºC, tube lens offset -95, collision pressure 1.9mTorr, collision energy 44V. The chromatogram for trans-androsterone glucuronide, dihydrotesosterone glucuronide and testosterone glucuronide with a capilliary LC-MS/MS method is shown in Figure 2.4.

Figure 2.4. Chromatograms of trans-androsterone glucuronide, dihydrotesosterone glucuronide and testosterone glucuronide with a capilliary LC-MS/MS method.

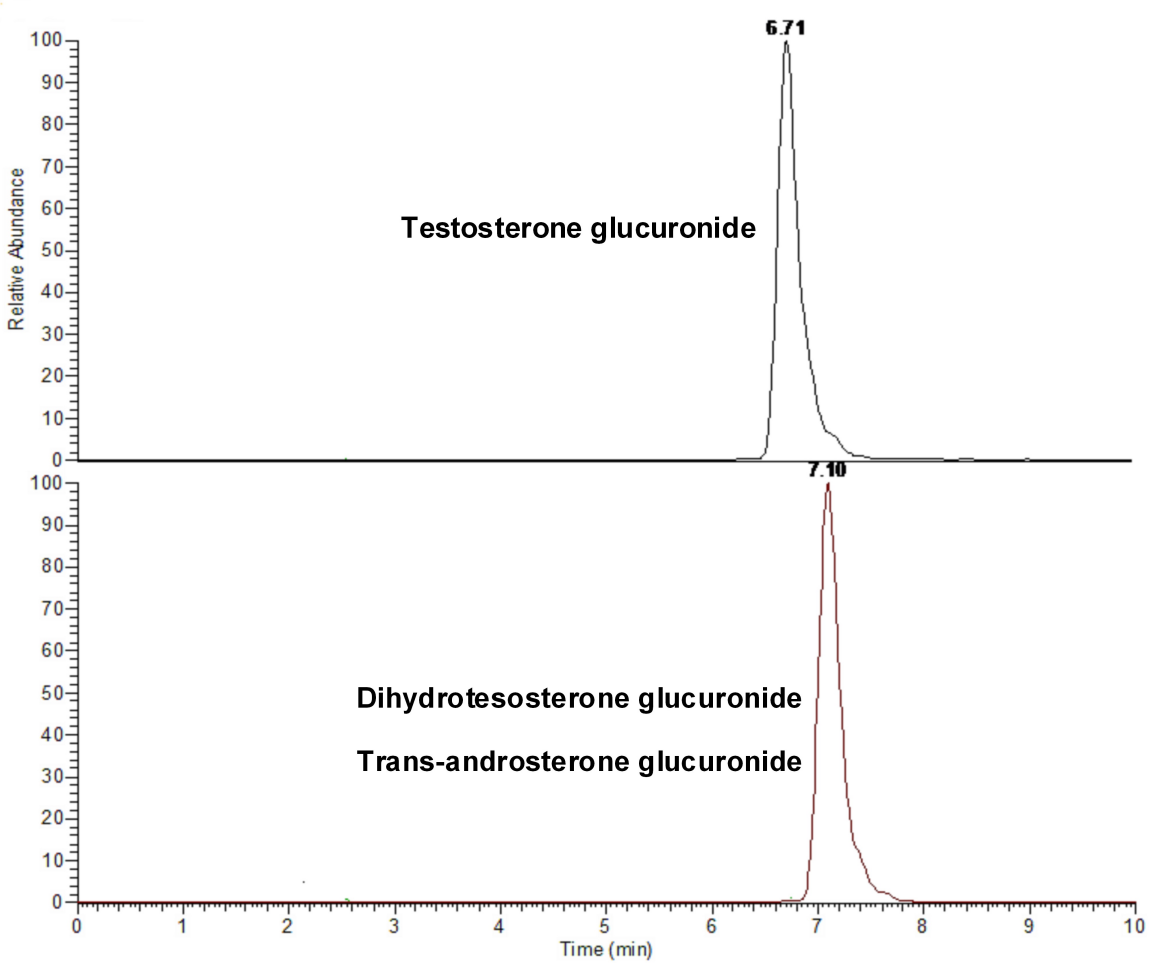

When co-incubated with a modifier, trans-androsterone glucuronide and dihydrotestosterone glucuronide were quantified by a LC-MS method with a Shimadzu LCMS-2010A system (Columbia, MD). Chromatographic separation was accomplished on a Haisil column (C8, 100 x 2.1 mm, 5 µm, Higgins, Mountain View, CA). For quantitation of dihydrotestosterone glucuronide, the mobile phase consisted of 0.1% of formic acid in water (A) and acetonitrile (B) delivered at a flow rate of 0.25 ml/min with a linear gradient elution program of: 30 to 67.5% of B over 5 min, followed by an isocratic hold at 95% of B for 5 min and a 4 min column re-equilibration at initial conditions. The retention times were for was 4.2 min for dihydrotestosterone glucuronide and 3.9 min for testosterone glucuronide. For the quantitation of trans-androsterone glucuronide, the same mobile phase was employed and a similar gradient elution program was applied: 30 to 60% B over 5 min, followed by an isocratic hold at 95% of B for another 5 min and a 4 min column re-equilibration at initial conditions. The retention times for trans-androsterone glucuronide and testosterone glucuronide were 3.60 and 3.23, respectively. The mass spectrometer was equipped with an ESI source operated in negative ion mode. Quantitation was accomplished in selected ion monitoring mode (SIM) by monitoring the respective $[M-H]^-$ ions: m/z=465 for trans-androsterone glucuronide and dihydrotestosterone glucuronide and m/z=463 for testosterone glucuronide. The MS parameters were as follows: nebulizing gas flow=1.5 L/min; interface bias = -3.50KV; interface current= -9.20 µA; heating block temperature= 200 ℃; focus lens= +2.5V; entrances lens= 50.0V; RF gain= 5660; RF offset= 5210; prerod bias= +4.2V; main-rod bias=

+3.5V; aperture= -20.0V; conversion dynode= +7.0kV; detector= -1.9KV; CDL voltage= -25.0kV; Q-array DC= -35.0 V; Q-array RF= +150.0V. The chromatograms are shown in Figure 2.5.

Figure 2.5. Chromatograms of trans-androsterone glucuronide, dihydrotesosterone glucuronide and testosterone glucuronide with LC-MS

A: For dihydrotesosterone glucuronide and testosterone glucuronide, the linear gradient elution program is as follows: 30 to 67.5% of B over 5 min, followed by an isocratic hold at 95% of B for 5 min and a 4 min column re-equilibration at initial conditions, B: For trans-androsterone glucuronide and testosterone glucuronide, the linear gradient elution program is as follows: 30 to 60% B over 5 min, followed by an isocratic hold at 95% of B for another 5 min and a 4 min column re-equilibration at initial conditions.

A

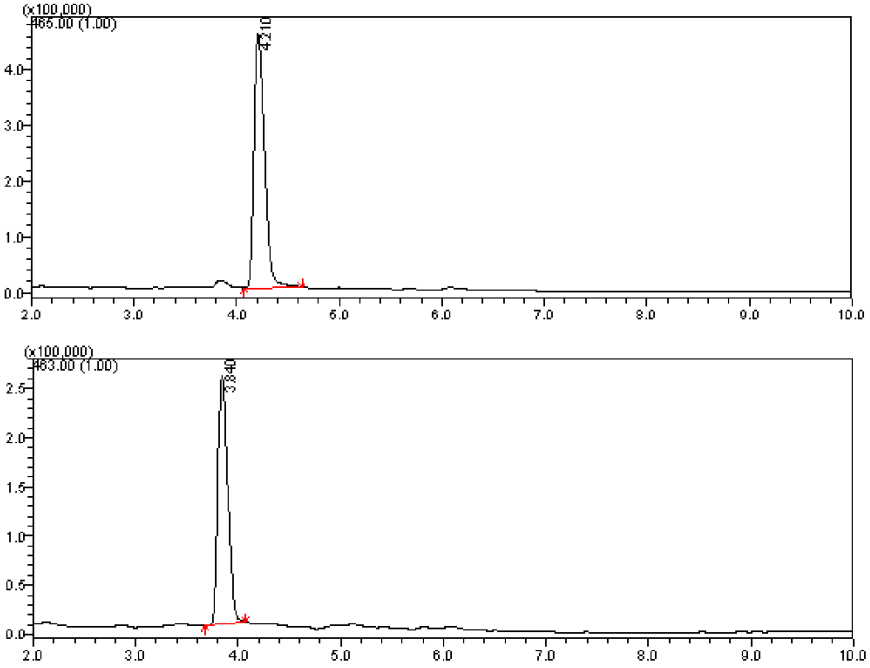
(x100,000)
465.00 (1.00)
4.210
(x100,000)
463.00 (1.00)
3.840

B

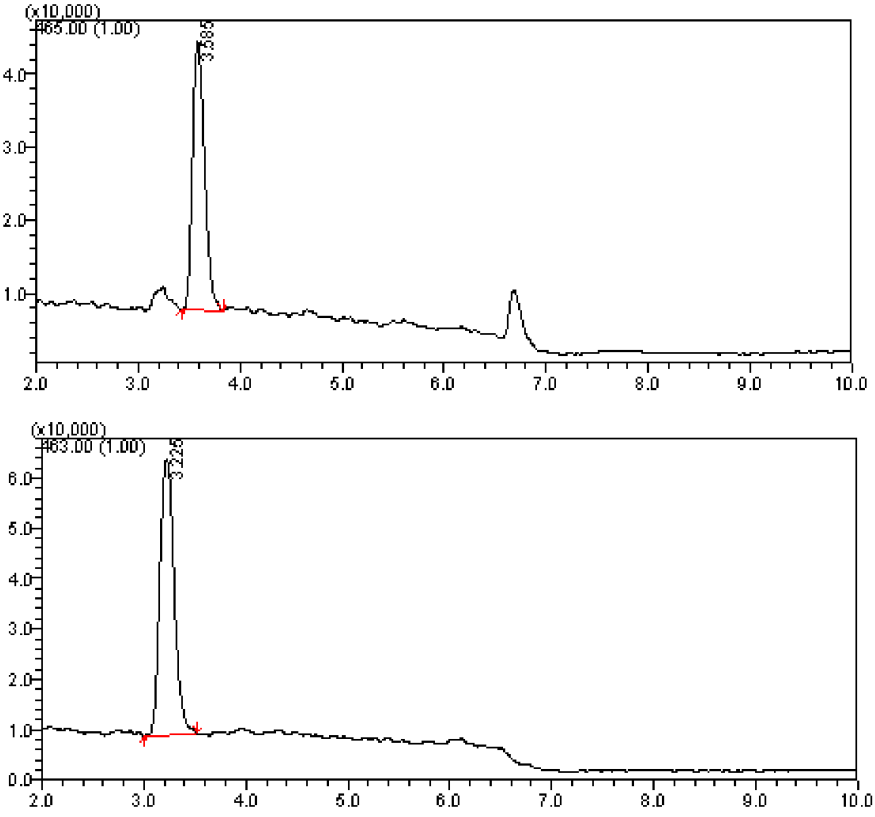
(x10,000)
465.00 (1.00)
3.585
(x10,000)
463.00 (1.00)
3.225

Both tamoxifen-N-glucuronide and lamotrigine-N_2-glucuronide were quantified by LC-MS methods (Shimadzu LCMS-2010A, Columbia, MD). Chromatographic separation was accomplished on a Haisil column (C18, 100 x 2.1 mm, 5 µm, Higgins, Mountain View, CA). Mobile phase, 0.1% formic acid (A) and 0.1% formic in methanol (B) was delivered at a flow rate of 0.25 ml/min with the following linear gradient elution programs: for lamotrigine-N_2-glucuronide, 5% to 40% of B for 5 min, 40 to 80% of B for 3 min, an isocratic hold at 95% of B for 3 min, and column re-equilibration for 4 min (Lamotrigine glucuornide eluted at 6.1 min and the internal standard morphine-3-glucuronide at 2.9 min); for tamoxifen-N-glucuronide, 5 % to 40% of B for 5 min, 40 to 90% of B for 10 min, an isocratic hold at 95% of B for 3 min and, column re-equilibration for 4 min (Tamoxifen-N-glucuronide eluted at 15.7 min and internal standard lamotrigine glucuronide eluted at 6.0 min). The mass spectrometer was operated in positive ion mode with an ESI interface. Quantification was performed in single ion monitoring mode (SIM) by monitoring m/z=432 ($[M]^+$) for lamotrigine-N_2-glucuronide, m/z=548 ($[M]^+$) for tamoxifen-N-glucuronide and m/z=462 ($[M+H]^+$) for morphine-3-glucuronide. The MS parameters were set as follows: nebulizing gas flow=1.5 L/min; interface bias = +4.50KV; interface current= 11.60 µA; heating block temperature= 200 ℃; focus lens= -2.5V; entrances lens= -50.0V; RF gain= 5620; RF offset= 5060; prerod bias= -4.2V; main-rod bias= -3.5V; aperture= +20.0V; conversion dynode= -8.0kV; detector= -1.5KV; CDL voltage= +25.0kV; Q-array DC= +35.0 V; Q-array RF= +150.0V. The chromatograms for tamoxifen-N-

glucuronide and lamotrgine –N2-glucuronide are shown in Figure 2.6 and Figure 2.7.

Figure 2.6. Chromatograms of tamoxifen-N-glucuronide and internal standard lamotrigine-N2-glucuronide with LC-MS

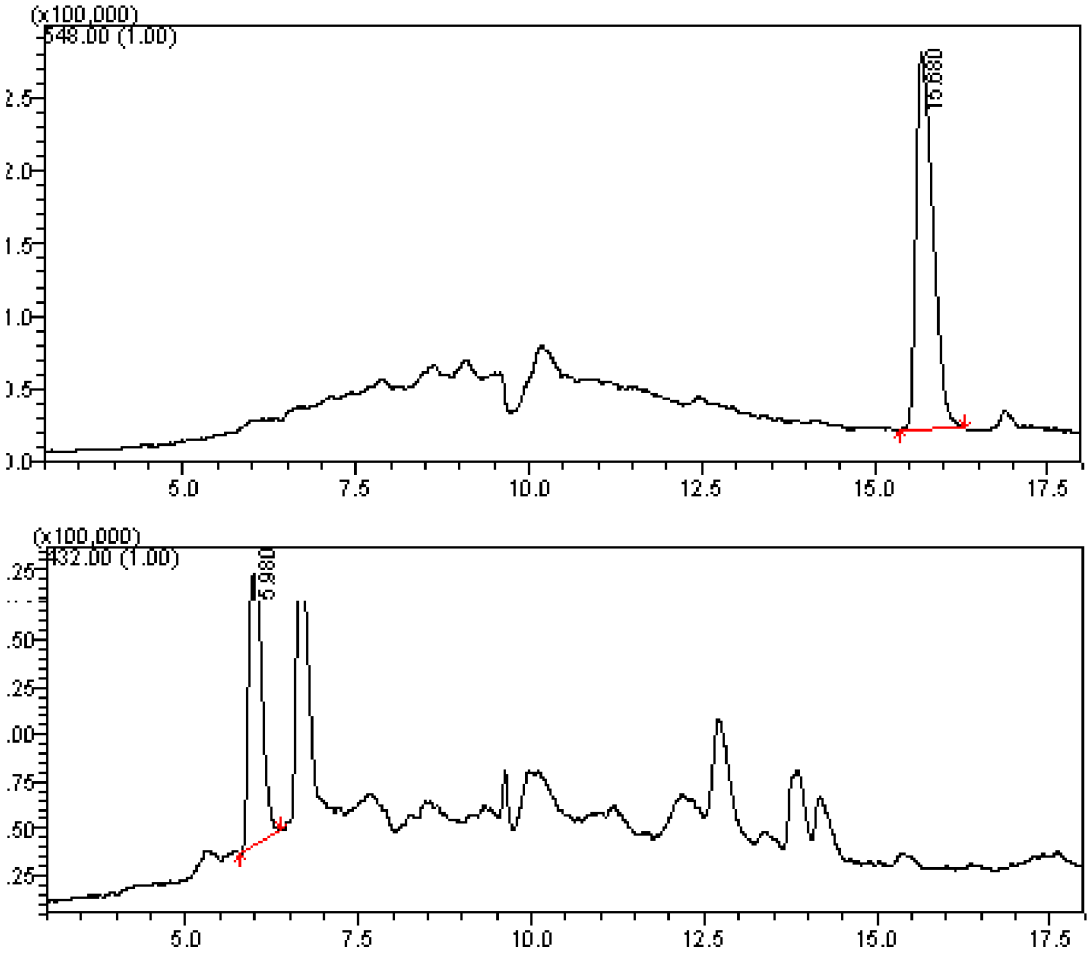

Figure 2.7. Chromatograms of lamotrigine-N2-glucuronide and internal standard morphine-3-glucuronide with LC-MS

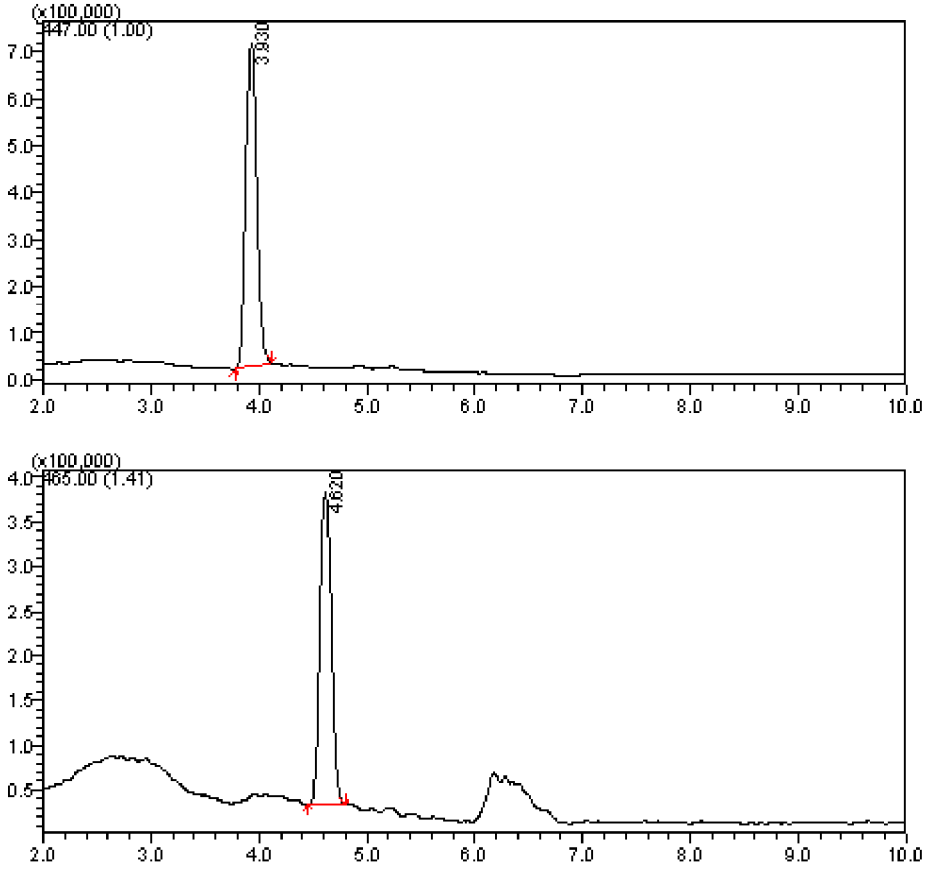

Estimation of Non-specific Protein Binding. Free fractions of DHT, t-AND, TAM and LTG in incubation were estimated with the Hallifax-Houston model (Equation 2.1)(Hallifax and Houston, 2006), where C is protein concentration in milligrams per milliliter and the logP values of DHT, t-AND , TAM and LTG are 3.428, 3.428, 6.064, 2.04 respectively and were calculated with Molinspiration-Interactive logP calculator (http://www.molinspiration.com/services/logp.html).

$$f_u = \frac{1}{1 + C \bullet 10^{0.072 \bullet \log P^2 + 0.067 \bullet \log P - 1.126}} \quad \text{(Equation 2.1)}$$

Data Analysis. Glucuronidation kinetic data for each substrate in the absence of modifiers were analyzed by fitting the Michaelis-Menten equation (Equation 2.2) or an empirical uncompetitive substrate inhibition equation (Equation 2.3) to the data with Sigma Plot 9.0 (Systat Software Inc., San Jose, CA) and by non-linear regression.

$$V_0 = \frac{V_{max} \times [S]}{K_m + [S]} \quad \text{(Equation 2.2)}$$

$$V_0 = \frac{V_{max}}{1 + \frac{K_m}{[S]} + \frac{[S]}{K_{si}}} \quad \text{(Equation 2.3)}$$

The V_{max} and K_m in Equation 2.2 were defined as the maximum velocity and substrate concentration at which velocity is equal to half of the maximum velocity. The V_{max} and K_m in Equation 2.3 have the same definition as in Equation 2.2 and K_{si} is the substrate inhibition constant. Selection of the appropriate model was determined by visual inspection of the Eadie-Hofstee plots and comparison of the Second-Order Akaike Information Criterion and the residual sum of squares.

Kinetic parameters were estimated by nonlinear regression analysis with Sigma Plot 9.0.

Glucurondation kinetics in the presence of modifiers were analyzed initially by calculating the percentage of rate of control (in the absence of modifiers). Modifiers that increased or decreased glucuronidation rate by greater than 20% were considered to exhibit activation or inhibition effects respectively. One-site competitive (Equation 2.4), noncompetitive (Equation 2.5), and mixed inhibition (Equation 2.6) models were applied to analyze the kinetic data, when only inhibition was observed. The V_{max} and K_m in Equation 2.4, 2.5, and 2.6 has the same definition as above. K_i is the inhibition constant. The parameter α reflects changes in the inhibition constant K_i. Selection of the appropriate model was determined by visual inspection of the Dixon plots and comparison of the Second-Order Akaike Information Criterion.

$$V_0 = \frac{V_{max} \times [S]}{K_m \times (1 + \frac{[I]}{K_i}) + [S]} \quad \text{(Equation 2.4)}$$

$$V_0 = \frac{V_{max} \times [S]}{K_m \times (1 + \frac{[I]}{K_i}) + [S] \times (1 + \frac{[I]}{K_i})} \quad \text{(Equation 2.5)}$$

$$V_0 = \frac{V_{max} \times [S]}{K_m \times (1 + \frac{[I]}{K_i}) + [S] \times (1 + \frac{[I]}{\alpha K_i})} \quad \text{(Equation 2.6)}$$

Various two-site kinetic models were applied to describe substrate inhibition kinetics as well as the interactions between TAM and DHT or TAM and t-AND (Figure 2.8-2.11 and Equation 2.7-2.11). Kinetic models with two-substrate

binding sites have been successfully utilized to explain substrate inhibition kinetics (Houston and Kenworthy, 2000; Fisher et al., 2001; Schrag and Wienkers, 2001). The two-site substrate inhibition model, incorporated herein, (Figure 2.8, Equation 2.7) assumes one reaction site and sequential binding of substrate molecules (Galetin et al., 2002). Kinetic models shown in Figure 2.9(Equation 2.8) and Figure 2.10 (Equation 2.9) were used to describe the interactions between TAM and DHT. In these models, DHT (assumed to have one binding site in UGT1A4) interacts with the substrate inhibition site of TAM (assumed to have two binding sites in UGT1A4). Two kinetic models (Figure 2.11A and Equation 2.10; Figure 2.11B and Equation 2.11) were utilized to explain the effect of t-AND on TAM glucuronidation. These two models assume both t-AND and TAM have two binding sites in UGT1A4 and they compete for binding to UGT1A4 at both binding sites. In Figure 2.11A (Equation 2.10), the reaction site of t-AND overlaps with the reaction site of TAM. In Figure 2.11B (Equation 2.11), the reaction site of t-AND reaction overlaps with the substrate inhibition site of TAM. All the aforementioned two-site kinetic models assume rapid equilibrium (Segel, 1993). The kinetic parameter V_{max} equates to $k_p[E]_t$, where $[E]_t$ is the total enzyme concentration and k_p is effective catalytic rate constant . K_s, K_{DHT}, $K_{t\text{-}AND}$, K_{TAM} are binding affinity constants. Constants b and c reflect changes in k_p. Constant d reflects changes in binding affinity. Surface plots were generated by fitting various two-site models to the kinetic data. Kinetic parameters were estimated with non-linear regression. Goodness of fit was

determined by the residual sum of squares, Second-Order Akaike Information Criterion, standard errors of the parameter estimates and R^2.

$$V_0 = \frac{V_{\max} \bullet (\frac{[S]}{K_s} + \frac{b \bullet [S]^2}{K_s{}^2})}{1 + \frac{[S]}{K_s} + \frac{[S]^2}{K_s{}^2}}$$ (Equation 2.7)

$$V_0 = \frac{V_{\max} \bullet (\frac{[DHT]}{K_{DHT}} + \frac{c \bullet [TAM] \bullet [DHT]}{d \bullet K_{TAM} \bullet K_{DHT}})}{1 + \frac{[DHT]}{K_{DHT}} + \frac{[TAM]}{K_{TAM}} + \frac{[TAM]^2}{K_{TAM}{}^2} + \frac{[TAM] \bullet [DHT]}{d \bullet K_{TAM} \bullet K_{DHT}}}$$ (Equation 2.8)

$$V_0 = \frac{V_{\max} \bullet (\frac{[TAM]}{K_{TAM}} + \frac{b \bullet [TAM]^2}{K_{TAM}{}^2} + \frac{c \bullet [TAM] \bullet [DHT]}{d \bullet K_{TAM} \bullet K_{DHT}})}{1 + \frac{[DHT]}{K_{DHT}} + \frac{[TAM]}{K_{TAM}} + \frac{[TAM]^2}{K_{TAM}{}^2} + \frac{[TAM] \bullet [DHT]}{d \bullet K_{TAM} \bullet K_{DHT}}}$$ (Equation 2. 9)

$$V_0 = \frac{V_{\max} \bullet (\frac{[TAM]}{K_{TAM}} + \frac{b \bullet [TAM]^2}{K_{TAM}{}^2} + \frac{c \bullet [TAM] \bullet [t-AND]}{d \bullet K_{TAM} \bullet K_{t-AND}})}{1 + \frac{[t-AND]}{K_{t-AND}} + \frac{[t-AND]^2}{K_{t-AND}{}^2} + \frac{[TAM]}{K_{TAM}} + \frac{[TAM]^2}{K_{TAM}{}^2} + \frac{2 \bullet [TAM] \bullet [DHT]}{d \bullet K_{TAM} \bullet K_{t-AND}}}$$

(Equation 2.10)

$$V_0 = \frac{V_{\max} \bullet (\frac{[TAM]}{K_{TAM}} + \frac{b \bullet [TAM]^2}{K_{TAM}{}^2} + \frac{c \bullet [TAM] \bullet [t-AND]}{d \bullet K_{TAM} \bullet K_{t-AND}})}{1 + \frac{[t-AND]}{K_{t-AND}} + \frac{[t-AND]^2}{K_{t-AND}{}^2} + \frac{[TAM]}{K_{TAM}} + \frac{[TAM]^2}{K_{TAM}{}^2} + \frac{[TAM] \bullet [DHT]}{d \bullet K_{TAM} \bullet K_{t-AND}}}$$

(Equation 2.11)

Figure 2.8. A two-site kinetic model for substrate inhibition kinetics (Equation 2.7)

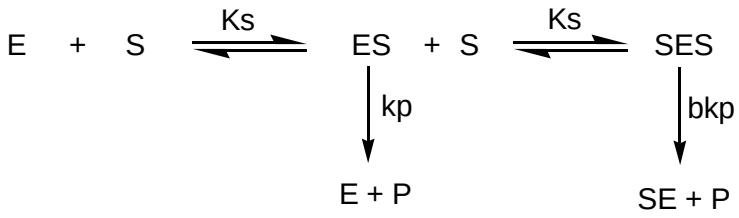

Figure 2.9. A two-site kinetic model to explain the effect of TAM on DHT glucuronidation (Equation 2.8)

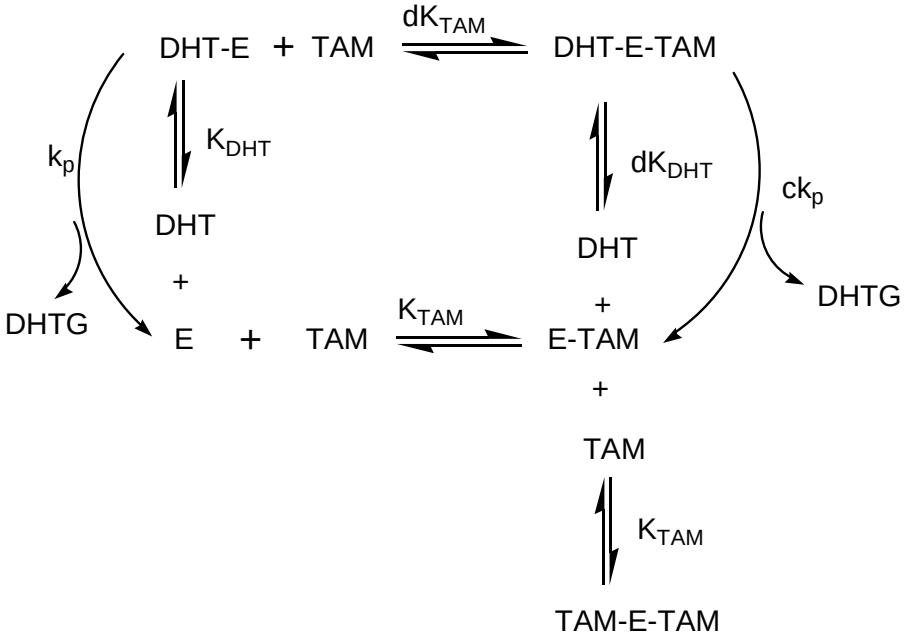

Figure 2.10. A two-site kinetic model to explain the effect of DHT on TAM glucuronidation (Equation 2.9)

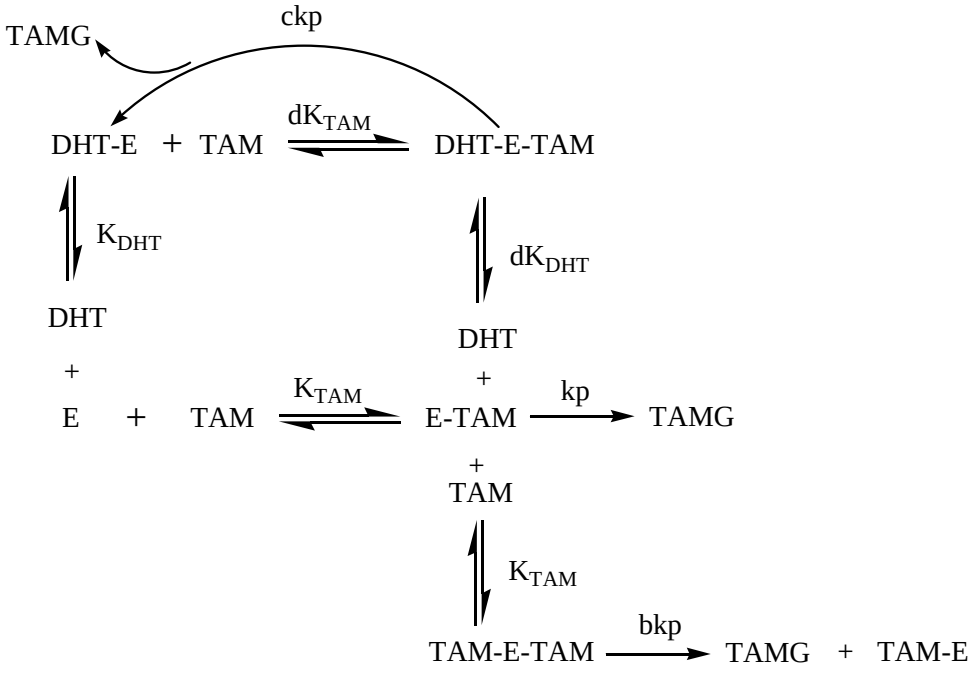

Figure 2.11. Two-site kinetic models to explain the effect of t-AND on TAM glucuronidation (Equation 2.10 and 2.11)

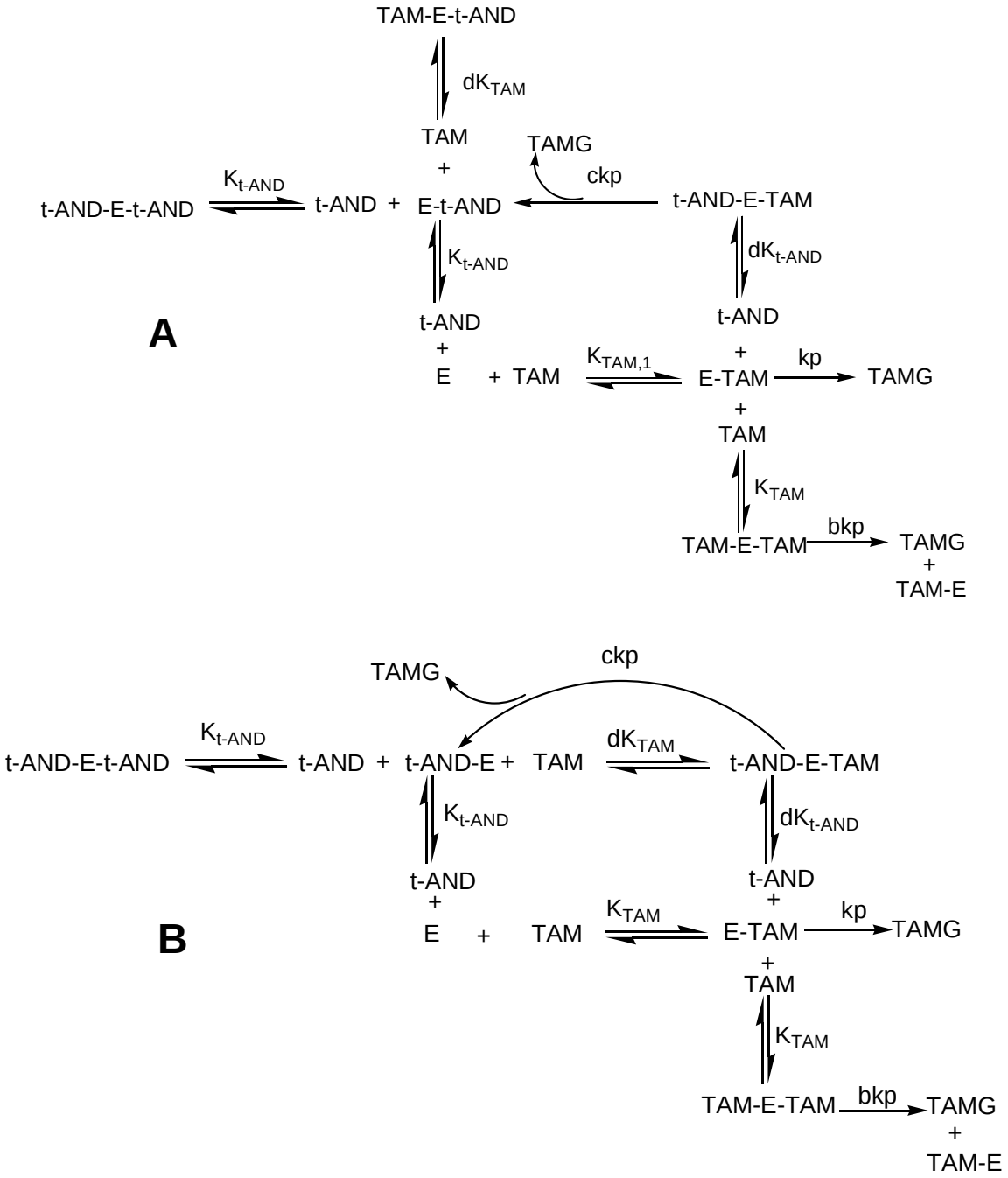

Results

Non-Specific Binding of DHT, t-AND, TAM and LTG. The estimated free fractions of DHT and t-AND were both 81.2% in incubations with 0.25 mg/ml of protein and 91.8% at a protein concentration of 0.1mg/ml of protein. The free fraction of LTG (0.25 mg/ml of protein) was estimated to be 95.2%, which is consistent with the negligible binding of LTG to HEK293 cell lysate reported by Rowland et al (Rowland et al., 2006). Since the estimated non-specific binding of DHT, t-AND and LTG under the incubation conditions employed was less than 20%, the concentration of DHT, t-AND and LTG added to the incubation mixtures was not corrected for non-specific protein binding in calculations of kinetic parameters. However, the estimated free fraction of TAM was 11.4% (0.1 mg/ml of protein) or 4.5% (0.25mg/ml of protein). TAM concentrations added to the incubation mixtures were corrected for binding when estimating kinetic parameters.

Kinetics of DHT and t-AND Glucuronidation. Initial efforts focused on conducting a detailed evaluation of the kinetics of DHT and t-AND glucuronidation. The Michaelis-Menten equation (Equation 2.2) was fit to the data for DHT glucuronidation whereas an empirical uncompetitive substrate inhibition equation (Equation 2.3) were fit to the data for t-AND glucuronidation. Results are presented in Figure 2.12 and the kinetic parameters obtained by non-linear regression are presented in Table 2.1. Though data for t-AND glucuronidation was not visually different from fits with the Michaelis-Menten equation in the Rate~[S] plot , fitting the uncompetitive substrate inhibition equation to the data

for t-AND glucuronidation generated a lower Second-Order Akaike Information Criterion (AICc) than fitting the Michaelis-Menten model to the data. (ΔAICc was 19; a value for ΔAICc greater than 10 indicates essentially no support for the unfavorable model (Collom et al., 2008)). Also, Eadie-Hofstee plots of each dataset (Figure 2.12) clearly demonstrated differences between the kinetic profiles of DHT and t-AND glucuronidation. A two-site substrate inhibition model (Figure 2.8, Equation 2.7) was also utilized to describe the data for t-AND glucuronidation. The estimated kinetic parameters with this model are presented in Table 2.2.

Table 2.1. Kinetic parameters for the glucuronidation of DHT, t-AND, TAM and LTG by recombinant UGT1A4

[a] Standard errors; [b] Not applicable

Substrate	K_m *(μM)*	V_{max} *(pmol/min/mg of protein)*	K_{si} *(μM)*	*Kinetics Model*	R^2
DHT	20 (2.2)[a]	17 (0.44)[a]	NA[b]	Michaelis-Menten (Equation 2.2)	0.94
t-AND	24 (3.1)[a]	110 (7.2)[a]	510 (130)[a]	Uncompetitive substrate inhibition (Equation 2.3)	0.98
TAM	0.90 (0.14)[a]	450 (37)[a]	4.6 (0.71)[a]	Uncompetitive substrate inhibition (Equation 2.3)	0.96
LTG	1600 (130)[a]	1100 (33)[a]	NA[b]	Michaelis-Menten (Equation 2.2)	0.99

Table 2.2. Kinetic parameters obtained by fitting various two-site models to kinetic data

[a] Standard errors; [b] Not applicable, K_{sub} and K_{mod} refer to the binding affinity of the substrate and modifier to the enzyme.

Substrate	*Modifier*	V_{max} *(pmol/min/mg of protein)*	K_{sub} *(μM)*	K_{mod} *(μM)*	*b*	*c*	*d*	Kinetic model	R^2
t-AND	without modifier	130 (19)[a]	33 (6.0)[a]	N.A.	0.56 (0.12)[a]	N.A.	N.A.	Equation 7	0.97
TAM	without modifier	630 (22)[a]	1.4 (0.12)[a]	NA[b]	0.12 (0.02)[a]	N.A.	N.A.	Equation 7	0.97
DHT	TAM	9.8 (0.45)[a]	18 (2.2)[a]	0.35 (0.020)[a]	N.A	8.4 (3.0)[a]	4.4 (2.1)[a]	Equation 8	0.99
TAM	DHT	560 (43)[a]	1.8 (0.24)[a]	58 (17)[a]	0.10 (0.04)[a]	0.52 (0.20)[a]	2.9 (1.9)[a]	Equation 9	0.97
TAM	t-AND	760 (51)[a]	1.3 (0.11)[a]	110 (21)[a]	0.18 (0.03)[a]	0.28 (0.12)[a]	1.2 (0.33)[a]	Equation 10	0.98
TAM	t-AND	760 (51)[a]	1.3 (0.11)[a]	110 (21)[a]	0.18 (0.03)[a]	0.14 (0.06)[a]	0.57 (0.17)[a]	Equation 11	0.98

<u>Figure 2.12.</u> Kinetic plots (Rate versus [S]) for DHT (A) and t-AND (B) glucuronidation by recombinant UGT1A4

The bars indicate the range of triplicate measurements. The embedded figures are Eadie-Hofstee plots for the same data. The Michaelis-Menten equation (Equation 2.2) was fit to the data for DHT glucuronidation. The uncompetitive substrate inhibition equation (Equation 2.3) was fit to the data for t-AND glucuronidation.

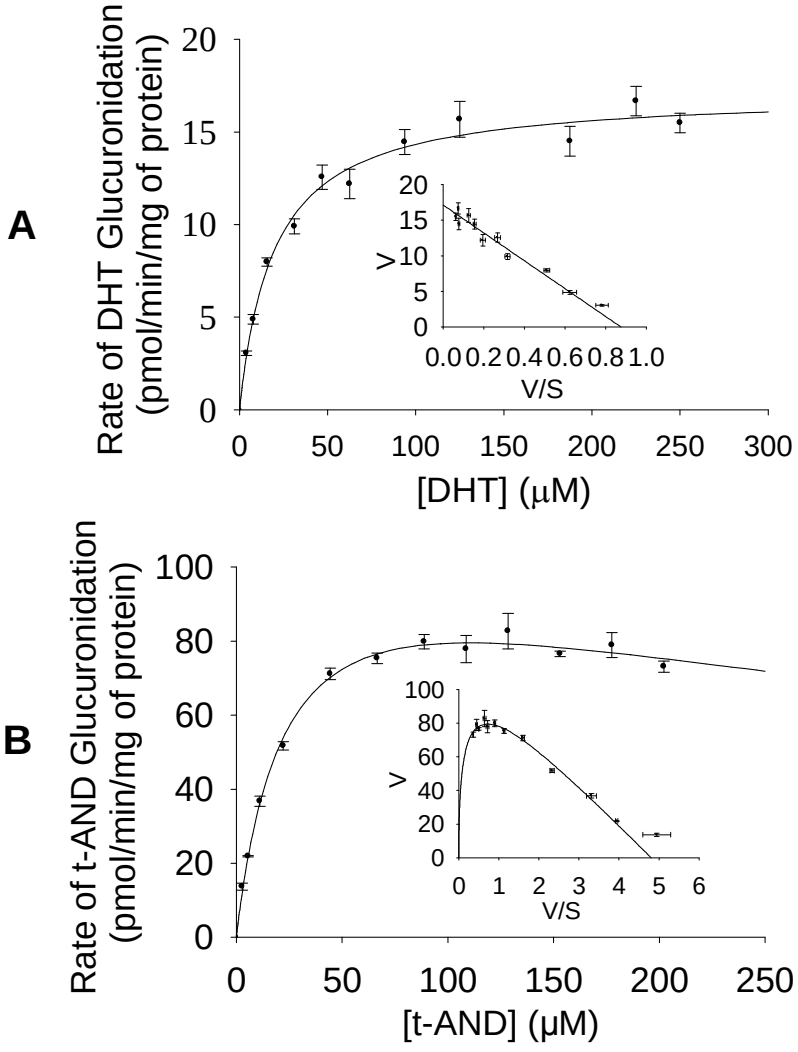

Effect of TAM on DHT and t-AND Glucuronidation. To test whether differential inhibition can be observed, DHT or t-AND, was co-incubated with a high affinity UGT1A4 substrate, TAM. TAM, a tertiary amine, forms a quaternary ammonium glucuronide upon UGT1A4-catalyzed N-glucuronidation. The reported K_m for TAM glucuronidation with recombinant UGT1A4 is 2.0 ± 0.51 µM (uncorrected for non-specific binding) (Sun et al., 2006), which was approximately 10-fold lower than the K_m values for glucuronidation of t-AND and DHT observed in the present study, suggesting that TAM may serve as a good competitive inhibitor. However, in contrast to the expected competitive inhibition, TAM caused concentration-dependent activation/ inhibition of both DHT and t-AND glucuronidation (Figure 2.13 A and 2.13 B). Notably, for DHT glucuronidation (Figure 2.13 A), the maximum velocities occurred at concentrations below the highest TAM concentration; i.e. the velocities of DHT glucuronidation initially increased but later decreased as TAM concentration was increased. In addition, the extent of activation effect increased as DHT concentration increased and the greatest activation was observed at the highest substrate concentration. Statistical comparison of DHT glucuronidation in the presence and absence of 10 µM TAM (uncorrected concentration) at 40 µM DHT indicated that the degree of activation by TAM was statistically significant (Student's t-test, $P<0.001$, $n=6$). With respect to t-AND glucuronidation (Figure 2.13 B), the activation effect of TAM was less pronounced, but similar features as described above were noted (Figure 2.13B). The velocity of t-AND glucuronidation initially increased but later

decreased with increasing TAM concentration and the extent of activation increased as t-AND concentration was increased.

<u>Figure 2.13</u>. Rate percentage of control versus [S] plots for the effect of TAM on DHT glucuronidation (A) and for the effect of TAM on t-AND glucuronidation (B)

Symbols in Figure A represent DHT concentrations: 2.5 (●), 5 (○), 10 (▼), 20 (Δ), 40 (■), 80 (□), 100 (♦). Symbols in Figure B represent DHT concentrations: 10 (●), 20(○), 40 (▼) μM. Controls refer to incubations in which the concentration of the modifier was zero.

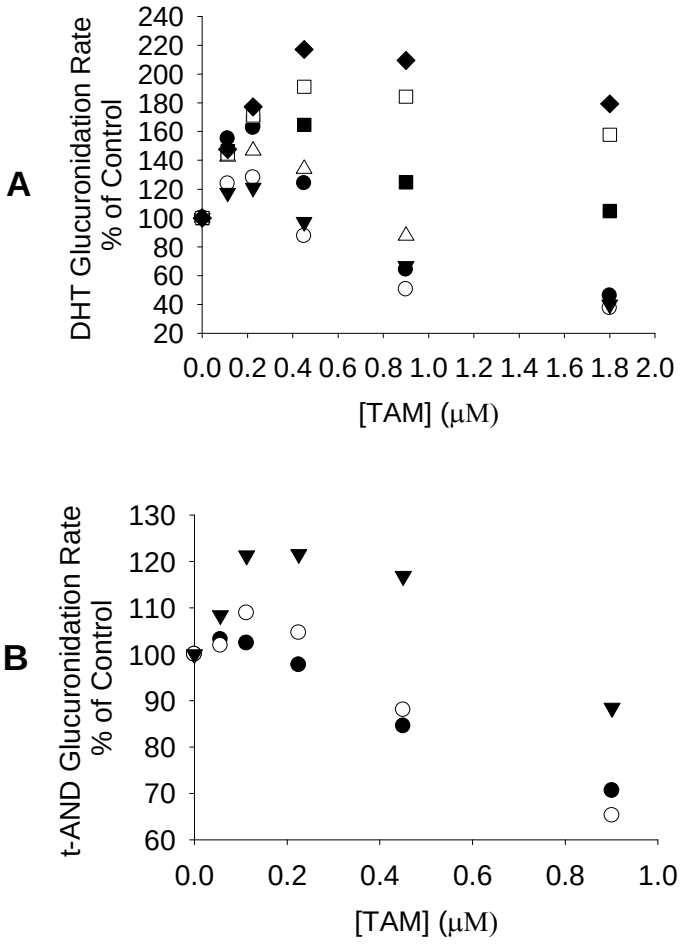

To better understand the unexpected mixed effects of TAM on DHT glucuronidation, the Michaelis-Menten model (Equation 2.2) was fit to individual kinetic data sets. The obtained kinetic parameters are shown in Table 2.3. Both K_m and V_{max} of DHT glucuronidation increased as TAM concentration was increased. Also simultaneously fitting of all kinetic data with a proposed two-site model (Figure 2.9 and Equation 2.8) was conducted and is presented in Figure 2.14. Estimated kinetic parameters are presented in Table 2.2. In the two-site model (Figure 2.9 and Equation 2.8), DHT competes with TAM for binding to the substrate inhibition site of TAM. Models in which DHT competes with TAM for binding to the reaction site of TAM were also used to describe the kinetic data but much larger standard errors of the parameter estimates and Second-Order Akeike Information Criterion were obtained.

<u>Figure 2.14.</u> Kinetic modeling for the effect of TAM on DHT glucuronidation

The surface plot was predicted with Equation 2.8 (Figure 2.9) and the TAM concentration in the plot was corrected for non-specific protein binding.

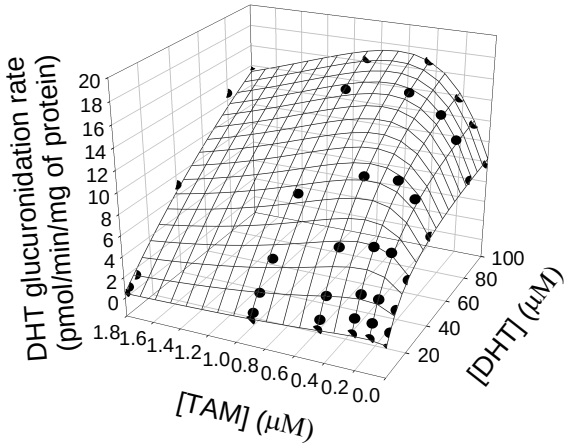

Table 2.3. Kinetic parameters for DHT glucuronidation in the presence or absence of TAM

The Michaelis-Menten equation (Equation 2) was used to fit individual kinetic data set. [a] Standard errors; CL_{int} equates to V_{max}/K_m; The TAM concentration was corrected for non-specific binding.

[TAM] (μM)	K_m (μM)	V_{max} (pmol/min/mg of protein)	CL_{int} (μl/min/mg of protein)
0	17 (1.6) [a]	9.5 (0.3) [a]	0.55
0.11	22 (2.5) [a]	15 (0.60) [a]	0.67
0.23	29 (3.3) [a]	18 (0.79) [a]	0.63
0.45	61 (4.9) [a]	27 (1.1) [a]	0.45
0.90	190 (32) [a]	47(5.7) [a]	0.25
1.80	227 (89) [a]	47 (14) [a]	0.20

Kinetics of TAM Glucuronidation. Because of the unexpected effect of TAM on DHT and t-AND glucuronidation, the kinetics of TAM glucuronidation with recombinant UGT1A4 were evaluated. TAM glucuronidation exhibited substrate inhibition kinetics (Figure 2.15). Both the uncompetitive substrate inhibition model (Equation 2.3) and a two-site model (Equation 2.8) were fit to the kinetic data. The derived kinetic parameters are presented in Table 2.1 and 2.2 respectively. A constant free fraction of 11.4% for TAM was assumed in calculations of the kinetic parameters.

<u>Figure 2.15.</u> Kinetic plots (Rate versus [S]) for TAM glucuronidation by recombinant UGT1A4

The bars indicate the range of triplicate measurements. The embedded figures are Eadie-Hofstee plots for the same data. A two-site model (Figure 2.8 and Equation 2.7) was fit to the data.

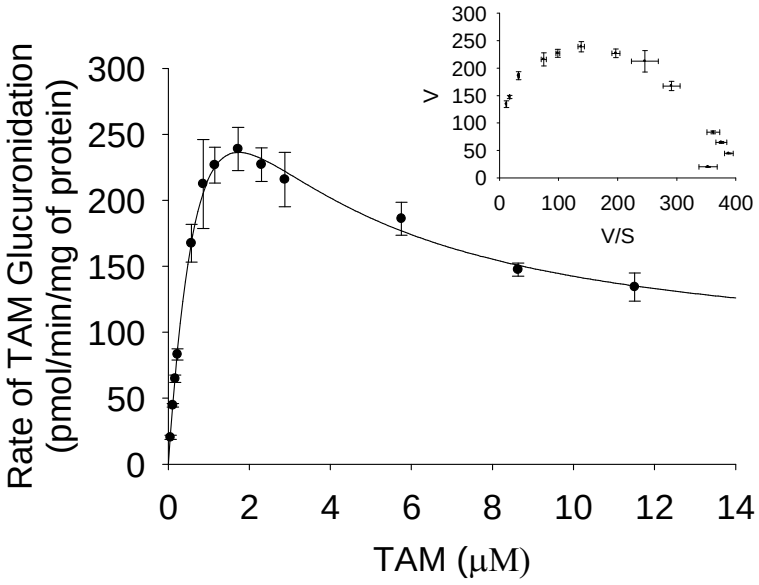

Effect of LTG on DHT and t-AND Glucuronidation. Another amine substrate of UGT1A4, LTG, was also evaluated as a modifier of DHT and t-AND glucuronidation. LTG also forms a quaternary ammonium glucuronide upon UGT1A4-catalyzed-N-glucuronidation. Initially, the kinetics of LTG glucuronidation were evaluated alone. LTG glucuronidation exhibited a hyperbolic kinetic profile (Figure 2.16) with an estimated K_m of 1.6 ± 0.13 mM (Table 1). LTG at concentrations ranging from ~0.25 Km to ~3 Km inhibited DHT and t-AND glucuronidation (Figure 2.17A and 2.17B). Single-site competitive, noncompetitive and mixed inhibition models were evaluated to describe the inhibition data. The noncompetitive inhibition model was associated with the lowest AICc values in both cases. The model-predicted lines and observed data are shown in Dixon plots (Figure 2.18A and 2.18B). The derived K_i were 3.25 ± 0.26 mM and 2.16 ± 0.24 mM for DHT and t-AND glucuronidation respectively.

<u>Figure 2.16.</u> Kinetic plots (Rate versus [S]) for LTG glucuronidation by recombinant UGT1A4

The bars indicate the range of duplicate measurements. The embedded figures are Eadie-Hofstee plots for the same data. Michaelis-Menten model (Equation 2.2) was fit to the data.

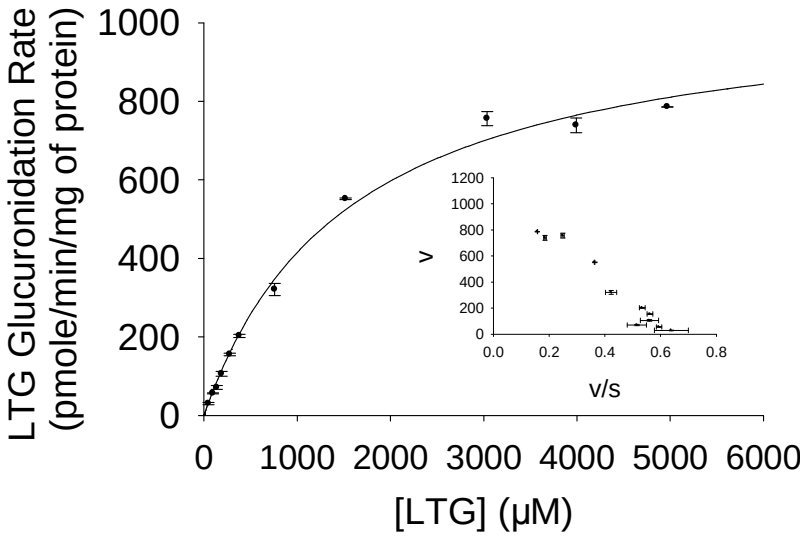

<u>Figure 2.17.</u> Rate percentage of control versus [S] plots for the effect of LTG on DHT glucuronidation (A) and for the effect of LTG on t-AND glucuronidation (B)

Data points are means of duplicate measurements. Coefficients of variation are all within 10%. Symbols represent DHT and t-AND concentrations: 10 (●), 20(○), 40 (▼) µM. TAM concentration in the plots was corrected for non-specific protein binding. Controls refer to incubations in which the concentration of the modifier was zero.

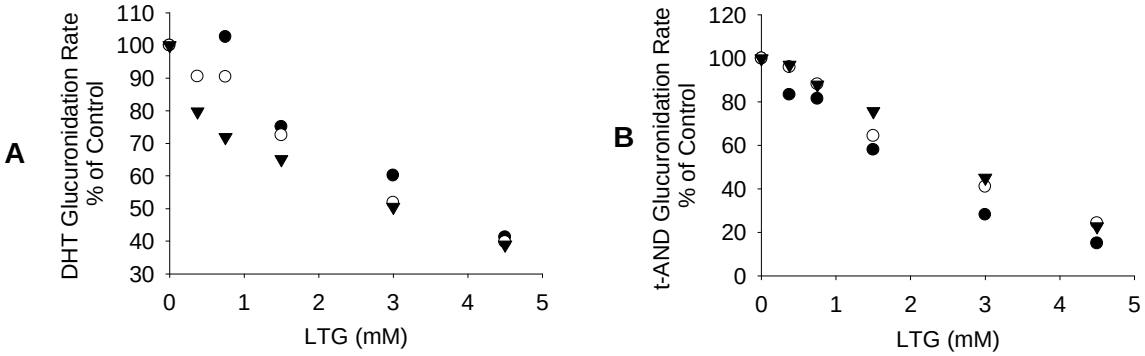

<u>Figure 2.18.</u> Dixon plots for inhibition of DHT glucuronidation by LTG (A) and for inhibition of t-AND glucuronidation by LTG (B)

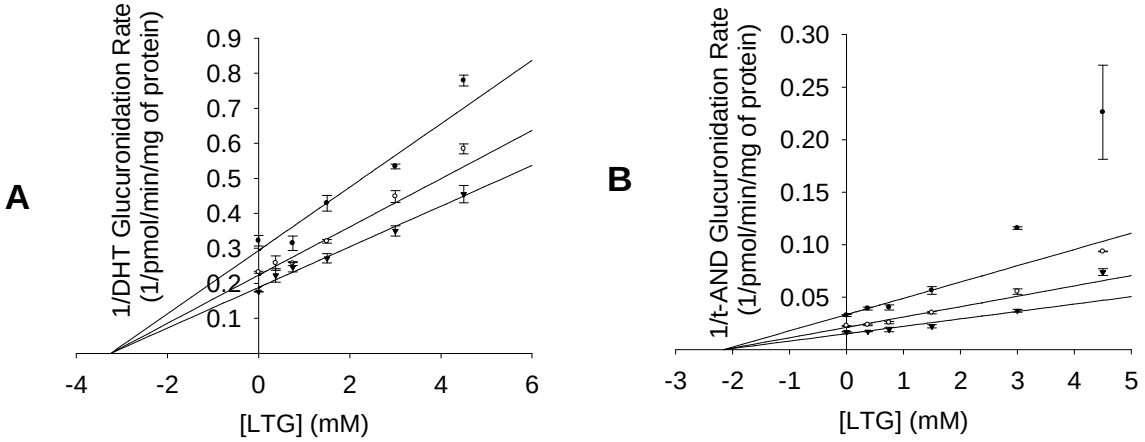

Effects of TAM on LTG glucuronidation. To investigate whether TAM can activate UGT1A4 with substrates not based on the steroidal ring structure, we also studied the effect of TAM on LTG glucuronidation. At all TAM concentrations tested in the present study, LTG glucuronidation was inhibited (Figure 2.19A). A one-site competitive inhibition model was best fit to the inhibition data (Figure 2.19B). The K_i for this interaction was 0.31µM (TAM concentration was corrected for non-specific protein binding).

<u>Figure 2.19.</u> Rate percentage of control versus [S] plots (A) and Dixon plot for the effect of TAM on LTG glucuronidation

Symbols in A represent LTG concentrations: 0.75 (●), 1.5(○), 3.0(▼) mM. TAM concentration in the plots was corrected for non-specific protein binding. Controls refer to incubations in which the concentration of the modifier was zero.

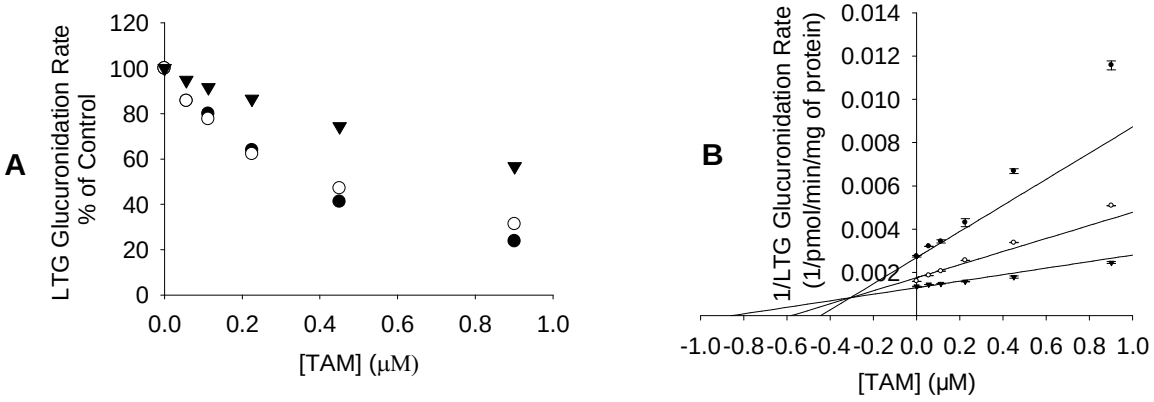

Effects of DHT and t-AND on TAM glucuronidation. Finally, the effects of DHT and t-AND on TAM glucuronidation were evaluated to assess whether the activation effects were bi-directional. Both t-AND and DHT inhibited TAM glucuronidation in a preliminary study. To gain further insight into the interactions of DHT and t-AND on TAM glucuronidation, the kinetics of TAM glucuronidation were evaluated in the presence of six concentrations of DHT or t-AND. A two-site substrate inhibition model (Equation 2.8) was applied to fit the individual kinetic data sets. Although there were no clear trends of changes in the predicted kinetic parameters as DHT or t-AND concentration increased, the substrate inhibition kinetic profile of TAM glucuronidation became more hyperbolic (Figure 2.20). Various two-site models were tested to simultaneously fit the kinetic data. The derived kinetic parameters are presented in Table 2.2. Kinetic model in Figure 2.10 (Equation 2.9) adequately described the effect of DHT on TAM glucuronidation and the fit of the data is presented in Figure 2.21A. For TAM glucuronidation kinetics in the presence of t-AND, two kinetic models (Figure 2.11A and Equation 2.10; Figure 2.11B and Equation 2.11) were applied to describe the kinetic data and similar goodness of fit was obtained. The fit of data to Equation 2.11 (Figure 2.11B) is illustrated in Figure 2.21B.

Figure 2.20. Kinetic plots (Rate versus [S]) for TAM glucuronidation by recombinant UGT1A4 in the presence of 250 μM of DHT (A) or 250μM of t-AND (B)

The embedded figures are Eadie-Hofstee plots for the same data. TAM concentration was corrected for non-specific protein binding

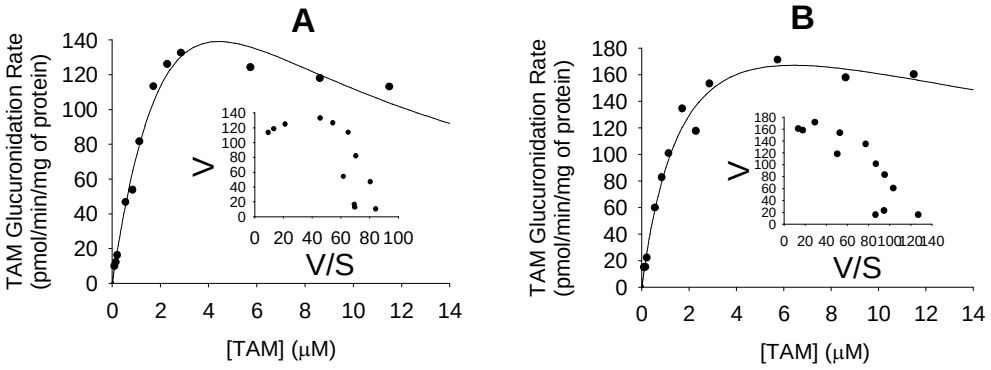

Figure 2.21. Kinetic modeling for effect of DHT (A) and t-AND (B) on TAM glucuronidation

The surface plot in Figure A is a predicted result with Equation 2.10 (Figure 2.9) and the surface plot in Figure B is a predicted result with Equation 2.11 (Figure 2.11B). The TAM concentration was corrected for non-specific protein binding.

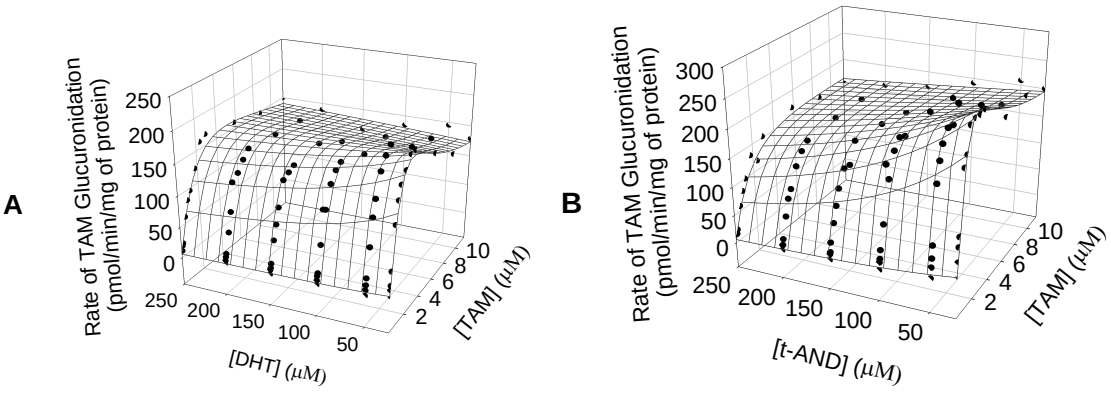

Discussion

In this part of the study, DHT and t-AND (more commonly known as epiandrosterone) were used as probe substrates to evaluate the potential existence of multiple aglycone substrate binding sites in UGT1A4. Glucuronidation of DHT and t-AND by HEK293-expressed UGT1A4 was evaluated in the presence of another UGT1A4 substrate, TAM or LTG. Unexpectedly, neither TAM nor LTG competitively inhibited DHT and t-AND glucuronidation. Noncompetitive inhibition was observed when LTG was used as the modifier, whereas concentration-dependent activation/ inhibition was observed with TAM as the modifier. These results, combined with kinetic modeling using various two-site models, suggest that multiple substrate binding sites exist in UGT1A4.

The glucuronidation kinetics of the four UGT1A4 substrates under investigation were carefully characterized. DHT and LTG exhibited hyperbolic kinetics, whereas t-AND and TAM displayed substrate inhibition kinetics. Although previous studies reported hyperbolic kinetics for TAM glucuronidation by UGT1A4 (Kaku et al., 2004; Sun et al., 2006), there are possible explanations for this discrepancy. In one report, a narrow TAM concentration range (1-6 µM, uncorrected for non-specific binding) was employed, potentially precluding the observation of substrate inhibition at higher TAM concentrations (Sun et al., 2006). In the second case, a one-hour incubation was conducted (Kaku et al., 2004), suggesting that linear incubation conditions may not have been operational. Our preliminary studies to determine linearity with incubation time

and protein concentration for TAM glucuronidation indicated that a low protein concentration and short incubation time were required to maintain steady state conditions.

In the present study, TAM and t-AND substrate inhibition were described with a two-site model, as depicted in Figure 2.7 (Equation 2.7). In both cases, the estimated b values were less than 1, indicating that the SES complex is less productive than the ES complex. Also, consistent with the more pronounced substrate inhibition of TAM glucuronidation, the estimated b value for TAM glucuronidation is smaller than the b value obtained for t-AND glucuronidation.

For UGT-catalyzed glucuronidation, substrate inhibition kinetics can also be explained by the aglycone substrate binding to the enzyme-UDP complex, resulting in a non-productive dead-end complex (Luukkanen et al., 2005). However, such mechanism where only one aglycone substrate binding site is incorporated inadequately explain the activation effect of TAM on DHT and t-AND glucuronidation. UDP, a product of catalysis, has been reported to be an inhibitor for UGT1A4 (IC_{50}=31μM) (Fujiwara et al., 2008). It is also possible that the observed substrate inhibition is due to the increased amount of UDP formation at high substrate concentrations. However, the calculated maximum UDP concentration was ~0.5 μM in our study. Thus, the inhibition of UGT1A4 by UDP should be negligible under the incubation conditions used herein.

A few cases of heteroactivation have been reported with UGTs (Williams et al., 2002; Mano et al., 2004; Pfeiffer et al., 2005; Mano et al., 2007; Uchaipichat et al., 2008; Hyland et al., 2009). Interestingly, in the present study TAM both

activated and inhibited DHT glucuronidation in a concentration-dependent fashion. A two-site kinetic model (Figure 2.8, Equation 2.8) which considers the kinetic properties of DHT and TAM adequately explained the effect of TAM on DHT glucuronidation. In this model, the overall effect of TAM is controlled by three enzyme-associated complexes (E-TAM, TAM-E-TAM, and TAM-E-DHT). Complexes E-TAM and TAM-E-TAM are not productive. The presence of these complexes results in less enzyme available for association with the substrate (DHT), producing an inhibition effect. However, the DHT-E-TAM complex is more productive than the DHT-E complex (c=8.36). The presence of the DHT-E-TAM complex leads to activation. At low TAM concentrations, the activation resulting from the presence of the DHT-E-TAM complex overcomes the inhibition effect, resulting in an overall activation effect. At high TAM concentrations, the TAM-E-TAM complex becomes the dominant form for TAM associating with the enzyme, resulting in an overall inhibition effect. Also interestingly, in contrast to most previous reports of enzyme heteroactivation, where the extent of heteroactivation decreases as the substrate concentration increases (Hutzler et al., 2001; Kenworthy et al., 2001; Hutzler et al., 2002; Uchaipichat et al., 2008), DHT glucuronidation is increasingly heteroactivated by TAM as the substrate (DHT) concentration was increased. This discrepancy is likely due to different mechanisms of heteroactivation. In previous cases, heteroactivation was largely due to the positive cooperative binding of substrates and modifiers to the enzyme (Hutzler et al., 2001; Kenworthy et al., 2001; Hutzler et al., 2002; Uchaipichat et al., 2008). However, in the present study, the increased glucuronidation

appeared to be due to the presence of a more productive modifier-E-substrate complex (DHT-E-TAM) (c=8.36). The percentage of the DHT-E-TAM complex among all enzyme complexes is greater at high substrate concentrations than at low substrate concentrations and therefore more activation was observed at high substrate concentrations.

Assuming the same binding scenario as in Figure 2.8 (Equation 2.8), kinetic model in Figure 2.9 (Equation 2.9) adequately explained the effect of DHT on TAM glucuronidation. But in this case, the predicted c value is less than 1, indicating the DHT-E-TAM complex is less productive than the E-TAM complex, consistent with the observed inhibition effect of DHT on TAM glucuronidation. In addition, in this model TAM substrate inhibition kinetics would be eliminated as DHT-E-TAM becomes the dominant productive complex, also consistent with our observation that the substrate inhibition kinetic profile of TAM glucuronidation became more hyperbolic as DHT concentration was increased.

Albeit modest activation, TAM exhibits the same effect on t-AND glucuronidation as on DHT glucuronidation: concentration-dependent activation/inhibition and greater activation at higher substrate concentrations. However, the kinetic model in Figure 2.9 (Equation 2.9) may not adequately explain the interactions of TAM on t-AND glucuronidation due to the substrate inhibition kinetics of t-AND (two t-AND binding sites). Kinetic models in which t-AND and TAM both have two binding sites on UGT1A4 may be applicable. Kinetic modeling with more data points than obtained in Figure 2.12B needed to adequately characterize the effect of TAM on t-AND glucuronidation.

Kinetic studies to characterize the effect t-AND on TAM glucuronidation was carefully conducted. Two kinetic models (Figure 2.10A and Equation 10; Figure 2.10B and Equation 11) in which the two binding sites of t-AND overlap with the two binding sites of TAM adequately explained the kinetic data. Again the predicted c values (less than 1) are consistent with the inhibition effect of t-AND on TAM glucuronidation and TAM substrate inhibition kinetics being eliminated as the less productive t-AND-E-TAM complex becomes the dominant productive complex in the models is consistent with our observation.

The unexpected heteroactivation on DHT and t-AND glucuronidation by TAM led us to investigate the effect of TAM on UGT1A4 activity with a different type of UGT1A4 substrate: LTG (an aromatic amine substrate of UGT1A4). In contrast to the concentration-dependent activation/inhibition on DHT and t-AND glucuronidation, LTG N-glucuronidation was competitively inhibited by TAM, suggesting that the heteroactivation of UGT1A4-catalyzed glucuronidation by TAM is substrate-dependent.

LTG was also evaluated as a modifier on DHT and t-AND glucuronidation. LTG inhibited both t-AND and DHT glucuronidation, but interestingly the one-site noncompetitive inhibition model (Equation 2.5) better described the kinetic data than the one-site competitive inhibition model (Equation 2.4). The observed noncompetitive inhibition of DHT glucuronidation by LTG suggests that these two UGT1A4 substrates have distinct binding sites within the active site of UGT1A4, assuming each has only one binding site.

The present study provides compelling evidence for the existence of at least two aglycone binding sites in UGT1A4. Though models can be developed to describe the kinetic data, additional biophysical/ biochemical studies are needed to delineate the specific binding region(s) of each molecule in UGT1A4. Additional kinetic studies with a wider range of UGT1A4 substrates are also needed to evaluate the range of substrates for which atypical kinetics are operable. UGT1A4 has been reported to form homodimers (Operana and Tukey, 2007), which may also play a role in these atypical kinetic phenomena. It is yet to be determined whether the two aglycone binding sites exist in different monomers or whether each monomer has two separate aglycone binding sites.

In vitro-in vivo extrapolations for UGT-catalyzed metabolism have proven problematic for a number of reasons, including inability to estimate in vivo UGT enzyme amounts, lack of isoform-specific probe substrates and inhibitors, overlapping substrate specificities (Miners et al., 2004; Miners et al., 2006) and “albumin effect”(Rowland et al., 2008). Accumulating evidence from the current study and others referenced above suggests that atypical kinetics involving this enzyme family may also contribute to the difficulty in making in vitro-in vivo correlations. Atypical kinetic profiles, such as the substrate inhibition observed in the present study, complicate the estimation of intrinsic clearance. Additionally, the presence of multiple aglycone binding sites and the substrate-dependent heteroactivation as observed in the present study, complicate the prediction of drug interactions. In summary, the present study reinforces the need for careful characterization of UGT1A4 kinetics and highlights the caveats of making in vitro-

in vivo correlations with this important metabolizing enzyme. For the purpose of screening for UGT1A4 inhibitors, the present study suggests the potential need to employ multiple probe substrates.

Part II: Function Analysis of UGT1A4.2 and UGT1A4.3 in Comparison with UGT1A4.1 on Dihydrotestosterone, Trans-Androsterone, and Tomoxifen Glucuronidation

Background

Single nucleotide polymorphisms (SNPs) commonly exist in UGT genes. To date, SNPs have been identified in the following UGT genes, including UGT1A1, UGT1A3, UGT1A4, UGT1A5, UGT1A6, UGT1A7, UGT1A8, UGT1A9, UGT1A10, UGT2B4, UGT2B7, UGT2B10, UGT2B15, UGT2B17, and UGT2B28 (Bock et al., Date Accessed: July 2010). Genetic polymorphisms in UGTs have shown to significantly affect the disposition of pharmacologically active compounds by changing the expression levels or activities of individual UGTs (Guillemette, 2003). For instance, several SNPs in UGT1A1 are linked to decreased bilirubin glucuronidation, which may result in different levels of unconjugated hyperbilirubinemia(Strassburg, 2008). SNPs in UGT1A1 are also associated with increased irinotecan toxicity as the glucuonidation of its active metabolite is reduced (Marcuello et al., 2004; Onoue et al., 2009). Thus, it is important to assess the effect of UGT genetic polymorphisms both *in vitro* and *in vivo*.

More than 100 SNPs have been identified in UGT1A4 gene (Bock et al., Date Accessed: July 2010). Among them, fourteen SNPs lead to amino acid changes: Arg3Thr, Gln6Arg, Arg11Trp, Pro24Thr, Leu48Val, Glu50Asp, His56Gln, His68Tyr, Arg91Cys, Arg109Gly, Leu132Pro, Ile176Phe, Ser250Asn, and Ile276Leu.(Bock et al., Date Accessed: July 2010) The two nonsynonymous SNPs investigated in the present study: UGT1A4*2 (70C>A, P24T) and

UGT1A4*3 (142T>G, L48V), were both identified in 2003 by two groups at approximately the same time (Ehmer et al., 2004; Wiener et al., 2004b). In Caucasians, the allelic frequencies of UGT1A4*2 and UGT1A4*3 are in the range of 6%-8% and 2.6%-9% respectively (Ehmer et al., 2004; Wiener et al., 2004b; Benoit-Biancamano et al., 2009). In Japanese populations, the allelic frequency of UGT1A4*3 was 16.5% or 12.9%, whereas UGT1A4*2 was not identified (Mori et al., 2005; Saeki et al., 2005).

Function analysis of these two variants has been conducted by several groups since their identification (Ehmer et al., 2004; Wiener et al., 2004a; Mori et al., 2005; Sun et al., 2006; Benoit-Biancamano et al., 2009) and the results of one of the studies particularly attracted our attention (Ehmer et al., 2004). In this study, the author evaluated the function of the two polymorphic enzymes against two steroids (dihydotesosterone and trans-androsterone) and two amines (benzidine and β-naphthylamine). They found that UGT1A4.3 almost completely lost its activity against the two steroids, however retained more than 50% of its activity against the two amine substrates. Contrarily, UGT1A4.2 retained more than 50% of the activity against the two steroids, but had markedly decreased activity on the two amine substrates (Ehmer et al., 2004). Their results indicated that the effects of these two polymorphisms may be dependent on the type of the substrate (steroids or amines) since similar effects were observed with the same type of compounds. In addition, dihydrotesosterone is the most potent endogenous androgen (Belanger et al., 2003).The fact that UGT1A4.3 completely lost its activity on dihydrotestosterone glucuronidation may potentially

have physiological consequences. However, the method they used to measure the enzyme activity (quanfication of glucuronide formation) was an insensitive TLC method and the activities of the three UGT1A4 enzymes were compared only at one substrate concentration (Ehmer et al., 2004), which may potentially lead to inaccurate estimation. In addition, their results that the two polymorphic enzymes showed decreased activities against all the four substrates evaluated didn't agree with the results reported by others (Wiener et al., 2004a; Mori et al., 2005; Sun et al., 2006). Wiener et al observed that microsomes from UGT1A4*2/*2 carriers exhibited higher activity on NNAL glucuronidation compared to the wild type carriers ($p<0.05$) (Wiener et al., 2004a). Mori et al reported that the cloned expressed UGT1A4.3 had increased intrinsic clearance against clozapine, trans-androsterone, imipramine, and cyprohepadine (Mori et al., 2005). Sun et al also reported that the cloned expressed UGT1A4.3 had higher CL_{int} on trans-OH-tamoxifen and cis-OH-tamoxifen glucuronidation compared to the wild type enzyme (Sun et al., 2006).

To better understand the function of the two polymorphic enzymes, previously our lab conducted detailed kinetic study on lamotrigine glucuronidation with recombinant UGT1A4.1, UGT1A4.2, and UGT1A4.3 (expressed in HEK293 cells). The CL_{int}s obtained with UGT1A4.2 and UGT1A4.3 were both about 50% of the CL_{int} obtained with wild type enzyme (Argikar, 2006). To further evaluate the function of the two polymorphic enzymes, in this part of the study we conducted detailed kinetic experiments with three additional UGT1A4 substrates: dihydrotestosterone, trans-androsterone and tamoxifen. The kinetic parameters

obtained with the two variants were compared with the kinetic parameters obtained in Part I with the wild type enzyme. In addition, in our previous study, we observed activation of DHT glucuronidation by tamoxifen with wild type UGT1A4. Because heteroactivation is a rare phenomenon for UGTs, in this part of the study, we also evaluated the effect of these two polymorphisms on the activation of DHT glucuronidation by tamoxifen.

Materials and Methods

Materials. All chemicals employed in the present study are the same as in Part I. Recombinant UGT1A4.2 and UGT1A4.3 were also produced in HEK293 cells (Gifts from Dr. Philips Larzarus at Pennsylvania State University). Cell lysate prepared with the same procedures as in Part I was added directly as the enzyme source for all the experiment conducted in this part of the study. Cell culture procedures were mentioned in detail in Part I.

Incubation Conditions. Incubation conditions for DHT, t-AND and TAM glucuronidation with the two variants were the same as previously described. To evaluate the effect of TAM on DHT glucuronidation with the two variants, 10µM or 100µM DHT were incubated with 10µM TAM.

Quantification of Glucuronides. Quantification of DHT, t-AND and TAM glucuronide was completed with LC-MS methods. The description of each method was mentioned with detail in Part I.

Western Blot Analysis.

HEK293 cell lysate (with or without UGT1A4) was diluted to 2 mg/ml with distilled water. 20 µl of each diluted cell lysate were mixed with 6 µl sample reducing agent (Invitrogen, NP0009, Carlsbad, CA) and 4 µl sample loading buffer (Invitrogen, NP0007, Carlsbad, CA). The resulting mixtures were boiled at 100^0C for 5 minutes and 5 µl of the resulting mixtures were loaded onto a 12% SDS-PAGE gel. Gel electrophoresis was then conducted at 150V for 2 hrs. The proteins were transferred onto a PVDF membrane (Millipore IPVH00010,

Billerica, MA) at 30V for 2 hours. The membranes were then blocked with 5% nonfat dry milk in TBS buffer (20mM Tris-base, 140mM NaCl, pH=7.6) containing 1% Tween 20 for 3 hours and were subsequently probed overnight with a rabbit polyclonal anti-UGT1A antibody in a 1:200 dilution (H-300, Santa Cruz Biotechnology, INC., Santa Cruz, CA) for UGT1A4 or a Monoclonal mouse Anti-β-Actin antibody (Sigma-Aldrich, St. Louis, MO) for the β-actin in 1:10,000 dilution. The bound antibodies were detected with anti-rabbit or anti-mouse peroxidase-coupled secondary antibodies (Santa Cruz Biotechnology, INC. Santa Cruz, CA) followed by detection using the Supersignal chemiluminescence system from Pierce (PI34080, Rockford, IL).

Data Analysis. Two-tailed Student *t* test was used to compare the kinetic parameters obtained with UGT1A4.2 or UGT1A4.3 against those obtained with the wild type UGT1A4. Estimation of kinetic parameters was as previously described.

Results

As shown in Figure 2.22, the expression levels of UGT1A4.2 and UGT1A4.3 in HEK293 cells were approximately 75% and 90% of the expression level for the wild type UGT1A4. These results were very close to the results reported by Sun and co-worker (the group, from which we obtained the UGT1A4-HEK293 cell lines)(Sun et al., 2006). The similar expression levels of the three UGT1A4s in HEK293 cells may indicate that the protein stability was not affected by the amino acid changes in codon 24 and codon 48.

Figure 2.22. Western blot analysis of UGT1A4 protein with anti-UGT1A antibody

The amount of UGT1A4 protein was normalized with the levels of actins in each lane and was quantified as densitometry relative. Blank HEK293 cell lysate was loaded on lane 4 as negative control. The relative ratios between the densitometry relative of the wild type lane and that of the UGT1A4.2 or UGT1A4.3 lane were calculated and the numbers were used to normalize the glucuronidation rates obtained when the variant-HEK 293 cell lysates were used as enzyme sources.

Relative ratios: 1.00 0.745 0.899

For all three substrates evaluated in the present study, the kinetic profiles obtained with the two variant enzymes were the same as with the wild type enzyme (Figure 2.23). For DHT glucuronidation, Michaelis-Menten kinetic profiles were observed with all three UGT1A4 enzymes, whearas for t-AND and TAM glucuronidation, substrate inhibition kinetic profiles were observed.

Figure 2.23. Rate versus [S] plots for DHT, t-AND and TAM glucuronidation with UGT1A4.1 (●), UGT1A4.2 (■) and UGT1A4.3 (○)

The bars indicate the range of triplicate measurements. The solid lines were generated b fitting Michaelis-menten equation (DHT) or uncompetitive substrate inhibition equation (t-AND and TAM) to kinetic data.

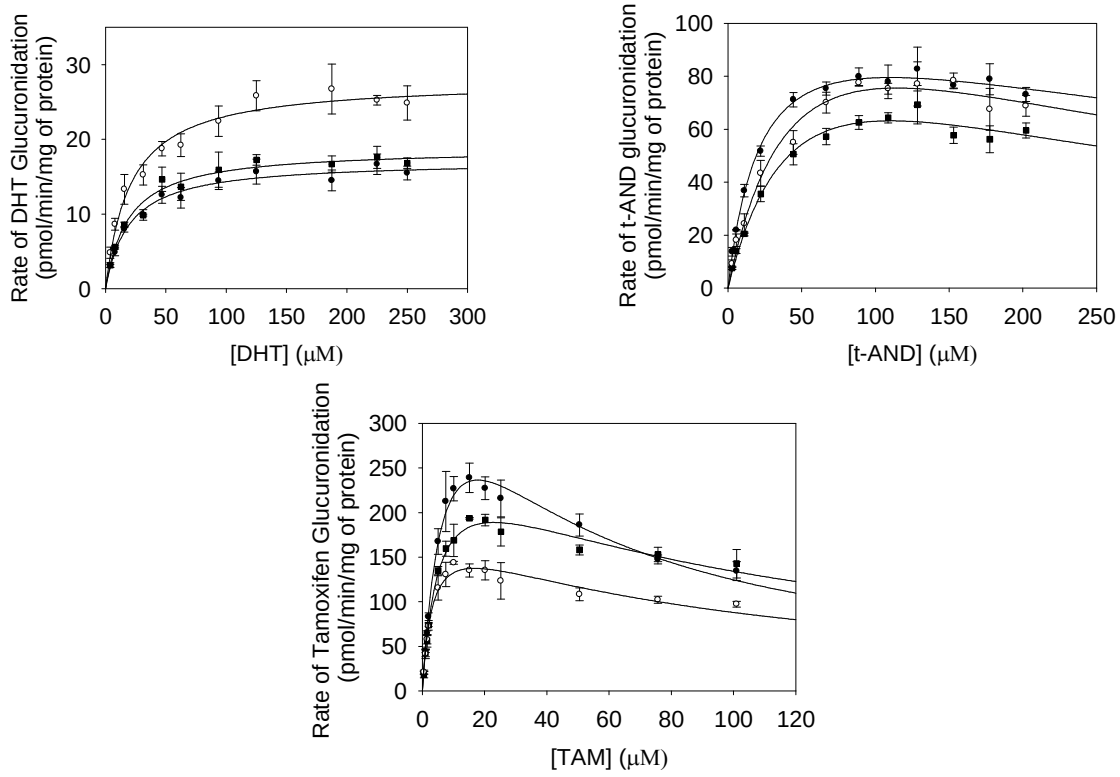

The kinetic parameters by fitting the Michaelis-Menten equation (Equation 2.1) or the uncompetitive substrate inhibition equation (Equation 2.2) to the

corresponding kinetic data are presented in Table 2.4. For DHT glucuronidation, P24T variant had very similar CL_{int} as compared with the wild type UGT1A4. Both K_m and V_{max} obtained with this variant are close to the values obtained with the wild type UGT1A4. L48V variant on the other hand exhibited significantly higher CL_{int} (~1.5-fold) on DHT glucuronidation compared to the wild type enzyme. The increased CL_{int} with L48V variant was due to a statistically significant increase in V_{max}, whereas the K_m obtained with this variant was close to the K_m obtained with the wild type enzyme. For t-AND glucuronidation, both variant showed significantly lower CL_{int} compared to the wild type UGT1A4. The calculated CL_{int} on t-AND glucuronidation with the two variants were about 50% of CL_{int} obtained with the wild type UGT1A4. In both cases, the decreased CL_{int}s were results of significant increases in K_m (~2-fold). A modest but significant increase in V_{max} and a significant decrease in K_{si} were also observed with L48V variant. For TAM glucuronidation, both P24T and L48V mutations resulted in significant decreases in K_m and V_{max}. However, because these two kinetic parameters were decreased to the same extent, the CL_{int} obtained with the two variants were close to the CL_{int} obtained with the wild type UGT1A4. In addition, the K_{si} obtained with the variants were significantly higher than the K_{si} of the wild type enzyme.

Table 2.4. Kinetic parameters for DHT, t-AND and TAM glucuronidation with UGT1A4.1, UGT1A4.2 or UGT1A4.3

Data are presented as the mean ± standard deviation for three replicates. Values that are significantly different from the wild type are labeled with *(P<0.05), ** (p<0.005), and *** (p<0.001). CL_{int} was calculated as V_{max}/K_m with the mean of the V_{max} and K_m

Substrate (Kinetic Model)	Enzyme	V_{max}	K_m	CL_{int}	K_{si}
DHT (Michaelis-Menten)	WT	17± 0.91	20± 2.4	0.88± 0.065	N. A.
	P24T	19±0.75	20±4.4	1.0± 0.17	N. A.
	L48V	**28±2.3	21±4.5	*1.4± 0.17	N. A.
t-AND (Uncompetitive substrate inhibition)	WT	110±11	24 ±3.5	4.8± 0.27	540±180
	P24T	130±22	*57±13v	***2.3± 0.15	230±91
	L48V	*150±12	**55±6.9	***2.7 ± 0.22	*240±25
TAM (Uncompetitive substrate inhibition)	WT	450 ±62	7.9±0.57	57 ± 3.9	40 ±8.1
	P24T	*280±5.7	**5.3±0.40	53± 4.7	*100±12
	L48V	**190 ±15	***3.2±0.45	60± 7.2	*89±5.1

In this part of the study, we also investigated the interaction of TAM on DHT glucuronidation with the two variants. In our previous study, we observed that TAM activated both DHT and t-AND glucuronidation with the wild type UGT1A4 (Figure 2.13). Because the activation effect of TAM on DHT glucuronidation was much higher than on t-AND glucuronidation, previously we also conducted a detailed kinetic study to further characterize the interaction of TAM on DHT glucuronidation with the wild type UGT1A4 (Figure 2.14). As discussed in part I, with the wild type UGT1A4, TAM activated DHT glucuronidation in a concentration-dependent fashion: higher activation effect was observed as the substrate (DHT) concentration was increased. This property differs from most activation effects observed with CYPs (Hutzler et al., 2001; Kenworthy et al., 2001) and was explained with a two–site kinetic model (Figure 2.9, Equation 2.8). It is interesting to find out whether we can still observe the same activation effect of TAM on DHT glucuronidation with the two polymorphic enzymes. Based on the results in Figure 2.13A, the experiment was conducted with two DHT concentrations (10 and 100µM) and 10 µM TAM. As shown in Figure 2.24, for the wild type enzyme, in the presence of 10 µM TAM, DHT glucuronidation rate was increased by ~2-fold at 100µM DHT, but at a lower DHT concentration (10µM), DHT glucuronidation rate wasn't affected by 10µM TAM. The extent of the activation with wild type enzyme was very close to the results obtained in our previous study (Figure 2.13A). For the two polymorphic enzymes, activation effect was observed at both DHT concentrations. But same as the wild type UGT1A4, the observed activation effects were higher at higher DHT

concentration (100μM) for both P24T and L48V. At 100μM of DHT, 10μM TAM increased DHT glucuronidation to 186% and 248% of the control for P24T and L48V respectively. At 10μM of DHT, the same concentration of TAM increased DHT glucuronidation rate to 136% and 128% of the control for P24T and L48V.

Figure 2.24. Effect of 10 μM TAM on DHT glucuronidation by wild type UGT1A4, UGT1A4 P24T, or UGT1A4 L48V

Box Bars and error bars present the means and standard deviations of three measurements. Values that are significantly different from the wild type are labeled with *($p<0.001$)

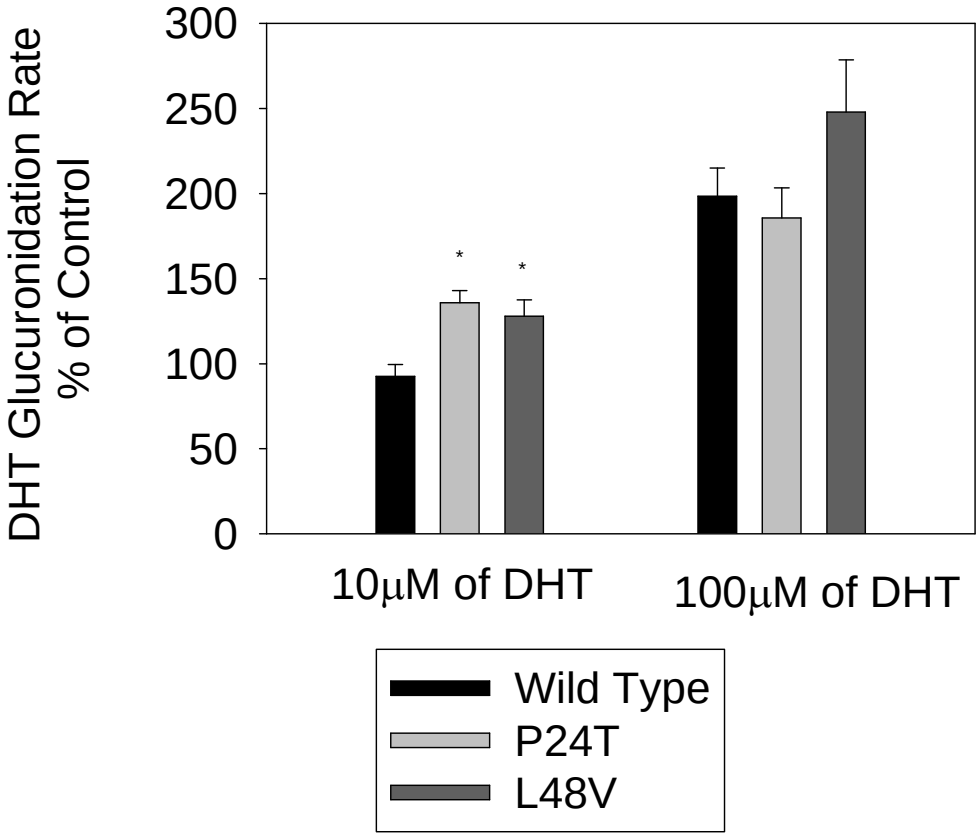

Discussion

In this part of the study we evaluated the function of two UGT1A4 variants (P24T and L48V) against DHT, t-AND and TAM glucuronidation. Both SNPs are commonly present in Caucasians(Ehmer et al., 2004; Benoit-Biancamano et al., 2009). In Japanese populations, although P24T were not detected, the allelic frequency of L48V is more than 10%(Wiener et al., 2004b; Mori et al., 2005; Saeki et al., 2005). Therefore, these two polymorphisms may play important roles in inter-individual variability associated with UGT1A4-catalyzed metabolism. Function analysis on these two variants has been conducted against several UGT1A4 substrates by different groups. Both increased and decreased enzyme activities as compared to the wild type enzyme were reported with the two variants against different UGT1A4 substrates, indicating that the effects of these two mutations are substrate dependent (Ehmer et al., 2004; Wiener et al., 2004b; Sun et al., 2006; Benoit-Biancamano et al., 2009). This property was further confirmed in our study. For the three UGT1A4 substrates evaluated in the present study, P24T mutation either had no effect on enzyme efficiency (CL_{int}) as compared to the wild type enzyme (DHT and TAM glucuronidation), or resulted in a decrease in enzyme efficiency (t-AND glucuronidation). The changes in CL_{int} by L48V mutation also depends upon the substrate. Increased, decreased or similar CL_{int} as compared to the wild type enzyme was observed against DHT, t-AND or TAM glucuronidation respectively.

The results obtained in our study on DHT and t-AND glucuronidation are quite different from the results reported by Ehmer et al (Ehmer et al., 2004). They

reported that L48V variant had very low or undetectable activity on both t-AND and t-DHT glucuronidation, and based on this result, the authors postulated that this polymorphism may have an impact on steroid metabolism and thus may be associated with steroid-dependent diseases (Ehmer et al., 2004). However, in our study, instead of showing undetectable activity on DHT glucuronidation, L48V variant displayed ~1.5-fold higher CL_{int} compared to the wild type UGT1A4. For t-AND glucuronidation, instead of retaining only ~ 2% of the enzyme activity, L48V variant retained about ~50% of the enzyme efficiency as compared to the wild type enzyme. Because the differences in enzyme efficiency between the L48V variant and the wild type enzyme are less than two folds and also because multiple UGTs are involved in the catalysis of DHT and t-AND glucuronidation, L48V polymorphism is not likely to have a big impact on DHT or t-AND metabolism in vivo.

As mentioned in Part I, DHT and t-AND are regioisomers with very similar structures (Figure 2.1). It is interesting to note that both mutations had differential effects on DHT and t-AND glucuronidation, especially that both mutations increased the K_m of t-AND glucuronidation but had no effect on the K_m of DHT glucuronidation. Assuming the enzyme-substrate association/dissociation rate constants are much higher than the rate constant for converting the substrate to the product after it associates with the enzyme, K_m is equivalent to K_s (binding constant of the substrate)(Segel, 1993). Therefore, the results we observed on DHT and t-AND glucuronidation with the two variants would indicate that these mutations decreased the binding affinity of t-AND, but had no effect on DHT

binding affinity. It is likely that DHT and t-AND may bind to different regions in the active site of UGT1A4 despite their structure similarities. Based on the fact that t-AND displayed substrate inhibition kinetics whereas DHT exhibited Michaelis-Menten kinetics with the three UGT1A4s, DHT may have one binding site in UGT1A4 whereas t-AND has two binding sites.

TAM is a non-steroid antiestrogen commonly used for the treatment and prevention of breast cancer (Fisher et al., 1998; Osborne, 1998). Significant inter-individual variability in TAM efficacy as well as toxicities has been observed in patients under TAM therapy and was associated with the polymorphisms of CYP2D6, the enzyme catalyzing 4-OH tamoxifen formation (Flockhart, 2008). In addition to form hydroxyl metabolites, TAM also undergoes glucuronidation, forming N-glucuronide. N-glucuronidation represents an important elimination pathway for TAM and is mainly catalyzed by UGT1A4 (Kaku et al., 2004). Thus, it is possible that polymorphisms in UGT1A4 may also contribute to the inter-individual variability in TAM therapy. In this study, we evaluated the potential effect of P24T and L48V polymorphisms on UGT1A4-catalyzed tamoxifen N-glucuronidation. In our study, although both V_{max} and K_m of TAM N-glucuronidation were decreased significantly by these two mutations, due to the same extent of changes in both kinetic parameters, the variants exhibited similar enzyme efficiency on TAM glucuronidation as compared to the wild type enzyme. Thus, our results predict that P24T and L48V polymorphisms may not have an impact on TAM N-glucuronidaiton in vivo.

Similar CL_{int}s by the three UGT1A4 enzymes against TAM glucuronidation were also observed by Sun et al (Sun et al., 2006), from whom we obtained the UGT1A4-HEK293 cell lines. However, Benoit-Biancamano reported L48V mutation resulted in a two-fold increase in CL_{int}. The increased CL_{int} in their study was due to a 2.5 fold decrease in K_m (similar to our study) but a relatively smaller decrease in V_{max}.(Benoit-Biancamano et al., 2009) The discrepancy between their results and ours on the V_{max} changes by L48V mutation is likely due to different amounts of active protein in different enzyme sources. Although they also used HEK293 cells as the expression system and the UGT1A4 protein amounts were normalized based on western blots, the amount active UGT1A4 relative to the total UGT1A4 protein may vary between different labs.

Our results on the function of L48V variant against t-AND glucuronidation were also different from the results reported by another group (Mori et al., 2005). Mori et al found L48V variant expressed in COS-7 cells had increased V_{max} (2.5-fold) and decreased K_m (4-fold) against t-AND glucuronidation. The overall CL_{int} of the L48V variant was approximately 10-fold the CL_{int} of the wild type enzyme, whereas in our study, L48V variant displayed decreased CL_{int} on t-AND glucuronidation(Mori et al., 2005). This discrepancy indicated that the function of UGT1A4 variants varies between different expression systems. Thus although function differences between the recombinant wild type enzyme and variants were observed in the present study and by other groups, studies such as comparison studies between liver microsomes from variant-carriers and wild type–carriers, are needed to further evaluate the effect of polymorphisms.

Part III: Effects of Ethinyl Estradiol and Estradiol Sulfate on UGT1A4-Catalyzed Lamotrigine-N2-glucuronidation

Background

Lamotrigine (LTG) is a phenyltriazine anticonvulsant, which is increasingly used for the treatment of various epilepsy and psychiatric disorders (Malik et al., 2006). LTG is often selected as a first-line antiepipletic drug for women with epilepsy during their reproductive years (Morrell et al., 2003). However, LTG clearance was increased by the estrogen component of oral contraceptives (Reimers et al., 2005; Sidhu et al., 2006; Ohman et al., 2008) and was almost doubled in pregnant women (Tran et al., 2002; Pennell et al., 2004). Because about 80% of LTG is eliminated by N2-glucuronidation (Malik et al., 2006), and the main enzyme that catalyzes this reaction is UGT1A4 (Rowland et al., 2006), the observed increased clearance is likely due to induction and/or activation of UGT1A4 by estrogens. In our previous studies (Part I and Part II), we clearly demonstrated that heterotropic activation was operable for UGT1A4. Thus, in this part of study, we investigated whether hetrotropic activation is one of the mechanisms that cause increased clearance of LTG in pregnant women and women with oral contraceptives. For this purpose, we evaluated the effect of ethinylestradiol (the estrogen component of most oral contraceptives) and estradiol-3-sulfate (an important circulating form of estradiol (Pasqualini et al., 1989)) on the LTG glucuronidation with a recombinant UGT1A4 system.

Materials and Methods

Materials. Ethinylestradiol was purchased from CalBiochem (San Diego, CA). Estradiol 3-sulfate was purchased from Sigma-Aldrich (St. Louis, MO). All the other chemicals employed in this part of the study were the same as in Part I.

Methods. All experiments were conducted by co-incubating the effector (ethinyl estradiol or estradiol sulfate) and the substrate (LTG) with recombinant UGT1A4. The enzyme source was cell lysate of HEK293 cells transfected with UGT1A4 gene (refer to Part I). Incubations were performed with the procedure in Part I. The rates of LTG glucruonidation were measured by quantifying the production of lamotrigine-N2- glucuronide (LTGG) with a LC-MS method and were compared with controls (no effector). LTGG quantification method was described with detail in Part I. The kinetic data for the interaction of ethinylestradiol on LTG glucuronidation were analyzed with Sigmaplot Enzyme Kinetics 1.3 (Systat Software Inc., San Jose, CA). A mixed partial inhibition model (Figure 2.25, Equation 2.12) best described the kinetic data. In this model, the inhibitor is able to bind to the free enzyme (E) and the enzyme –substrate complex (E-S), but with different binding constants (K_i). The binding constant of the inhibitor to E-S is α-fold the binding constant of the inhibitor to the free enzyme. In addition, the formed substrate-enzyme-inhibitor complex is also productive, but its efficiency differs from that of the enzyme-substrate complex by β-fold. In Equation 2.12, V_{max} refers to the maximum velocity of the substrate; K_s and K_i are binding constants of the substrate and the inhibitor; constant α and β reflect the changes

in binding constants and the effective catalytic rate constant (k_p) respectively (Segel, 1993).

<u>Figure 2.25</u>. A mixed partial inhibition model (Segel, 1993)

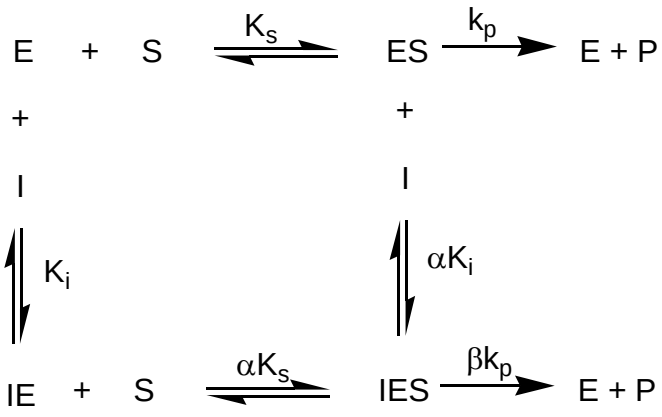

$$V_0 = \frac{V\max \bullet (1 + \frac{\beta[I]}{\alpha \bullet Ki}) \Big/ (1 + \frac{[I\}}{\alpha \bullet Ki})}{1 + \frac{Ks}{[S]} \bullet (1 + \frac{[I]}{Ki}) \Big/ (1 + \frac{[I]}{\alpha \bullet Ki})} \qquad \text{(Equation 2.12)}$$

Results and Discussion

To evaluate the effect of ethinylestradiol on LTG glucuronidation, interaction experiments were initially conducted with one concentration of LTG (0.625mM) and a wide range of ethinylestradiol concentration (2nM-25μM). In these experiments, ethinylestradiol either had no effect on LTG glucuronidation rate or inhibited LTG glucuronidation at higher concentrations (Figure 2.26), indicating that ethinylestradiol is not a heteroactivator for LTG glucuronidation. The inhibition effect of ethinylestradiol on LTG glucuronidation was further evaluated with multiple LTG concentrations (0.375-3.002 mM). A mixed partial inhibition model best described the inhibition data (Figure 2.27). The estimated Ki, α, and β are 7.9±0.7μM, 3.4±0.9, and 0.2±0.05 respectively.

<u>Figure 2.26</u> Rate percentage of control versus [S] plots for the effect of ethinylestradiol on LTG glucuronidation

The incubation mixtures contained UGT1A4-HEK293 cell lysate (0.5mg/ml), lamotrigine (0.625mM), alamethacin (50 µg/mg protein), saccharo-1,4-lactone (5mM), $MgCl_2$(5mM), Tris buffer (100mM), UDPGA(3mM) and ethinyl estradiol. The incubation time was 30 mins. The incubations were conducted in duplicate. The data in the plot were the mean of the duplicate determinations (< 20% of variation in all cases).

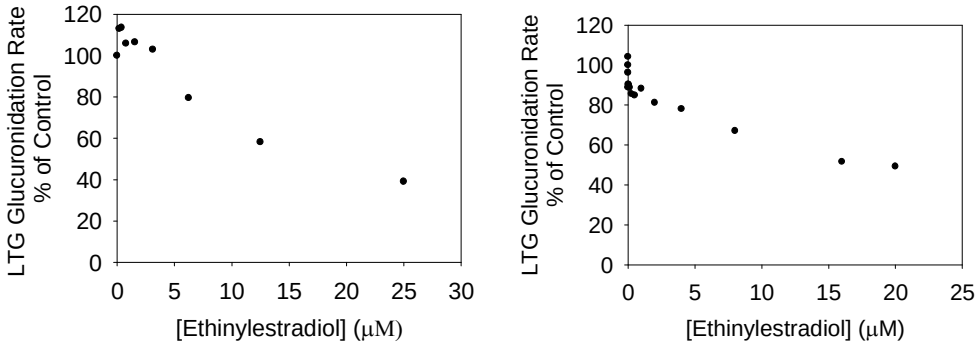

<u>Figure 2.27.</u> A Dixon plot of lamotrigine-N2-glucuronidation in the presence of different concentrations of ethinylestradiol (inhibitor)

Symbols represent LTG concentrations: 0.375 (●), 0.751(○), 1.501(▼), and 3.002 (∆) mM.

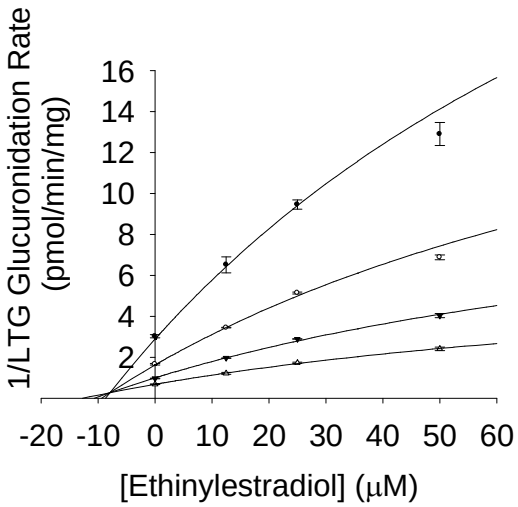

Because the estradiol sulfate conjugate is an important circulating form of estradiol(Pasqualini et al., 1989), we also conducted a co-incubation experiment to evaluate the effect of estradiol sulfate conjugate on LTG glucuronidation. In this experiment, a wide range of estradiol sulfate concentration (2.44nM to 20.0μM) was employed against one concentration of LTG (0.625mM). Our results as shown in Figure 2.28 demonstrated that estradiol sulfate at those concentrations (2.44nM to 20.0μM) had no effect on LTG glucuronidation.

<u>Figure 2.28.</u> Rate percentage of control versus [S] plots for the effect of estradiol sulfate conjugate on LTG glucuronidation

The data in the plot were the mean of the duplicate determinations (< 10% of variation in all cases).

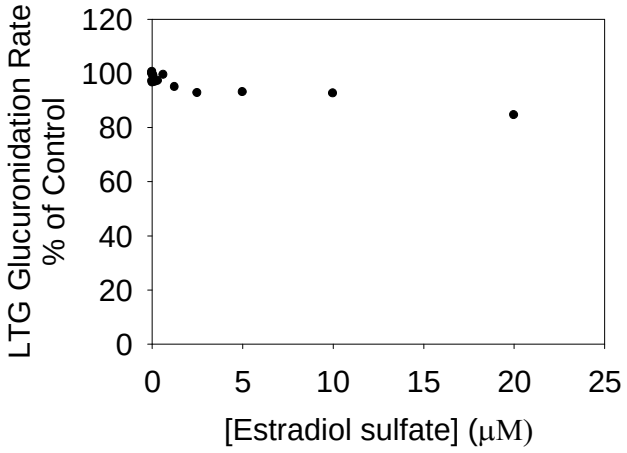

The two compounds we evaluated in the present study both did not show activation effect on LTG glucuronidation. It likely that the increased LTG clearance in pregnant women and women with oral contraceptives are due to other mechanisms. A recent paper by Chen et al demonstrated estradiol up-regulated UGT1A4 in HepG2 cells through specificity protein-1 (Sp1) and estrogen receptor alpha(Chen et al., 2009). Thus, induction of UGT1A4 may be one the mechanisms for increased LTG elimination in pregnant women. Recent functional analysis of UGT2B10 indicated that this orphan UGT is capable of catalyzing tertiary amine glucuronidation with higher efficiency than UGT1A4 (Chen et al., 2008; Zhou et al., 2010b). However, the involvement of UGT2B10 in lamotrigine glucurondiation has never been characterized. Whether increased

LTG elimination is partly due to induction or activation of other UGT enzymes such as UGT2B10 needs to be investigated.

CHAPTER 3 - KINETIC ANALYSIS ON UGT1A1-CATALYZED GLUCURONIDATION

Part I: Bilirubin Glucuronidation Revisited: Proper Assay Conditions to Estimate Enzyme Kinetics with Recombinant UGT1A1

Background

Bilirubin is a toxic waste product, formed from heme degradation. In humans, appproximately 250-400 mg of bilirubin are produced each day (Brierley and Burchell, 1993). Glucuronidation of bilirubin, catalyzed primarily by UGT1A1, is an obligatory step for bilirubin elimination and takes place in the liver and intestine (Kadakol et al., 2000). In this reaction, a glucuronosyl moiety is conjugated to one of the propionic acid side chains, located on the C8 and C12 carbons of the two central pyrrole rings of bilirubin, resulting in two mono-glucuronides (BMGs), which can be further glucuronidated, forming an 8,12-di-glucuronide (Crawford et al., 1992). Both BMGs and BDG are excreted into bile by an ATP-dependent transporter, multidrug resistance-associated protein 2 (Kamisako et al., 2000). BDG is the major bilirubin pigment (~80%) found in bile (Crawford et al., 1992).

Because glucuronidation by UGT1A1 is an essential step in bilirubin elimination, genetic polymorphisms resulting in partial or complete loss of UGT1A1 activity can lead to accumulation of unconjugated bilirubin in plasma (Kadakol et al., 2000). Typically, bilirubin is highly bound to plasma albumin, but in

hyperbilirubinemic situations, plasma albumin may become saturated. The unbound bilirubin is then free to cross the blood-brain barrier. Progressive accumulation of bilirubin in the brain can result in neurological damages, kernicterus and eventually death (Brierley and Burchell, 1993). Type I and II Crigler-Najjar syndromes and Gilbert's syndrome represent three grades of unconjugated hyperbilirubinemia. Patients with type I Crigler-Najjar syndrome are unable to conjugate bilirubin and exhibit serum bilirubin concentration typically in the range of 20-50mg/dl (normal serum bilirubin <0.9mg/ml) (Brierley and Burchell, 1993). Type II Crigler-Najjar syndrome (serum bilirubin level ~7-20mg/dl) is characterized as a severe but only partial loss of UGT1A1 activity and can be treated by administration of UGT1A1 inducers, such as phenobarbital (Brierley and Burchell, 1993). More than 50 genetic variants, mostly in the exons of UGT1A1, have been associated with Crigler-Najjar syndromes (Kadakol et al., 2000). The mildest form of unconjugated hyperbilirubinemia is Gilbert's syndrome, The serum bilirubin levels in patients with Gilbert's syndrome typical fluctuating between normal to 5 mg/dl (Kamisako et al., 2000). Two types of genetic mutation have been associated with Gilbert's syndrome. In Caucasians, Gilbert's syndrome is most frequently associated with a genetic mutation in the promoter region of UGT1A1 (UGT1A1*28). Characterized as an insertion of TA in the promoter A(TA)6TAA sequence, UGT1A1*28 has been observed to exhibit an allelic frequency of ~40% in Caucasians (Strassburg, 2008). Other genetic mutations associated with Gilbert's syndrome are missense mutations in exon 1 such as G71R. This type of mutation is rare in Caucasian populations but is

common in Asians. The allelic frequency for G7R in a Japanese population has been reported to be 24%. (Kamisako, 2004; Takeuchi et al., 2004)

Xenobiotics that inhibit UGT1A1 may also cause an elevation of bilirubin in blood and further exacerbate the hyperbilirubinemia observed in patients with Gilbert's syndrome or Crigler-Najjar syndrome (Rotger et al., 2005; Gupta et al., 2007). Therefore, in drug discovery settings, the in vitro ability of new drug candidates to inhibit bilirubin glucuronidation is commonly evaluated. For this, a simple and robust bilirubin glucuronidation assay is critical. However, the instability of bilirubin (Doumas et al., 1973) and its glucuronides (Jansen, 1973; Blanckaert et al., 1978; Adachi et al., 1985) makes in vitro bilirubin glucuronidation assays technically challenging. Furthermore, since the glucuronidation of bilirubin involves a sequential reaction that produces two mono-glucuronides and a di-glucuronide, establishment of initial rate conditions can be difficult, if not given particular attention. These challenges have manifest in significant disparities in estimated kinetic parameters for bilirubin glucuronidation. One group has reported that substrate inhibition kinetics are operable (Udomuksorn et al., 2007) whereas others have reported hyperbolic (Michaelis-Menten) kinetics (Senafi et al., 1994; Seppen et al., 1994). Likewise, estimates of Km have ranged from 0.26 μM (Udomuksorn et al., 2007) to as high as 24 μM (Senafi et al., 1994; Seppen et al., 1994). To more carefully characterize the necessary initial rate (linear) conditions for bilirubin glucuronidation by HEK293-expressed UGT1A1, the present study evaluated the effect of incubation time and protein concentration on bilirubin glucuronidation over a broader range of values. In addition, a

sensitive and robust assay was developed to measure the mono-glucuronides and di-glucuronide of bilirubin, providing the necessary analytical capabilities for evaluating these incubation conditions.

Materials and Methods

Materials. Bilirubin used in the present study was bilirubin IXα and was purchased from Frontier Scientific (Logan, UT). Uridine-diphosphate glucuronic acid (UDPGA), Trizma base, Trizma HCl, D-saccharic acid 1,4-lactone, and alamethicin were purchased from Sigma-Aldrich (St. Louis, MO). $MgCl_2$ was purchased from Mallinckrodt Corp. (Hazelwood, MO). All other chemicals employed in the glucuronidation incubations, as well as the HPLC solvents were HPLC grade and obtained from standard sources. Recombinant human UGT1A1 was expressed in HEK293 cells (gifts from Dr. Philip Lazarus, Penn State University, Hershey, PA). Cell lysates were prepared as previously mentioned (Chapter 2) and were added directly to the incubations as the enzyme source.

Incubation conditions. Incubations were conducted at 37℃ in a shaking water bath. Incubation mixtures (final volume 0.2 ml) contained UGT1A1-HEK293 cell lysate, bilirubin, Tris-HCl buffer (0.1M, pH 7.4 at 37℃), $MgCl_2$ (5mM), D-saccharic acid 1,4-lactone (5mM), UDPGA (3mM) and alamethicin (50 µg/mg protein). Bilirubin was dissolved in 100% DMSO just prior to addition to the incubation mixtures. The final DMSO concentration in the incubations was 1%. Cell lysate was pre-treated with alamethicin on ice for 30 minutes, prior to addition to the incubations. The reaction was initiated by addition of UDPGA, after a 3-min pre-incubation at 37° and was terminated by addition of 0.2 ml of cold methanol containing 200mM ascorbic acid. Protein was precipitated by centrifugation at 13,000 X g for 5 mins at 4℃ and 200µl supernatant were

injected onto the HPLC system for quantification. To characterize initial rate (linear) conditions with respect to protein concentration and incubation time, 10 µM bilirubin was incubated with different concentrations of protein (0.05 to 1mg/ml) for 5 or 6 mins or with 0.5 mg/ml of protein over the time range of 2 to 50 minutes. Based on the results of these experiments, the incubation conditions used to characterize UGT1A1 mediated bilirubin glucuronidation kinetics were 5-min (incubation time) and 0.05 mg/ml (protein concentration) or 6-min and 0.5 mg/ml. Rates of formation of bilirubin glucuronides under these incubation conditions and at different bilirubin concentrations (0.05 µM to 2µM) were determined and expressed as pmol/min/mg of protein. Bilirubin and bilirubin glucuronide solutions were stored in amber vials and handled and processed under conditions of reduced light.

Quantification of Bilirubin Monoglucuronides and Diglucuronide. Quantification of bilirubin monoglucuronides and diglucuronide was conducted with a Shimadzu LC-10ADVP system (Shimadzu, Columbia, MD) coupled with a Shimadzu SPD-10ADVP UV-Vis detector. The mobile phase consisted of 0.1% formic acid in water (A) and 100 % methanol (B) delivered at a flow rate of 0.5 ml/min. A linear gradient elution program was employed beginning with 60% of mobile phase B, then increasing mobile phase B linearly from 60% to 95% over 15 minutes, holding at 95% B for 7 mins, and then re-equilibrating the column at initial conditions for 4 mins. The HPLC column was a Zorbax Eclipse XDB-C18 column (150 X 3mm, 5µM, Agilent Technologies, Inc., Santa Clara, CA). Bilirubin glucuronides and bilirubin were detected at a visible wavelength of 450nm.

Figure 3.1 depicts representative chromatograms of the supernate fractions from incubations conducted in the presence and absence of UDPGA. Three additional peaks were detected in the presence of UDPGA. The peaks at 9.7 and 10.2 min were assigned as the monoglucuronides and the peak at 6.5 min as the bilirubin diglucuronide (Figure 3.1). Peak assignment was based on lipophilicities of the glucuronides and retention times reported by others (Adachi et al., 1985; Udomuksorn et al., 2007). The combined peak areas from the products eluting at 9.7 and 10.5 min were used to estimate the concentration of total monoglucuronides. Because bilirubin glucuronides were not commercially available, the UV absorbance response for bilirubin was used to estimate bilirubin glucuronide concentration, assuming that bilirubin and bilirubin glucuronides have the same molar extinction coefficient. Since the added glucuronic acid moiety does not absorb at the 450nm wavelength, the molar extinction coefficient of the parent compound is not affected, upon which the assumption of equal extinction coefficients is based. Bilirubin standards were prepared just before analysis. Each standard also contained the same concentrations of Tris-HCl buffer, $MgCl_2$, D-saccharic acid 1,4-lactone and HEK293 cell lysate as the incubation reactions. Protein in the standards was precipitated by addition of 100% cold MeOH instead of ascorbic acid-MeOH solution due to the potential precipitation of bilirubin under acidic conditions. Supernatants of 200 µl were injected onto HPLC column. The limit of quantification (LOQ) for bilirubin was set at the lowest concentration in the linear standard curve and was equal to 3.1 nM. For accuracy and precision

determinations, standard curves were constructed on eight separate days. The average accuracy and between-day precision at LOQ were 109.4% and 18.6% respectively. Accuracy at LOQ was calculated as the measured value divided by the true value times 100. The precision is calculated as the standard deviation divided by the mean concentrations times 100.

<u>Figure 3.1.</u> Chromatograms for bilirubin glucuronidation in the presence (A) or absence (B) of UDPGA

Incubations were conducted with 50µM of bilirubin at 0.5 mg/ml of protein for 30 mins in the presence or absence of UDPGA. 20µl of the incubation supernatant were injected onto HPLC for analysis.

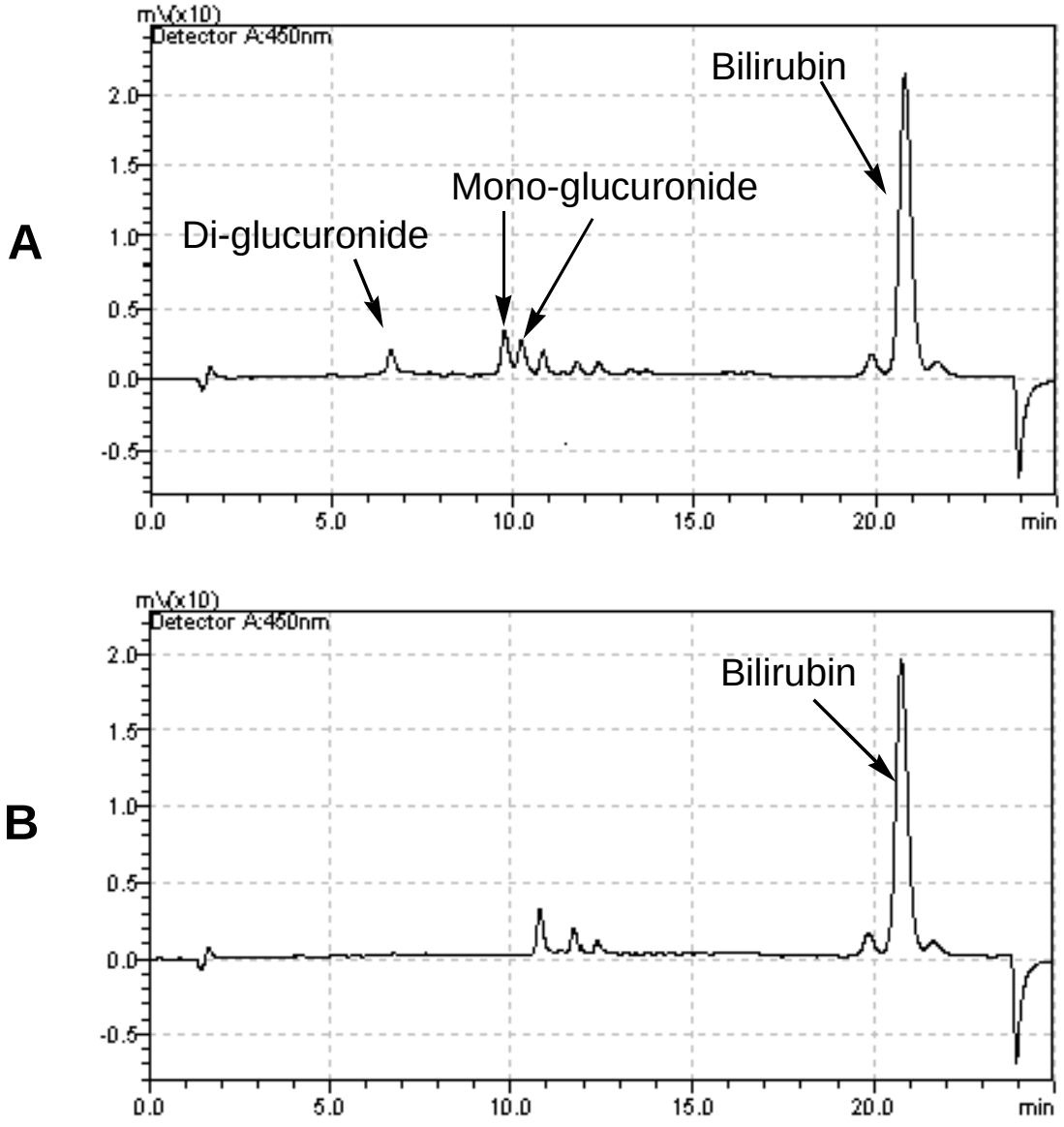

Data Analysis. Kinetic data were analyzed by fitting the Michaelis-Menten equation (Equation 3.1) or the Hill equation (Equation 3.2) to the kinetic data with Sigma Plot 9.0 (Systat Software Inc., San Jose, CA). The parameters V_{max} and K_m in Equation 1 are defined as the maximum velocity (V_{max}) and the substrate concentration at which velocity equals to half of the maximum velocity (K_m). The parameter V_{max} in Equation 3.2 has the same definition as in Equation 3.1. S_{50} and *n* are defined as substrate concentration at which velocity equals to half of the maximum velocity and the Hill coefficient, respectively. Determination of model appropriateness was determined by visual inspection of the Eadie-Hofstee plots, comparison of the Second-Order Akaike Information Criterion and the residual sum of squares.

$$V_0 = \frac{V_{\max} \times [S]}{K_m + [S]} \quad \text{(Equation 3.1)}$$

$$V_0 = \frac{V_{\max} \times [S]^n}{S_{50}{}^n + [S]^n} \quad \text{(Equation 3.2)}$$

Results and Discussion

Several factors contribute to the substantial technical challenges in the quantitation of bilirubin glucuronidation assay. Bilirubin itself is highly water insoluble at pH values below 8 (Heirwegh et al., 1972). Thus, to achieve desired concentrations for in vitro assays, bilirubin is commonly dissolved in alkaline solutions, followed by pH adjustment (Gordon et al., 1983; Seppen et al., 1994), or in 100% organic solvents (Ciotti et al., 1998; Zhang et al., 2005; Udomuksorn et al., 2007). Due to its instability under these conditions, alkaline solutions of bilirubin must be prepared immediately prior to addition to the incubations (De Ewenson et al., 1966; Doumas et al., 1973) and one must be concerned about the potential precipitation of bilirubin after adjusting the pH to the neutral range. To address this issue, addition of albumin has been employed to stabilize bilirubin solutions prepared in this manner (Black et al., 1970; Crawford et al., 1992). However, because bilirubin extensively binds to albumin, decreased rates of glucuronidation (Crawford et al., 1992) and non-Michaelis-Menten kinetics (Heirwegh et al., 1972) may be observed. In the present study, bilirubin was dissolved in 100% DMSO and stability was established for at least 8.5 hrs at room temperature and at least 7 days at -80℃.

Equally as problematic is the instability of bilirubin glucuronides, especially the mono-glucuronides (Jansen, 1973; Blanckaert et al., 1978; Adachi et al., 1985). In aqueous solutions, the mono-glucuronides rapidly disproportionate to diglucuronide and parent bilirubin (Adachi et al., 1985). This non-enzymatic conversion confounds kinetic determinations, due to loss of one molecule of total

glucuronide (two molecules of mono-glucuronide transform to one molecule of diglucuoronide and one molecule of bilirubin). However, this conversion can be strongly inhibited by high concentrations of reducing agents, bovine serum albumin, or rat liver cytosolic proteins (Adachi et al., 1985). Thus, to eliminate the conversion of BMGs to BDG during sample analysis, a high concentration of ascorbic acid in methanol (200 mM final concentration) was used to terminate the reactions. Under these conditions, BMGs and BDG were stable in the final incubation supernate for at least 17 hours at room temperature.

Because of the disparate kinetic profiles obtained previously by others (Senafi et al., 1994; Seppen et al., 1994; Udomuksorn et al., 2007), the effects of protein concentration and incubation time on bilirubin glucuronidation were carefully examined to accurately establish linear (initial rate) conditions. Formation of BDG or BMGs was linear at protein concentrations up to 0.5mg/ml (Figure 3.2). However, linearity with respect to incubation time was different for BDG and BMGs. Formation of BDG was linear at incubation times up to 30 mins, whereas for the BMGs, linearity was only observed up to 6 mins (Figure 3.3). These results are consistent with a sequential formation process for BMG and BDG. Based on these results, experiments were initially conducted at a high protein concentration (0.5mg/ml) for 6 mins.

<u>Figure 3.2.</u> Effects of protein concentration on BDG (A and B), BMG (C and D), and total glucuronide (E and F) formation

Data are means of triplicate measurements (CV %< 15%). The y-axes present the ratios between peak heights and protein concentrations, which are constant under linear conditions. The embedded figures are protein concentration versus peak height plots for the same data.

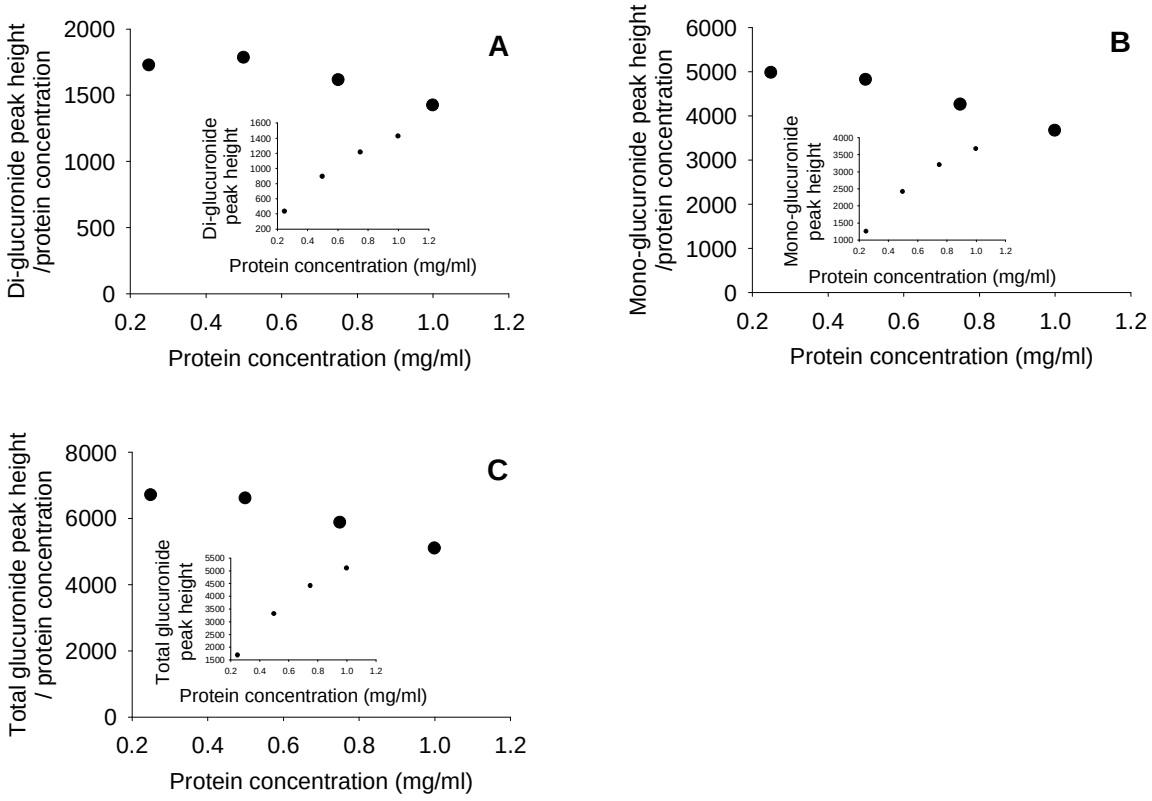

<u>Figure 3.3.</u> Effects of incubation time on BDG (A and B), BMG (C and D), and total glucuronide (E and F) formation

Data are means of triplicate measurements (CV %< 15%).The y-axes present the ratios between peak heights and incubation time, which are constant under linear conditions. The embedded figures are incubation time versus peak height plots for the same data.

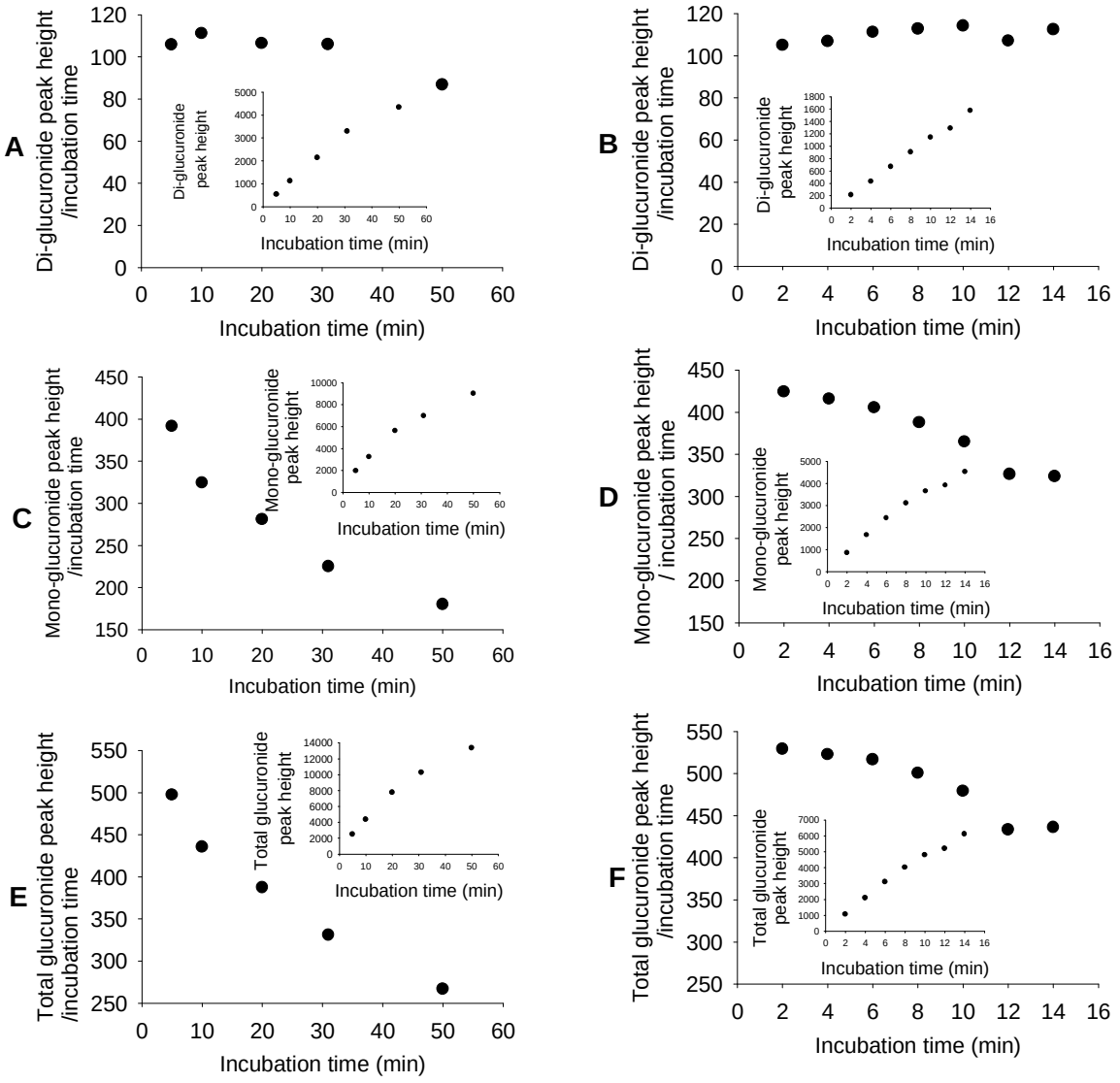

The K_m for bilirubin glucuronidation with recombinant UGT1A1 has previously been reported to range between 0.26 - 24μM (Senafi et al., 1994; Seppen et al., 1994; Zhang et al., 2005; Udomuksorn et al., 2007). To assure this range of concentrations was bracketed; experiments were initially conducted over the concentration range of 1.25 μM to 80 μM of bilirubin. However, under the conditions employed in the present study, no change in bilirubin glucuonidation rate was noted over this concentration range suggesting that the reaction was already at V_{max} even at 1.25 μM bilirubin (Figure 3.4).

Figure 3.4. Effects of bilirubin concentration (1.25-80 μM) on total glucuronide formation rate

The bars indicate the range of triplicate measurements.

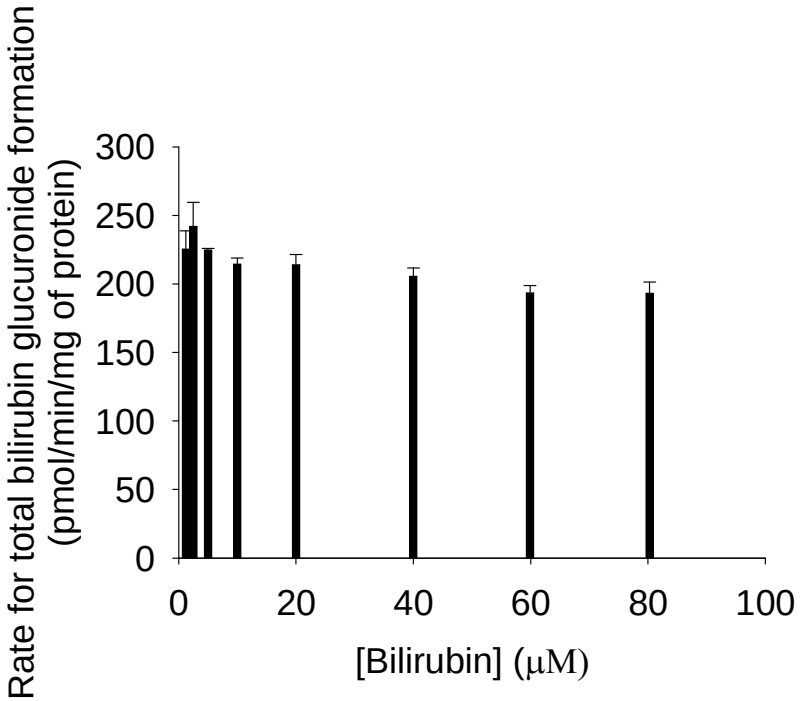

Thus, even lower bilirubin concentrations (0.05 μM to 2 μM) were evaluated to allow estimation of K_m and V_{max}. As depicted in Figure 3-5B, the kinetic profile for total bilirubin formation deviated from the classic hyperbolic (Michaelis-Menten) profile and was best described by fitting the data to the Hill Equation (Equation 3.2). The derived S_{50}, V_{max} and *n* values were 0.30 ± 0.02μM, 199 ± 6.1 pmol/min/mg of protein and 1.47 ± 0.09 respectively. However, amounts of the total glucuronides formed in this experiment were, on a molar basis, greater than 90% of the amount of bilirubin added to the incubation mixtures at low bilirubin concentrations, indicating this experiment was not conducted under initial rate conditions. To address this issue, 0.05mg/ml of protein and a 5-min incubation time were then evaluated. Under these conditions (Figure 3.5A), formation of bilirubin glucuronides followed hyperbolic (Michaelis-Menten) kinetics with estimates of K_m = 0.20 ± 0.018μM and V_{max} = 165±4.3 pmol/min/mg of protein. Substrate consumption under these conditions was <20% at all substrate concentrations. It is interesting to note that although a different kinetic model was used by Udomuksorn *et al.*(Udomuksorn et al., 2007) as compared to our study, the K_m for total bilirubin glucuronide formation was very similar to the value we obtained. The low K_m observed in the present study and also reported by Udomuksorn (Udomuksorn et al., 2007) suggest that saturation of glucuronidation will occur at relatively low substrate concentrations in vivo.

Figure 3.5. Substrate-concentration versus rate plots for total bilirubin glucuronide formation

A: incubations with 0.05 mg/ml of protein for 5 mins; B: incubations with 0.5 mg/ml of protein for 6 mins. The bars indicate the range of triplicate measurements. The embedded figures are Eadie-Hofstee plots for the same data. Data in A were fit to the Michaelis-Menten equation. Data in B were fit to the Hill equation.

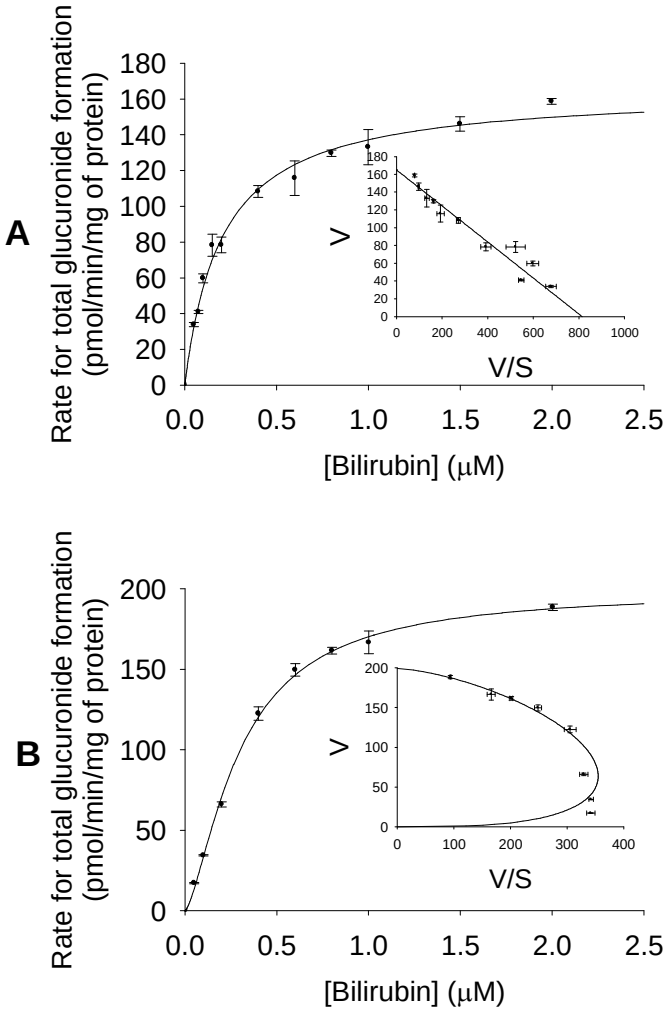

To assure that the saturation of velocity observed in the present study (the plateau in the hyperbolic kinetic profile) truly represents the V_{max} of the enzyme,

and is not due to saturation of bilirubin solubility in the incubation solution, we compared the peak areas of bilirubin in buffer solutions, where different concentrations of bilirubin in DMSO were added. A linear increase in bilirubin peak area was observed up to 10 µM final bilirubin concentration. Thus, the saturation of velocity observed around ~2uM (Figure 3.5A) is a reflection of achieving maximum velocity of the enzyme and not artificially due to limits on bilirubin solubility. However, the peak areas observed from measuring bilirubin in buffer solutions were lower than the same concentrations of bilirubin in 100% acetonitrile. Over the range of 0.05 -2µM bilirubin, the peak areas of bilirubin in buffer solutions were about 60-80% of the peak areas in acetonitrile. This is likely due to the non-specific binding of bilirubin to walls of the test tubes that occurs when bilirubin is in aqueous environment. In vivo, bilirubin also is highly bound to albumin in the systemic circulation and to cytosolic proteins (ligandin: a dimer of GSTA1 and/or GSTA2 and Z class proteins) present in hepatocytes (Kamisako et al., 2000). It is likely, under the present incubation conditions, a portion of bilirubin non-specifically binds to the proteins in the incubation although the protein concentration in the present study is low (0.05mg/ml) which would serve to minimize this binding. Also, because bilirubin is highly lipophilic, it may also partition into the membranes of the cell lysate. For the above reasons, the K_m observed in the present study (0.2µM) likely represents an apparent K_m and the actual K_m of bilirubin glucuronidation is likely lower than 0.2 µM.

Several groups have reported that their proportions of BDG and BMGs formed in incubation were bilirubin-concentration dependent (Blanckaert et al., 1979;

Gordon and Goresky, 1980; Gordon et al., 1983; Senafi et al., 1994). At low bilirubin concentrations, BDG was reported to be the dominant species formed whereas BMGs formation predominated at high bilirubin concentrations (Blanckaert et al., 1979; Gordon and Goresky, 1980; Gordon et al., 1983; Senafi et al., 1994). Senafi *et al.* conjectured that this kinetic phenomenon might be the reason that BDG is the predominant species found in bile since the free concentration of bilirubin in plasma is extremely low (Senafi et al., 1994). Only under non-initial rate conditions were our results congruent with these reports (Figure 3.6B). When true initial rate conditions were used, the proportions of BMGs and BDG formed were constant, with BMGs being the predominant species formed (~70%) (Figure 3.6A). Thus, in the previously reported work (Senafi et al., 1994), the higher percentages of BDG formed at low bilirubin concentrations were most likely due to depletion of bilirubin and subsequent accumulation of BMGs in the *in vitro* incubations. In addition, it is well established that bilirubin glucuronidation by UGT1A1 is a sequential reaction (Peters and Jansen, 1986; Crawford et al., 1992; Senafi et al., 1994) and the kinetic model can be simplified as Figure 3-7. In this model, BMG can either be directly converted to BDG without releasing from the enzyme or it is released from the enzyme, but can quickly rebound to the enzyme and then be converted to BDG. Based on the kinetic model, the ratio between initial rates for BMG and BDG formation equates to $k_{-4}/k_{3,}$ independent of bilirubin concentration. (See Appendix 3-2) Thus, the observed constant proportion between BMGs and BDG across the

range of bilirubin concentrations under true linear conditions (Figure 3-6A) is consistent with the sequential kinetic model in Figure 3-7.

<u>Figure 3.6.</u> Effects of bilirubin concentration on the proportions of BMGs or BDG

A: incubations with 0.05 mg/ml of protein for 5 mins; B: incubations with 0.5 mg/ml of protein for 6 mins. Symbol ● represents BDG and Symbol ■ represents BMG.

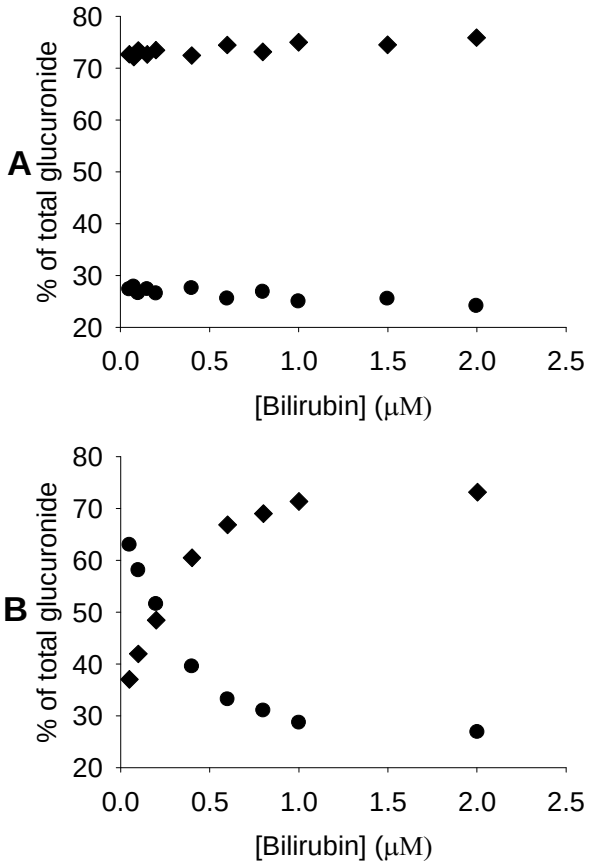

<u>Figure 3.7.</u> Kinetic scheme for bilirubin glucuronidation

k_1, k_{-1}, k_2, k_3, k_4, k_{-4}, k_5 and k_{-5} refer to the rate constants of the corresponding reaction steps.

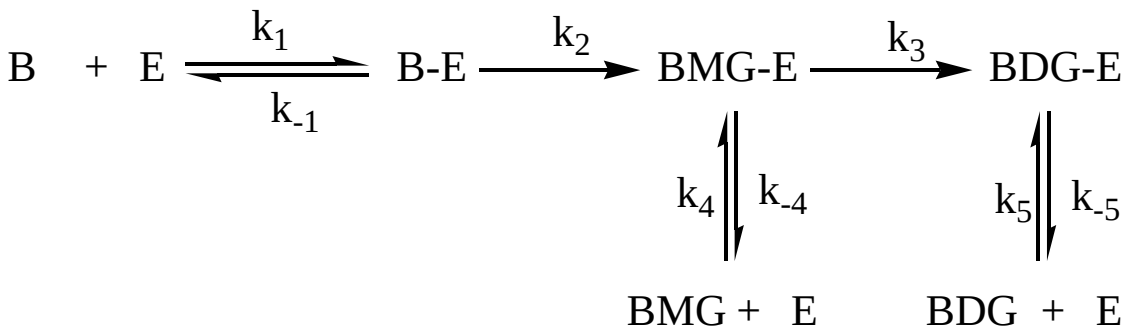

In summary, the present study established the proper conditions to conduct bilirubin glucuronidation with HEK293-expressed UGT1A1. Under true linear conditions, bilirubin glucuronidation displayed Michaelis-Menten kinetics with a K_m of 0.2 μM and the ratios of BMGs and BDG formation were constant across the range of bilirubin concentration evaluated. In addition, a robust assay that possessed sufficient sensitivity to permit characterization of low amounts of glucuronide formation was developed in the present study. We are currently employing this assay to evaluate a battery of UGT1A1 inhibitors on bilirubin glucuronidation.

Part II: Correlation between Bilirubin Glucuronidation and Estradiol-3-Gluronidation in the Presence of Model UGT1A1 Substrates/Inhibitors

Background

As mentioned in Part I, UGT1A1-mediated glucuronidation is an essential step for the efficient bilirubin elimination (Kadakol et al., 2000). Inhibition of UGT1A1 may cause unconjugated hyperbilirubinemia, thus in drug discovery settings the in vitro ability of new drug candidates to inhibit bilirubin glucuronidation is commonly evaluated. To evaluate the Inhibition potential of new chemical entities on UGT1A1 activity, ideally one would co-incubate the compound of interest with a UGT1A1-specfic probe substrate in human liver microsomes. Although bilirubin is highly specific for UGT1A1 and is the substrate of interest, it is less than an ideal UGT1A1 probe substrate for several reasons: a. bilirubin and bilirubin glucuronides are chemically unstable, b. authentic metabolite standards (bilirubin mono- and di-glucuronides) are not commercially available, c. bilirubin forms multiple metabolites and, d. sequential metabolism occurs during the formation of bilirubin glucuronides (Miners et al., 2010). To date, the most widely used probe substrate for UGT1A1 has been estradiol (Court, 2005; Miners et al., 2010). In human liver microsomes, estradiol is conjugated by UGTs to form either the 3- or 17 glucuronide. Estradiol-3-glucuronidation is primarily catalyzed in the liver by UGT1A1, with some involvement of UGT1A3 (Lepine et al., 2004). Furthermore, formation of estradiol-3-glucuronide is highly correlated with bilirubin glucuronidation in human liver microsomes (R^2=0.852) (Zhang et al.,

2007). In further support of the use of estradiol-3-glucuronidation as a measure of UGT1A1, beyond avoiding the technical challenges involved in measuring bilirubin glucuronidation, estradiol-3-glucuronide is commercially available and is easily measured. However, estradiol-3-glucuronidation has been reported to exhibit autoactivation (homotropic cooperativity) in human liver microsomes and recombinant UGT1A1 (Fisher et al., 2001; Udomuksorn et al., 2007).

Atypical kinetic profiles, classified by homotropic and heterotropic cooperativity, have been increasingly reported with UGTs. Similar to the CYPs, UGTs have been described to exhibit substrate-dependent autoactivation (Udomuksorn et al., 2007), substrate inhibition (Zhou et al., 2010c), and biphasic kinetics (Stone et al., 2003). Because of this propensity of the UGTs to exhibit atypical kinetic properties, a compound may activate the glucuronidation of one substrate, but inhibit or have no effect on the glucuronidation of a second substrate catalyzed by the same UGT (Uchaipichat et al., 2008; Zhou et al., 2010c). In Chapter 2, we investigated the effect of tamoxifen on UGT1A4-catalyzed dihydrotestosterone, trans-androsterone and lamotrigine glucuronidation and discovered that tamoxifen exhibited a concentration-dependent activation/inhibition of dihydrotestosterone and trans-androsterone glucuronidation, but only inhibited lamotrigine glucuronidation (Zhou et al., 2010c). Similar context-dependent heterotropic effects were also reported by Uchaipichat *et al* who reported that 4-methylumbelliferone activated UGT2B7-catalyzed 1-naphthol glucuronidation but inhibited zidovudine glucuronidation (Uchaipichat et al., 2008). Together, these results suggest the potential to make incorrect predictions of drug-drug

interactions involving UGT enzymes when assessed with a single probe substrate.

Therefore, in present study we evaluated the appropriateness of using estradiol-3-glucuronidation as an in vitro predictor for interactions with bilirubin glucuronidation. To this end, the kinetic profiles for both estradiol-3-glucuronidation and bilirubin glucuronidation with recombinant UGT1A1 were carefully characterized and the inhibition potentials of sixteen UGT1A1 substrates/inhibitors on each process were compared.

Materials and Methods

Materials. Ritonavir, anthraflavic acid, 1-naphthol, ketoconazole, carvedilol, 7-ethyl-10-hydroxycamptothecin (SN-38), 4-methylumbelliferone, 4'-OH-phenytoin, estradiol, estradiol-3-glucuronide, levothyroxine, uridine-diphosphate glucuronic acid (UDPGA), Trizma base, Trizma HCl, D-saccharic acid 1,4-lactone and alamethicin were purchased from Sigma-Aldrich (St. Louis, MO). Bilirubin IXα was purchased from Frontier Scientific (Logan, UT). Daidzein and riluzole were purchased from MP Biomedical LLC (Santa Ana, CA). Ethinylestradiol, raltegravir, niflumic acid, baicalein, and farnesol were purchased from CalBiochem (San Diego, CA), Toronto Research Chemicals Inc (North York, ON, Canada), Acros Organics (Fair Lawn, NJ), Indofine Chemical Company, Inc. (Hillsborough, NJ) and TCI American (Portland, OR), respectively. $MgCl_2$ was purchased from Mallinckrodt Corp. (Hazelwood, MO). All other chemicals employed were HPLC or reagent grade. Recombinant UGT1A1 was expressed in HEK293 cells (gift from Dr. Philip Lazarus, Penn State University, Hershey, PA). Cell lysate, prepared by sonication of UGT1A1-HEK293 cells in 10 mM Tris Buffer (pH=7.4 at 37˚C) containing 0.25 M sucrose for three 30-second bursts, each separated by 1-minute cooling on ice, was added directly to the incubation as the enzyme source. The protein concentration in the cell lysates was determined with the Pierce BCA™ protein assay kit (Thermo Fisher Scientific Inc., Rockford, IL).

Incubation Conditions to Characterize Kinetic Profiles. All incubations were conducted at 37℃ in a final volume of 0.2 ml in 100 mM Tris-HCl buffer with 5 mM $MgCl_2$, 5 mM D-saccharic acid 1,4-lactone, 3 mM UDPGA, cell lysate (0.05 or 0.25 mg/ml), alamethicin (50 µg/ mg of protein) and substrate. Estradiol and bilirubin were both dissolved in 100% DMSO before added to the incubation mixtures. The final DMSO concentration in the incubations was 1%. Cell lysates were pre-treated with alamethicin on ice for 30 minutes before reaction initiation. Preliminary experiments were conducted to ensure that all kinetic determinations were carried out under linear conditions with respect to time and protein concentration. For estradiol-3-glucurondation, incubations were carried out in the presence of 0.25mg/ml of protein for 30 mins with 13 different estradiol concentrations (3-100 µM). Reactions were terminated with 0.2 ml cold methanol, followed by addition of 20 µl of 1 µg/ml trans-androsterone glucuronide as internal standard. The samples were then centrifuged at 13,000 X g for 5 min to remove the precipitated protein. Five µl of supernate from each sample were injected onto the HPLC system for quantification. Detailed incubation conditions for bilirubin glucuronidation were as previously described (Zhou et al. submitted to DMD). Bilirubin incubations were conducted with 0.05 mg/ml of protein for 5 min. These conditions assured that bilirubin consumption was less than 20% in all incubations. Bilirubin concentrations for kinetic profile characterization ranged from 0.05 - 2 µM.

Interaction Studies. The effect of bilirubin on estradiol-3-glucuronidation (7.5, 15, 30 µM of estradiol), was evaluated in the absence or presence of 0.04-1 µM

bilirubin. For the converse, bilirubin glucuronidation (0.1, 0.2, 0.4 μM of bilirubin) was studied in the absence or presence of 3-30 μM estradiol. The effects of ritonavir, anthraflavic acid, 1-naphthol, ketoconazole, carvedilol, 7-ethyl-10-hydroxycamptothecin (SN-38), 4-methylumbelliferone, 4'-OH-phenytoin, levothyroxine, daidzein, riluzole, ethinylestradiol, raltegravir, niflumic acid, baicalein, and farnesol were initially evaluated with 15 μM of estradiol or 0.2 μM of bilirubin. The concentrations of the purported inhibitors were originally selected based on reported K_m or K_i values. The final range of concentrations ensured appropriate calculation of IC_{50s} and are presented in Table 1. Because of the observation of atypical effects with daidzein and SN-38 in the initial studies, the effects of daidzein (0 and 3.125 - 50 μM) and SN-38 (0 and 25 - 200 μM) on estradiol-3-glucuronidation were further evaluated with multiple concentrations of estradiol (4-75 μM).

Quantification of Estradiol-3-Glucuronide and Bilirubin Glucuronides. Methods for quantitation of bilirubin monoglucuronides and diglucuronide were as previously described (Part I of Chapter 3). Estradiol-3-glucuronide was quantified either through an LC-MS method with a Shimadzu LC-10ADVP system (Columbia, MD) or through a capillary LC-MS/MS method (for estradiol and bilirubin interaction experiments only) on a Thermo Finnigan TSQ Quantum Discovery Max MS system (Waltham, MA) coupled with an Agilent 1100 capillary HPLC system (Santa Clara CA). The mobile phase for both methods consisted of 0.1% formic acid in water (A)/methanol (B) gradient and was delivered at a flow rate of 0.25 ml/min for the LC-MS method or 12 μl/min for the capillary LC-

MS/MS method. The HPLC column used for the LC-MS method was a Haisil Higgins C8 column (100 X 2.1mm, 5μM, Mountain View, CA) and the column for the LC-MS/MS method was a Thermo BetaBasic-18 column (150 x 0.5 mm, 3 μm, Waltham, MA). Linear gradient elution programs were employed for both methods. For the LC-MS method, the initial mobile phase contained 40% B, which was linearly increased to 95% B over 5 mins and retained at 95% for an additional 5 mins. The column was then re-equilibrated at 40% of B for 4 mins. The elution program for the LC-MS/MS method was initiated at 50% B, then increased to 95% B over 3 minutes and then maintained at 95% B for an additional 9 minutes, followed by an 8-min column re-equilibration at 50% B. The mass spectrometers were both operated in negative ion mode with an ESI interface. Quantitation was performed in single ion monitoring (SIM) mode by monitoring m/z=447 ($[M-H]^-$) for estradiol-3-glucuronide and m/z=465 ($[M-H]^-$) for trans-androsterone glucuronide or in multiple reaction monitoring (MRM) mode by monitoring a transition pair of m/z 465→287 for estradiol-3-glucuronide and 447→227 for trans-androsterone glucuronide. The MS parameters for the LC-MS method were as follows: nebulizing gas flow = 1.5 L/min; interface bias = -3.50KV; interface current = -9.20 μA; heating block temperature = 200 ℃; focus lens = +2.5V; entrances lens = 50.0V; RF gain = 5660; RF offset = 5210; prerod bias = +4.2V; main-rod bias = +3.5V; aperture = -20.0V; conversion dynode = +7.0kV; detector = 2.5 KV; CDL voltage = -25.0kV; Q-array DC = -35.0 V; Q-array RF = +150.0V. In the LC-MS/MS method, argon was used as the collision gas. The MS operating conditions were as follows for the LC-MS/MS method:

spray voltage 2800V, sheath gas pressure 10mTorr, capillary temperature 350ºC, tube lens offset -300, source CID: 8V, collision pressure 2.2 mTorr, collision energy 42V, Quad MS/MS bias:1.4. The chromatograms for estradiol-3-glucuronide and internal standard trans-androsterone glucuronide with the LC-MS and the capilliary LC-MS/MS method are shown in Figure 3.8 and Figure 3.9.

Figure 3.8. Chromatograms of estradiol-3-glucuronide and trans-androsterone glucuronide with a LC-MS method

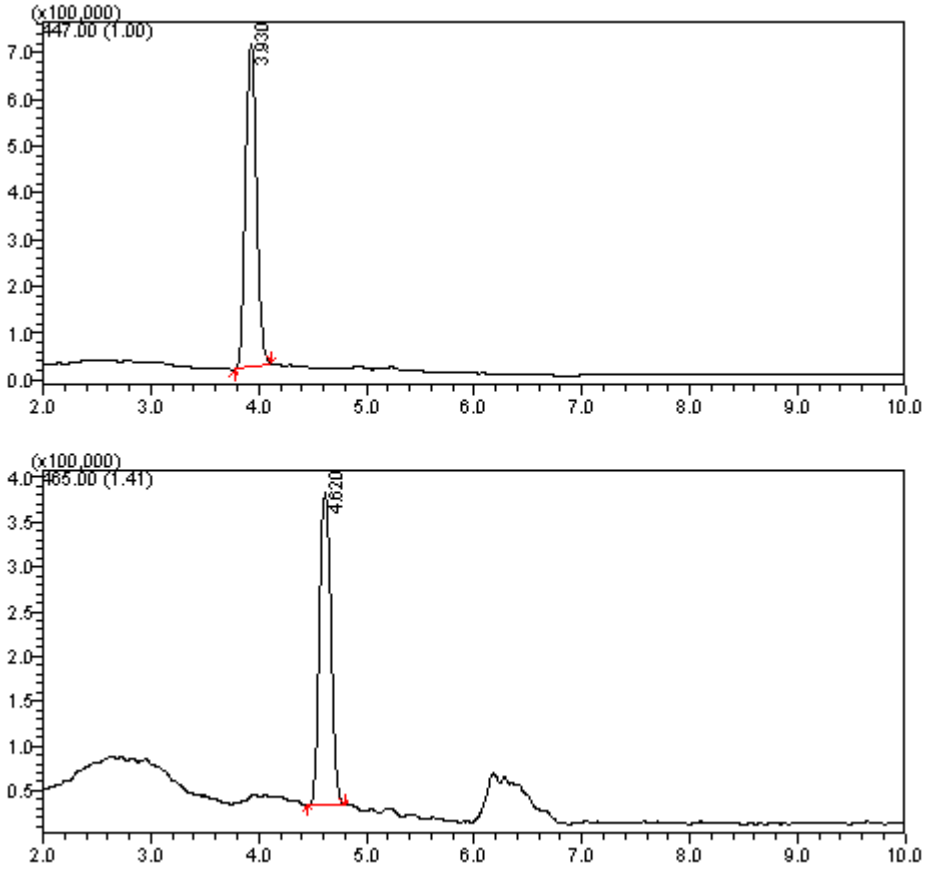

Figure 3.9. Chromatograms of estradiol-3-glucuronide and trans-androsterone glucuronide with a capilliary LC-MS/MS method

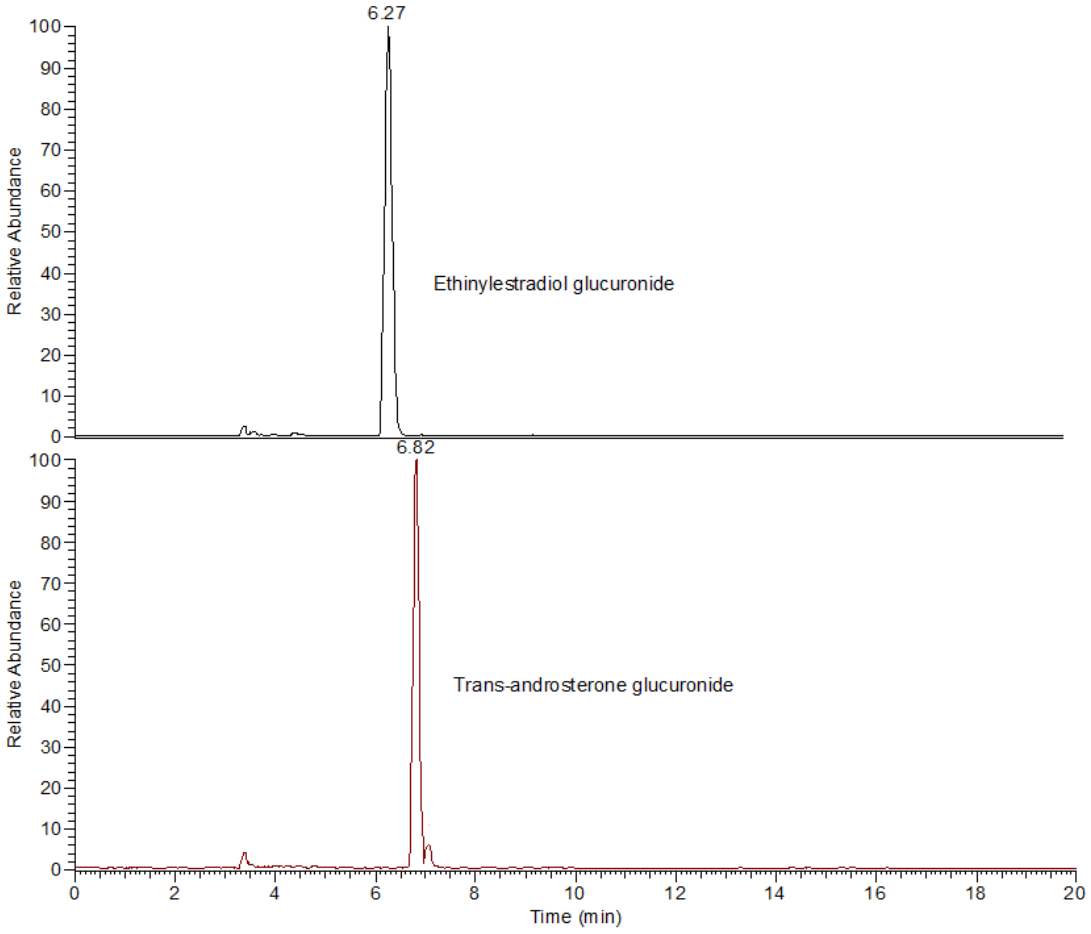

Data Analysis. Kinetic data for bilirubin glucuronidation and estradiol-3-glucuronidation were fit to the Michaelis-Menten equation (Equation 3.1) and Hill equation (Equation 3.2), respectively, via nonlinear regression with Sigma Plot 9.0 (Systat Software Inc., San Jose, CA). Selection of the appropriate model was determined by visual inspection of the Eadie-Hofstee plots, comparison of the Second-Order Akaike Information Criterion and the residual sum of squares.

For the interaction experiments, rates were expressed as percentage of control. Mean control values were determined for each experiment. A value of ≥ 20% was used for classification of compounds that increased or decreased estradiol-3-glucuronidation or bilirubin glucuronidation as activators or inhibitors. IC_{50} was determined by linear interpolation (Huber and Koella, 1993). IC_{50}s for bilirubin glucuronidation and for estradiol-3-glucuronidation were compared for correlation by linear regression and the coefficient of determination (R^2) was calculated.

A two-site model (Figure 3.10A, Equation 3.3) (Kenworthy et al., 2001) was applied to describe the interaction of daidzein on estradiol-3-glucuronidation. In this model, the substrate binds cooperatively to two binding sites in the enzyme and the modifier competes for both sites. The model also assumes that no interaction occurs between the two modifier molecules, but the binding of one modifier molecule to the enzyme induces a similar cooperativity to the substrate as the substrate itself. Thus, at low substrate and modifier concentrations,b enhancement of substrate binding induced by the modifier overcomes any competitive inhibition, resulting in activation. In addition, the modifier-enzyme-substrate complexes (AES and SEA in Figure 3.10A) are productive, but the

effective catalytic rate constants (k_p) of these complexes differ from that of the enzyme-substrate complex (ES) by a factor **c**, which determines the extent of the activation and the substrate concentration range in which activation may occur. The effect of SN-38 on estradiol-3-glucuronidation was best described with a three-site model (Figure 3.10B, Equation 3.4) (Kenworthy et al., 2001). In this model, the substrate binds cooperatively to two binding sites in the enzyme, whereas the inhibitor binds to a distinct binding site. Thus, inhibition of the reaction occurs by decreasing V_{max} rather than changing the binding constant of the substrate. In addition, the modifier does not affect the interaction between the two substrate molecules. Thus, the sigmoidicity of the reaction does not change with increasing modifier concentration. Also in this model, enzyme complexes containing the modifier are productive, resulting in incomplete inhibition even at a saturating concentration of inhibitor. Changes in the effective catalytic rate constant for enzyme complexes containing the inhibitor are reflected by the parameter "**c**". The aforementioned multiple-site models assume rapid equilibrium (Segel, 1975). The kinetic parameter V_{max} equates to 2 $k_p[E]_t$, where $[E]_t$ is the total enzyme concentration and k_p is effective catalytic rate cnstant . K_s, K_a and K_i are binding affintiy constants. The parameter ***c*** reflects changes in k_p, whereas the parameters ***a*** and ***d*** reflect changes in binding affinity of the substrate.

$$V_0 = \frac{V_{max} \bullet \left(\frac{[S]}{K_s} + \frac{[S]^2}{a \bullet K_s^2} + \frac{c \bullet [S] \bullet [A]}{a \bullet K_s \bullet K_a}\right)}{1 + \frac{2[S]}{K_s} + \frac{2[A]}{K_a} + \frac{[S]^2}{a \bullet K_s^2} + \frac{2 \bullet [S] \bullet [A]}{a \bullet K_s \bullet K_a} + \frac{[A]^2}{K_a^2}} \quad \text{(Equation 3.3)}$$

$$V_0 = \frac{V_{max} \bullet \left(\frac{[S]}{K_s} + \frac{[S]^2}{a \bullet K_s^2} + \frac{c \bullet [S] \bullet [I]}{d \bullet K_s \bullet K_i} + \frac{c \bullet [S]^2 \bullet [I]}{a \bullet d \bullet K_s^2 \bullet K_i}\right)}{1 + \frac{2[S]}{K_s} + \frac{[I]}{K_i} + \frac{[S]^2}{a \bullet K_s^2} + \frac{2 \bullet [S] \bullet [I]}{d \bullet K_s \bullet K_i} + \frac{[S]^2 \bullet [I]}{a \bullet d \bullet K_s^2 \bullet K_i}}$$ (Equation 3.4)

<u>Figure 3.10.</u> Multiple-site kinetic models for interactions of daidzein or SN-38 on estradiol-3-glucuronidation (adapted from (Kenworthy et al., 2001))

A: a kinetic model to explain the effect of daidzein on estradiol-3-glucuronidation (Equation 3-3); B: a kinetic model to explain the effect of SN-38 on estradiol-3-glucuronidation (Equation 3-4). k_p is the effective catalytic constant. K_s, K_a, K_i are binding affinity constants. Constant c reflects change in k_p and constant a and d reflect changes in binding affinity.

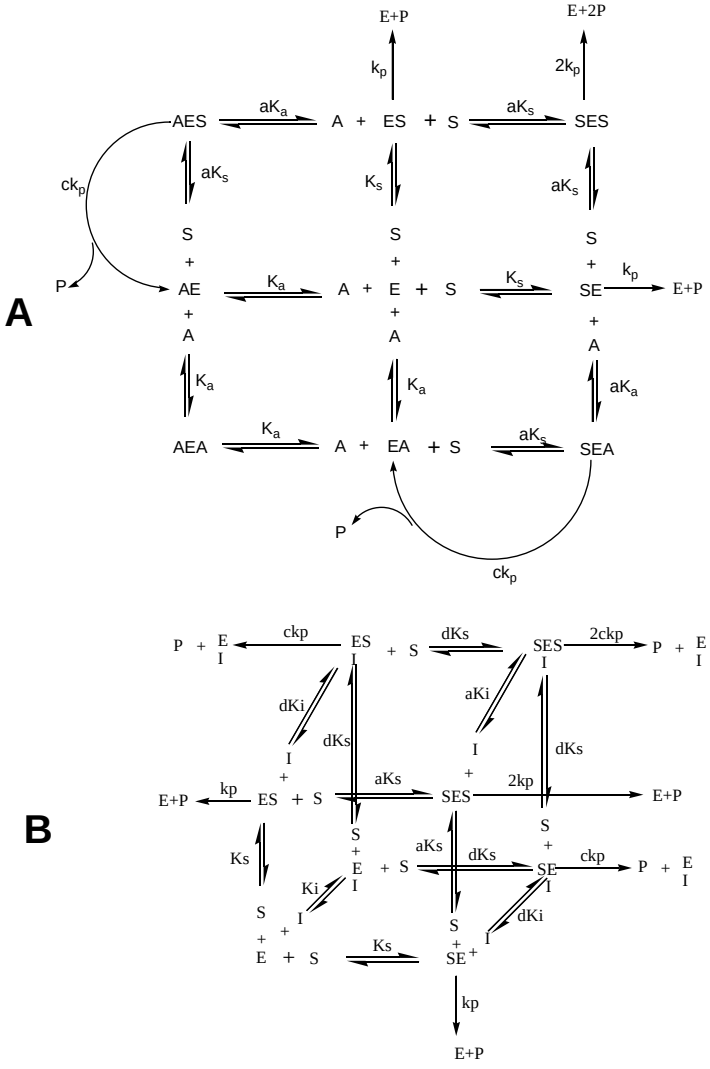

Results

Kinetics of bilirubin glucuronidation and estradiol-3-glucuronidation. The kinetic properties of bilirubin glucuronidation and estradiol-3-glucuronidation were carefully characterized in a recombinant human UGT1A1 system. Estradiol-3-glucuronidation exhibited characteristics of autoactivation, with a sigmoidal kinetic profile (Figure 3.11). The Hill equation (Equation 3.2) was fit to the kinetic data. The derived S_{50}, V_{max} and Hill coefficient (n) for estradiol-3-glucuronidation were 15.2±0.4 μM, 115±1.7 pmol/min/mg of protein and 1.9 ± 0.1. Bilirubin glucuronidation kinetics were described with details in Part I.

Figure 3.11. Kinetic plots (Rate versus [S]) for estradiol-3-glucuronidation

The bars indicate the range of triplicate measurements. The embedded figures are Eadie-Hofstee plots for the same data. The sigmoidal equation (Equation 3.2) was fit to the data.

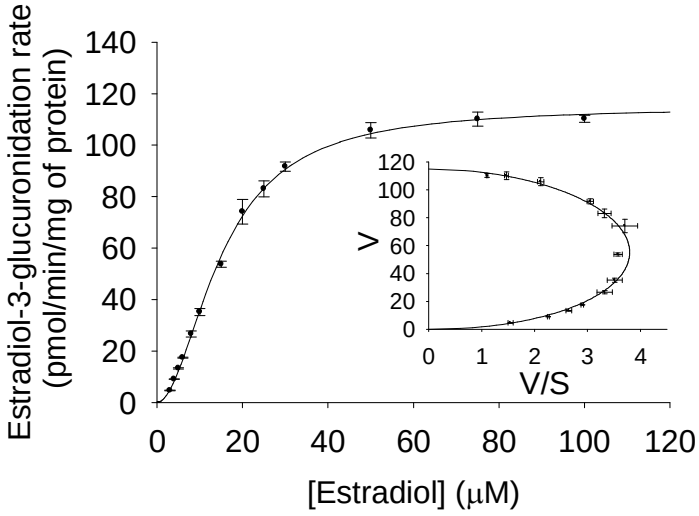

Interaction between bilirubin and estradiol glucuronidation. Both bilirubin and estradiol inhibited the glucuronidation of the other compound (Figure 3.12) and the effects were substrate-concentration dependent. As substrate concentration was increased, less inhibition was observed, as would be expected for competitive inhibition. However, due to the atypical kinetic properties of estradiol glucuronidation, a simple one-site competitive inhibition model did not adequately explain both sets of data. More data points are required to fit the results to a more complex model, and thus the results are reported in a qualitative manner (Figure 3.12).

<u>Figure 3.12.</u> Interactions between estradiol and bilirubin (rate percentage of control versus [modifier] plots)

A: effect of estradiol on bilirubin glucuronidation: Symbols represent bilirubin concentration: 0.1 (●), 0.2 (○), 0.4 (▼) μM. B: effect of bilirubin on estradiol-glucuronidation: Symbols represent estradiol concentrations: 7.5 (●), 15 (○), and 30(▼). Data points are means of duplicate measurements. Coefficients of variation are all within 10%.

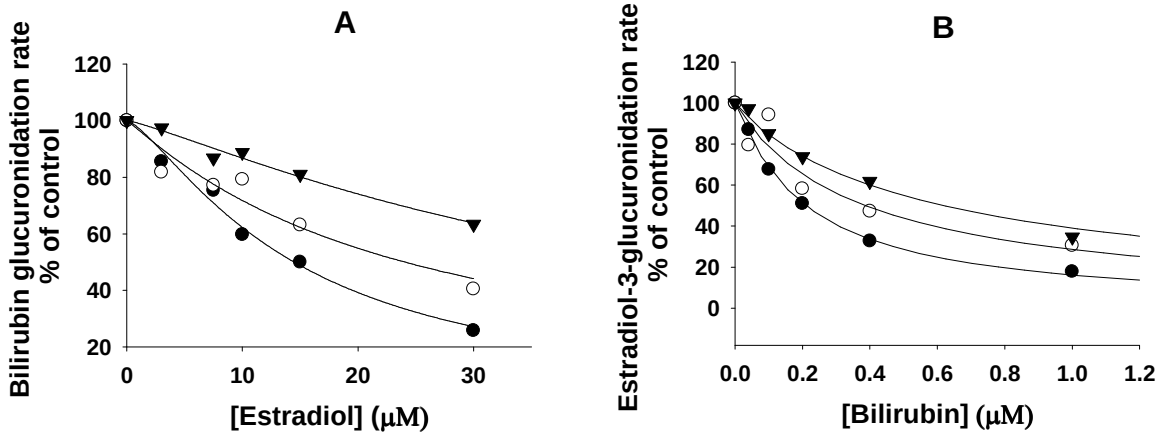

Effects of 16 model UGT1A1 substrates or inhibitors on bilirubin and estradiol glucuronidation. Fourteen of the studied compounds inhibited both bilirubin and estradiol glucuronidation (Table 3.1). Among these 14 compounds, ritonavir, anthraflavic acid, levothyroxine, riluzole, baicalein, farnesol, 4'-OH-phenytoin, 4 – methylumbelliferone, raltegravir and 1-naphthol exhibited very similar IC_{50}s (differences less than 2-fold) on both bilirubin glucuronidation and estradiol-3-glucuronidation (Table 3.1). Ketoconazole, carvedilol and niflumic acid exhibited more disparity with respect to inhibition of the two reactions in that these compounds exhibited at least two-fold higher IC_{50} value against bilirubin glucuronidation than against estradiol-3-glucuronidation. SN-38 only weakly inhibited bilirubin glucuronidation (IC_{50}=356 μM) and appeared to be a partial inhibitor of estradiol-3-glucuronidation. At even the highest SN-38 concentration, only 64% inhibition of estradiol-3-glucuronidation was noted. Two of the compounds examined ethinylestradiol and daidzein, exhibited concentration-dependent activation/inhibition effects on estradiol-3-glucuronidation but were pure inhibitors of bilirubin glucuronidation. Daidzein and ethinylestradiol both activated estradiol-3-glucuronidation at low concentrations but inhibited the reaction at higher concentrations. The activation effect resulted in higher IC_{50}s (apparent IC_{50}, calculated without including the activation data points) on estradiol-3-glucuronidation than on bilirubin glucuronidation, Daidzein, which activated estradiol-3-glucuronidation to 156% of control, exhibited a ~16-fold higher IC_{50} toward estradiol-3-glucuronidation than toward bilirubin glucuronidation. Ethinylestradiol, which modestly activates estradiol-3-

glucuronidation (128% of control) exhibited an IC_{50} toward estradiol-3-glucuronidation that was ~2-fold higher than the IC_{50} against bilirubin glucuronidation. The IC_{50} values for each inhibitor-substrate pair were plotted to assess whether a correlation existed in the inhibition of each substrate (bilirubin or estradiol) for these 16 compounds (Figure 3.14). Excluding the data from the two heteroactivators (ethinylestradiol and daidzein), the R^2 value for the correlation was 0.96 ($P<0.0001$). If the two heteroactivators were included, the R^2 decreased to 0.83 ($P<0.0001$).

Figure 3.13. **Structures of 16 model modifiers (14 UGT1A1 substrates and 2 UGT1A1 inhibitors)**

14 Substrates:

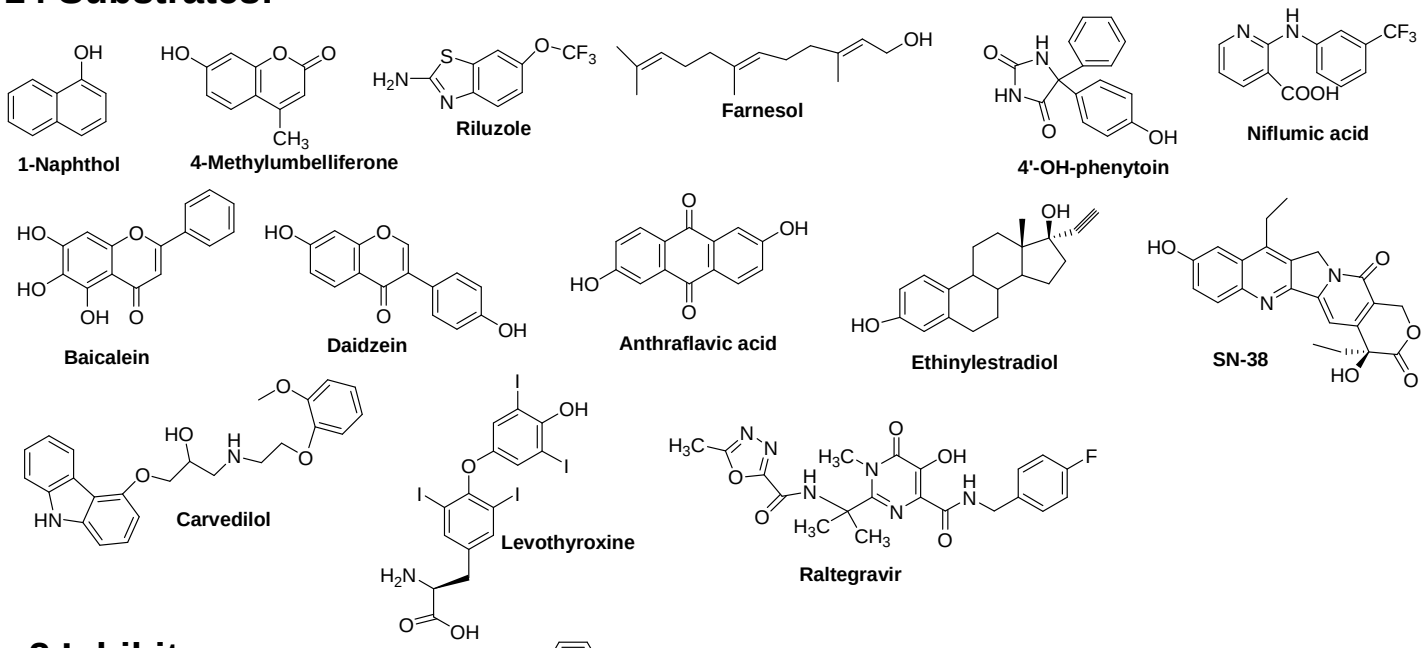

2 Inhibitors:

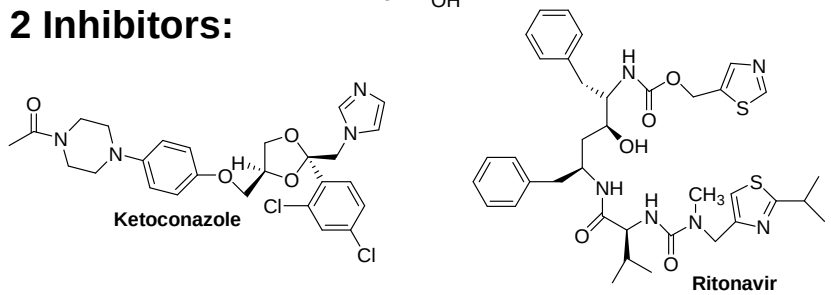

Table 3.1. Effects of 16 UGT1A1 substrates/inhibitors on bilirubin glucuronidation and estradiol-3-glucuronidation

[a] Concentration ranges of the modifiers used for IC_{50} determination.

Name	[a]Concentration (μM)	IC_{50}s on bilirubin glucuronidation (Effect)	IC_{50}s on estradiol-3-glucuronidation (Effect)
Ritonavir	1.3 to 50	3.0 (Inhibition)	1.7 (Inhibition)
Anthraflavic acid	2 to 40	3.6 (Inhibition)	4.0 (Inhibition)
Levothyroxine	0.6 to 10	4.9 (Inhibition)	5.6 (Inhibition)
Baicalein	0.5 to 10	7.0 (Inhibition)	4.4 (Inhibition)
Farnesol	13 to 60	47 (Inhibition)	40 (Inhibition)
4 - Methylumbelliferone	28 to 550	100 (Inhibition)	100 (Inhibition)
4'-OH-phenytoin	15 to 300	120 (Inhibition)	110 (Inhibition)
Raltegravir	25 to 200	170 (Inhibition)	190 (Inhibition)
Riluzole	25 to 500	180 (Inhibition)	160 (Inhibition)
1-Naphthol	88 to 1700	240 (Inhibition)	280 (Inhibition)
Ketoconazole	6.3 to 100	27 (Inhibition)	13 (Inhibition)
Carvedilol	2.5 to 50	27 (Inhibition)	12 (Inhibition)
Niflumic Acid	2 to 80	53 (Inhibition)	13 (Inhibition)
SN-38	6.3 to 400	360 (Inhibition)	N.A. (Partial inhibition)
Ethinylestradiol	2.5 to 50	21 (Inhibition)	44 (Activation and inhibition)
Daidzein	6.3 to 130	7.3 (Inhibition)	120 (Activation and inhibiton)

<u>Figure 3.14.</u> Comparison of IC_{50}s for bilirubin glucuronidation and IC_{50}s for estradiol-3-glucuronidation

Symbol ● represents modifiers that showed inhibition effect on both processes. Symbol ■ represents daidzein and estradiol which showed heteroactivation on estradiol-3-glucuronidation. IC_{50}s for bilirubin glucuronidation and IC_{50}s for estradiol-3-glucuronidation were compared by linear regression and the coefficient of determination (R^2) was calculated. Without the two heteroactivators (ethinylestradiol and daidzein), the R^2 for the correlation was 0.9702. If the two heteroactivators were included, the R^2 was 0.8435. The solid line represents the fit of all IC_{50}s to linear equation.

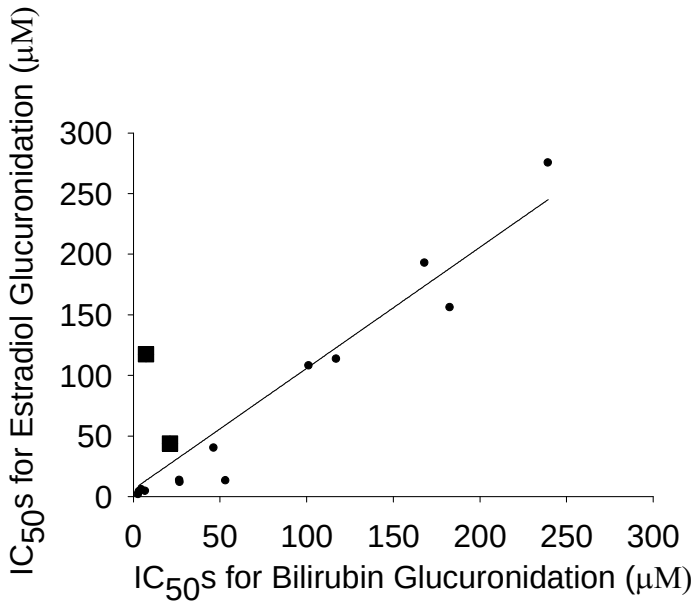

Kinetics of estradiol-3-glucuronidation in the presence of daidzein. To more completely characterize the mixed effects (activation/inhibition) of daidzein on estradiol-3-glucuronidation more detailed kinetics were assessed over a range of estradiol concentrations (4μM-75μM). As depicted in Figure 3.15A, the formation of estradiol-3-glucuronide was either activated or inhibited by daidzein depending on both the estradiol concentration and the daidzein concentration. With increasing daidzein concentrations, the rate of estradiol-3-glucuronidation increased to a maximum at ~6.25 μM daidzein and then decreased with increasing daidzein concentrations. It is notable that greater activation of estradiol-3-glucuronidation by daidzein was observed at lower concentrations of estradiol, as is typically noted with heteroactivation (Hutzler et al., 2001; Kenworthy et al., 2001; Uchaipichat et al., 2008). The most pronounced activation effect (392% of the control) was observed at the lowest substrate concentration (4 μM of estradiol) in the presence of 6.25 μM of daidzein. At 50 μM daidzein, slight inhibition of estradiol-3-glucuronidation was observed at estradiol concentrations greater than 15 μM. Interestingly, estradiol-3-glucuronidation displayed hyperbolic kinetics in the presence of daidzein, in contrast to the sigmoidal kinetic profile observed for this reaction when estradiol is incubated alone. The curvature noted in the Eadie-Hofstee plot for estradiol-3-glucuronidation in the presence of daidzein disappeared even at the lowest daidzein concentration (3.125 μM). The kinetic model presented in Figure 3.10A (Equation 3.3) adequately described the kinetics of estradiol-3-glucuronidation when co-incubated with daidzein. The estimated kinetic parameters obtained by

fitting the kinetic model (Equation 3.3) to the data are presented in Table 3.2 and the fit of data to Equation 3.3 is illustrated in Figure 3.15B.

Figure 3.15. Effect of daidzein on estradiol-3-glucuronidation

A: Rate percentage of control versus [modifier] plots. Symbols in Figure A represent estradiol concentrations: 4 (●), 6 (○), 8 (▼), 10 (Δ), 15 (■), 20 (□), 25 (♦), 30 (◊), 50 (▲), 75 (▽) μM; B: Surface plot. Generated by fitting a two-site model (Figure 3.10A, Equation 3.3) to the data.

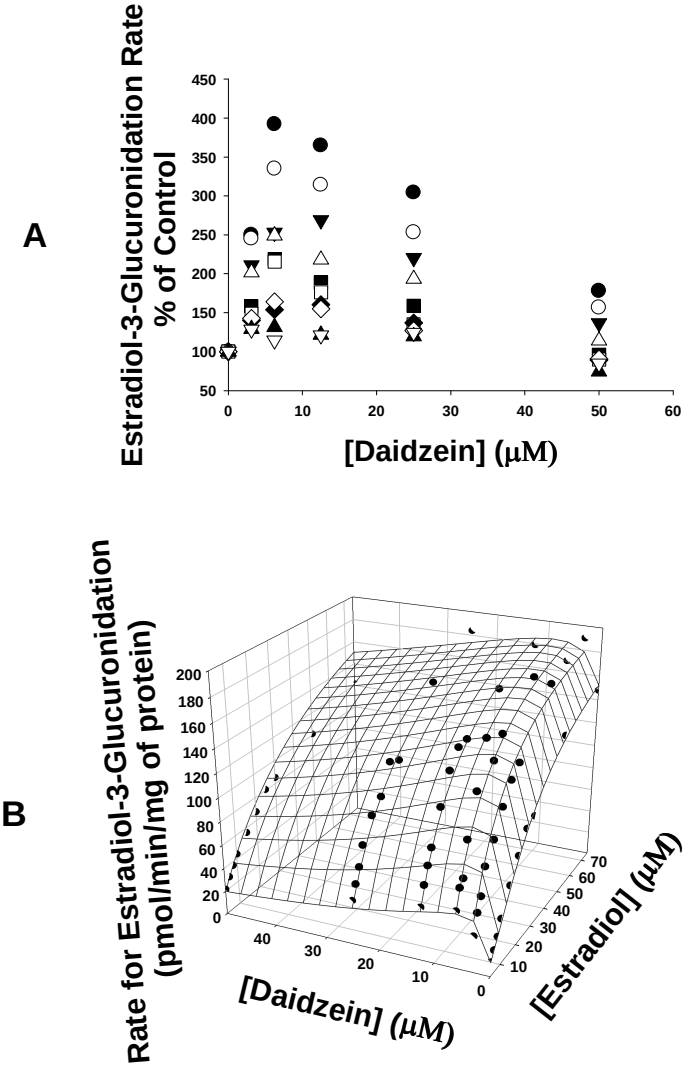

Kinetics of estradiol-3-glucuronidation in the presence of SN-38. The partial inhibition of estradiol-3-glucuronidation during co-incubation with SN-38 noted at 15 μM estradiol led us to further investigate the interactions of SN-38 on the kinetics of estradiol-3-glucuronidation over a range of estradiol concentrations (4μM-75μM). As depicted in Figure 3.16A, partial inhibition by SN-38 was observed at all estradiol concentrations and the extent of the maximum inhibition effect (~40%) was substrate-concentration independent. In addition, SN-38 did not alter the sigmoidicity observed with estradiol-3-glucuronidation by UGT1A1. Applying the Hill equation for analysis of the individual data sets at each inhibitor concentration demonstrated that the Hill coefficient *n* remained constant (CV% for the *n* values was 9%) over the full range of SN-38 concentrations. This was further confirmed graphically by comparison of the Eadie-Hofstee plots of the individual data sets, comparable curvatures were noted (data not shown), again indicating that the sigmoidicity of estradiol-3-glucuronidation did not change in the presence of SN-38. A three-site kinetic model (Figure 3.10B, Equation 3.4) adequately described the kinetics of estradiol-3-glucuronidation in the presence of SN-38. The kinetic parameters derived by simultaneous fitting of all kinetic data with the three-site model are shown in Table 3.2 and the fit is illustrated in Figure 3.16B.

<u>Figure 3.16.</u> Effect of SN-38 on estradiol-3-glucuronidation

A: **Rate percentage of control versus [modifier] plots.** Symbols in Figure A represent estradiol concentrations: 4 (●), 6 (○), 8 (▼), 10 (Δ), 15 (■), 20 (□), 25 (♦), 30 (◊), 50 (▲), 75 (▽) μM. B: **Surface plot.** Generated by fitting a three-site model (Figure 3.10B, Equation 3.4) to the data.

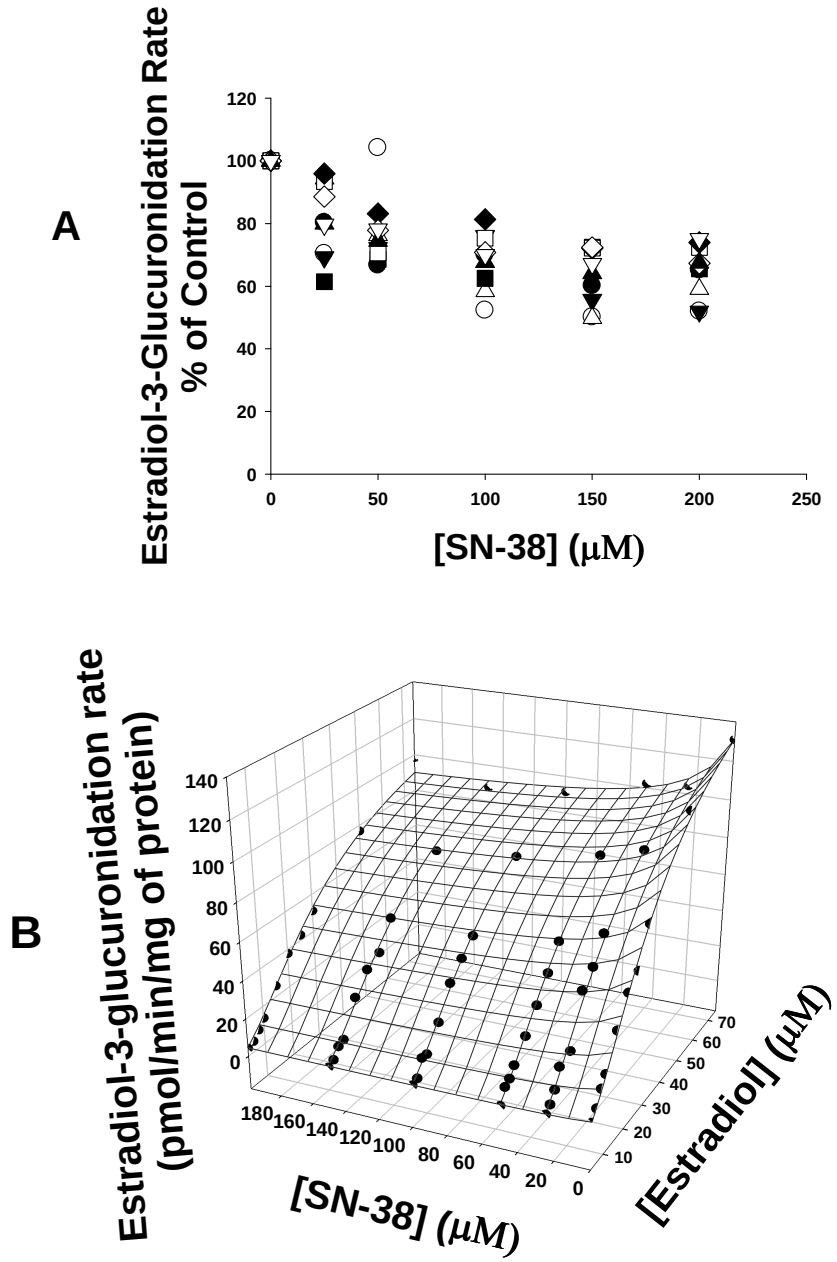

Table 3.2. Kinetic parameters obtained by using multiple-site models to explain the effect of daidzein or SN-38 on estradiol-3-glucuronidation

[a]Standard errors of estimate; [b] Not applicable, K_{sub} and K_{mod} refer to the binding affinity of the substrate and modifier to the enzyme.

Modifier	***V_{max} (pmol/min /mg of protein)***	***K_{sub} (μM)***	***K_{mod} (μM)***	***a***	***c***	***d***	**Kinetic model**	***R^2***
Daidzein	190 (11)[a]	81 (6.3)[a]	6.3 (0.57)[a]	0.11 (0.032)[a]	2.6 (0.22)[a]	N.A.	Equation 3	0.96
SN-38	170 (5.9)[a]	140 (21)[a]	24 (5.4)[a]	0.055 (0.018)[a]	0.65 (0.028)[a]	1.0 (0.11)[a]	Equation 4	0.99

Discussion

It is important to assess the potential for new chemical entities to affect UGT1A1-catalyzed bilirubin glucuronidation. However, due to technical challenges with the incubation and assay of bilirubin, it is desirable to develop alternate probes for this process. An alternate probe must be similar to bilirubin when assessed with a range of compounds that may be potential effectors of this process. Thus the present study evaluated whether estradiol may be an appropriate probe for predicting interactions with UGT1A1-catalyzed bilirubin glucuronidation. Sixteen UGT1A1 substrates or inhibitors, which exhibit a wide range of reported K_m or K_i values and possess diverse chemical structures, were used as model effectors. Their effects on UGT1A1-catalyzed estradiol-3-glucuronidation and bilirubin glucuronidation were evaluated with a recombinant UGT1A1 system. Fourteen of the sixteen compounds inhibited both reactions, with most exhibiting similar IC_{50} values toward both reactions. However, daidzein and ethinylestradiol resulted in concentration-dependent activation of estradiol-3-glucuronidation but not of bilirubin glucuronidation. Furthermore, SN-38, a UGT1A1 substrate, weakly inhibited bilirubin glucuronidation and exhibited only partial inhibition of estradiol-3-glucuronidation. Though differential effects on the two reactions were elicited by daidzein, ethinylestradiol and SN-38, the IC_{50} values of all compounds (SN-38 was excluded because 50% of inhibition was not obtained.) toward the two reactions were highly correlated (R^2=0.83, P<0.0001). This suggests that in general estradiol is a suitable probe for predicting inhibition of bilirubin glucuronidation by UGT1A1. However, for high-throughput screening assays

where one substrate and one effector concentration are used, direct extrapolation may be tenuous since some effectors may activate estradiol-3-glucuronidation but inhibit bilirubin glucuronidation at certain concentrations.

Consistent with previously reports (Fisher et al., 2001; Udomuksorn et al., 2007), in the present study estradiol-3-glucuronidation exhibited a sigmoidal kinetic profile. A widely accepted mechanism for sigmoidal kinetics involves cooperative binding of multiple substrate molecules to the enzyme. (Segel, 1975; Korzekwa et al., 1998; Shou et al., 2001; Houston and Galetin, 2005) Thus, the sigmoidal kinetic profile exhibited by estradiol-3-glucuronidation suggested that two estradiol molecules may bind in the UGT1A1 active site simultaneously. In addition, the presence of atypical kinetics, and by inference, the presence of two binding regions within the active site of UGT1A1, may result in differential inhibition of estradiol-3-glucuronidation depending on the inhibitor employed.

Mutual-inhibition was observed between estradiol and bilirubin. Bilirubin, unlike estradiol, displayed classic hyperbolic (Michaelis-Menten) kinetics. The observation of this type of kinetic profile implies that bilirubin either has one binding site or multiple identical and independent binding sites in UGT1A1 (Korzekwa et al., 1998).Nevertheless, the cross-inhibition between these two substrates together with the high correlation between bilirubin glucuronidation and estradiol-3-glucuronidation in the presence of model effectors suggests that the bilirubin binding region(s) and at least one of the estradiol binding regions are overlapping. In support of this hypothesis, Ciotti et al. conducted site-directed mutagenesis studies and reported that bilirubin and ethinylestradiol bind to

overlapping sites in UGT1A1 (Ciotti and Owens, 1996). Structurally, ethinylestradiol only differs from estradiol by an ethinyl group at the 17-position of the steroidal scaffold. Ethinylestradiol-3-glucuronidation by UGT1A1 also resulted in a sigmoidal kinetic profile with an estimated S_{50} value of 10 μM(Soars et al., 2003), similar to the S_{50} obtained in the present study for estradiol. By inference, it is thus likely that estradiol and ethinylestradiol also share the same multiple binding sites in UGT1A1, at least one of which overlaps with the binding site(s) of bilirubin.

Among the 16 compounds screened in the present study, ethinylestradiol and daidzein exhibited a heteroactivation effect on estradiol-3-glucuronidation. In both cases, the activation effect became less pronounced with increasing concentrations of either compound and at a high enough concentration inhibition of estradiol-3-glucuronidation was observed. This type of concentration-dependent activation/inhibition effect has also been reported with other UGT isoforms (Uchaipichat et al., 2008; Zhou et al.). Daidzein, a major isoflavone component in soy, is a substrate of UGT1A1 (Nielsen and Williamson, 2007). Activation of UGT1A1 activity by daidzein in human liver microsomes has been noted previously by Pfeiffer et al (Pfeiffer et al., 2005). We confirmed a similar concentration-dependent activation/inhibition relationship of daidzein on estradiol-3-glucuronidation with recombinant UGT1A1. Also in agreement with their observations, we noted that the kinetic profile of estradiol-3-glcurondiation in the presence of daidzein displayed a hyperbolic (Michaelis-Menten) kinetic profile (Pfeiffer et al., 2005).

Multiple binding site models have been successfully used to explain various atypical (non-Michaelis-Menten) kinetic phenomena, including heteroactivation (Korzekwa et al., 1998; Shou et al., 2001; Tracy and Hummel, 2004; Houston and Galetin, 2005). In the present study, we applied a two-site kinetic model (Kenworthy et al., 2001) (Figure 3.10A, Equation 3.3) to describe the heteroactivation effect by daidzein. As depicted in Figure 3.10A, both estradiol and daidzein are proposed to bind to two unique sites within UGT1A1 and compete for binding at these sites. The predicted parameter ***a*****,** which reflects changes in binding affinity of estradiol after one molecule of estradiol or daidzein binds to the enzyme, was substantially less than 1, indicating that binding of one molecule of either daidzein or estradiol to the enzyme facilitates the association of a second estradiol molecule to the other binding sites available within the enzyme active site. Additionally, the kinetic parameter ***c***, which is reflective of the formation of estradiol-3-glucuronide from the Estradiol-E-Daidzein complex, was estimated to be 2.6, suggesting that formation of the estradiol-3-glucuronide was 2.6-fold faster from this complex than from the Estradiol-E complex.

Ethinylestradiol also activated estradiol-3-glucuronidation in the present study. However, the magnitude of the effect was much less than observed with daidzein. Ethinylestradiol only slightly stimulated estradiol-3-glucuronidation (maximum of 128% of the control) at 15 μM of estradiol. A similarly modest activation with these compounds was also observed by Mano et al. with recombinant UGT1A1 expressed in baculovirus-infected insect cells (Mano et al., 2007) and by Williams et al with a human liver microsomal preparation (Williams

et al., 2002). Williams et al also noted an increase in the magnitude of activation with decreasing substrate concentrations (Williams et al., 2002). With these results as a guide, we also evaluated the effect of ethinylestradiol on estradiol-3-glucuronidation with 7.5 μM (0.5 S_{50}) of estradiol as substrate and observed a higher activation (up to 140% of the control).

SN-38, the active metabolite of irinotecan (an topoisomerase inhibitor used in cancer therapy) is primarily inactivated via glucuronidation and is a relatively specific UGT1A1 substrate (Mathijssen et al., 2001). SN-38 only partially inhibited estradiol-3-glucuronidation in a substrate-concentration independent manner. To model this type of inhibition, a three-site kinetic model (Houston and Galetin, 2005) was employed wherein SN-38 binds to a distinct site separate from the two binding sites of estradiol (Figure 3.10B, Equation 3.4). In this model, SN-38 did not alter the binding affinity of estradiol to the enzyme since the parameter ***d***, reflective of changes in substrate affinity was estimated to be approximately unity. The inhibition by SN-38 was noted to result solely in a decrease in V_{max}. The parameter ***c*** was estimated to be 0.65, indicating that the effective catalytic rate constant for ESI and ESI_2 was 35% lower than that of the ES complex.

The reported K_m for SN-38 glucuronidation by recombinant UGT1A1 is ~25 μM while it exhibited a hyperbolic kinetic profile (Hanioka et al., 2001). Interestingly, SN-38 only weakly inhibited bilirubin glucuronidation. As described by the Cheng-Prusoff equation, the IC_{50}s obtained at the apparent K_m should be twice the values of the K_i when the inhibition mechanism is competitive (Cheng and

Prusoff, 1973). However, the IC_{50} of SN-38 toward bilirubin glucuronidation was much higher than the predicted binding constant of SN-38 (Table 3.1) and the reported K_m for SN-38 glucuronidation. The discrepancy between the IC_{50} value of SN-38 and the reported K_m for SN-38 glucuronidation or its binding constant obtained in the present study suggest that the inhibition mechanism of SN-38 toward bilirubin glucuronidation was not competitive. It is likely SN-38 also affects bilirubin glucuronidation through a distinct binding site, similar to that predicted for its interaction with estradiol-3-glucuronidation. Lack of inhibition of bilirubin glucuronidation by the UGT1A1 substrate has also been reported by Rios and Tephly with buprenorphine (Rios and Tephly, 2002). These authors postulated that buprenorphine and bilirubin also bind to different domains within UGT1A1 (Rios and Tephly, 2002). It is tempting to speculate that buprenorphine and SN-38 may share the same UGT1A1 binding domain, separate from the binding domain of both bilirubin and estradiol. However, studies of the interaction of buprenorphine and SN-38 would be required to test this hypothesis.

In summary, by evaluating the effects of 16 various UGT1A1 substrates/inhibitors on UGT1A1-catalyzed bilirubin and estradiol-3-glcuruonidation, it was observed that estradiol-3-glucuronidation is an appropriate probe for predicting interactions with bilirubin glucuronidation since only minor disparities in correlation were noted. However, we have clearly identified compounds that are outliers. In addition, multi-site kinetic analysis on the interaction of SN-38 on estradiol-3-glucuronidation suggested that these two UGT1A1 substrates bind to different

bind sites in UGT1A1. These results suggest that multiple probes may still be necessary for predicting UGT1A1 inhibition or activation.

Future Directions

To summarize, kinetic studies with model UGT1A1/UGT1A4 substrates provided compelling evidence on multiple aglycone binding sites in these two glucuronidation enzymes. Thus, it may be necessary to use multiple probe substrates for reaction phenotyping and screening for drug-drug interactions involving UGT1A- and UGT1A4-catalyzed metabolism. In our study with UGT1A1, we found estradiol, a widely-used probe substrate of UGT1A1, is an adequate probe for predicting interactions with UGT1A1-catalyzed bilirubin glucuronidation. However, interactions of SN-38 on estradiol-3-glucuronidation strongly suggested that SN-38 and estradiol bind to different binding site(s) in UGT1A1. Thus, estradiol may not be a good probe for predicting interactions with SN-38 glucuronidation. Correlation study on SN-38 and estradiol-3-glucuronidation in the presence of a battery of UGT1A1 substrates/inhibitor is currently planned in our lab. In addition, because kinetic evidence suggested that SN-38 and estradiol bind to different binding site(s) in UGT1A1 and also because both SN-38 and estradiol are relatively specific substrates for UGT1A1, employment of both SN-38 and estradiol as probe substrates in *in vitro* inhibition study may increase the accuracy for predicting drug-drug interactions. Studies to evaluate SN-38 - estradiol combination in *in vitro* inhibition studies will also be conducted in the future.

For UGT1A4, trifluroperizine and hecogenin is typically used as a probe substrate. However, based on our study with this enzyme, using only one probe substrate in *in vitro* inhibition studies may lead to inaccurate prediction. To

search for a UGT1A4 substrate that may be used together with tripluroperizine in *in vitro* inhibition studies, we will evaluate the effect of a battery of UGT1A4 substrates on trifluroperizine glucuronidation with recombinant UGT1A4. For substrates that do not competitively inhibit trifluroperize glucuronidation, further investigation will be conducted to find out whether they can be used in combination with trifluroperizine in *in vitro* inhibition studies.

In addition, we also plan to conduct a pharmacokinetic study to evaluate the effect of atypical kinetics in vivo. In the present study, we observed a strong heteroactivation effect of daidzein on estradiol-3-glucuronidation (up to 4-fold). Interestingly, the activation effect of daidzein was increased as the substrate (estradiol) concentration was decreased. Because the concentration of estradiol *in vivo* is much lower than the concentration we used *in vitro*, it is likely that *in vivo* we would observe a much higher activation of estradiol-3-glucuronidation by daidzein. Since daidzein is a major isoflavone component in soy, it would be interesting to find out whether consumption of soy food would lead to inter-individual variability in estradiol therapy.

References

Adachi S, Uesugi T and Kamisaka K (1985) Study of bilirubin metabolism by high-performance liquid chromatography: stability of bilirubin glucuronides. *Arch Biochem Biophys* **241:**486-493.

Anderson GD, Yau MK, Gidal BE, Harris SJ, Levy RH, Lai AA, Wolf KB, Wargin WA and Dren AT (1996) Bidirectional interaction of valproate and lamotrigine in healthy subjects. *Clin Pharmacol Ther* **60:**145-156.

Argikar UA (2006) Effects of age, induction, regulation and polymorphisms on the metabolism of antiepileptic drugs, in: *Dept. of Medicinal Chemistry*, pp 227, University of Minnesota, Minneapolis.

Atkins WM (2005) Non-Michaelis-Menten kinetics in cytochrome P450-catalyzed reactions. *Annu Rev Pharmacol Toxicol* **45:**291-310.

Bailey MJ and Dickinson RG (2003) Acyl glucuronide reactivity in perspective: biological consequences. *Chem Biol Interact* **145:**117-137.

Battaglia E, Pritchard M, Ouzzine M, Fournel-Gigleux S, Radominska A, Siest G and Magdalou J (1994) Chemical modification of human UDP-glucuronosyltransferase UGT1*6 by diethyl pyrocarbonate: possible involvement of a histidine residue in the catalytic process. *Arch Biochem Biophys* **309:**266-272.

Beaulieu M, Levesque E, Hum DW and Belanger A (1998) Isolation and characterization of a human orphan UDP-glucuronosyltransferase, UGT2B11. *Biochem Biophys Res Commun* **248:**44-50.

Belanger A, Pelletier G, Labrie F, Barbier O and Chouinard S (2003) Inactivation of androgens by UDP-glucuronosyltransferase enzymes in humans. *Trends Endocrinol Metab* **14:**473-479.

Benoit-Biancamano MO, Adam JP, Bernard O, Court MH, Leblanc MH, Caron P and Guillemette C (2009) A pharmacogenetics study of the human glucuronosyltransferase UGT1A4. *Pharmacogenet Genomics*.

Bernard P, Goudonnet H, Artur Y, Desvergne B and Wahli W (1999) Activation of the mouse TATA-less and human TATA-containing UDP-glucuronosyltransferase 1A1 promoters by hepatocyte nuclear factor 1. *Mol Pharmacol* **56:**526-536.

Black M, Billing BH and Heirwegh KP (1970) Determination of bilirubin UDP-glucuronyl transferase activity in needle-biopsy specimens of human liver. *Clin Chim Acta* **29:**27-35.

Blanckaert N, Compernolle F, Leroy P, Van Houtte R, Fevery J and Heirwegh KP (1978) The fate of bilirubin-IXalpha glucuronide in cholestasis and during storage in vitro. Intramolecular rearrangement to positional isomers of glucuronic acid. *Biochem J* **171:**203-214.

Blanckaert N, Gollan J and Schmid R (1979) Bilirubin diglucuronide synthesis by a UDP-glucuronic acid-dependent enzyme system in rat liver microsomes. *Proc Natl Acad Sci U S A* **76:**2037-2041.

Bock KW (1992) Metabolic polymorphisms affecting activation of toxic and mutagenic arylamines. *Trends Pharmacol Sci* **13:**223-226.

Bock KW, Burchell B, Guillemette C, Mackenzie PI, Nebert DW, Court M and Owens I (Date Accessed: July 2010) UGT Alleles Nomenclature Home Page: http://www.ugtalleles.ulaval.ca.

Bock KW and Kohle C (2009) Topological aspects of oligomeric UDP-glucuronosyltransferases in endoplasmic reticulum membranes: advances and open questions. *Biochem Pharmacol* **77:**1458-1465.

Brierley CH and Burchell B (1993) Human UDP-glucuronosyl transferases: chemical defence, jaundice and gene therapy. *Bioessays* **15:**749-754.

Chen G, Dellinger RW, Sun D, Spratt TE and Lazarus P (2008) Glucuronidation of tobacco-specific nitrosamines by UGT2B10. *Drug Metab Dispos* **36:**824-830.

Chen H, Yang K, Choi S, Fischer JH and Jeong H (2009) Up-regulation of UDP-glucuronosyltransferase (UGT) 1A4 by 17beta-estradiol: a potential mechanism of increased lamotrigine elimination in pregnancy. *Drug Metab Dispos* **37:**1841-1847.

Cheng Y and Prusoff WH (1973) Relationship between the inhibition constant (K1) and the concentration of inhibitor which causes 50 per cent inhibition (I50) of an enzymatic reaction. *Biochem Pharmacol* **22:**3099-3108.

Chouinard S, Tessier M, Vernouillet G, Gauthier S, Labrie F, Barbier O and Belanger A (2006) Inactivation of the pure antiestrogen fulvestrant and other synthetic estrogen molecules by UDP-glucuronosyltransferase 1A enzymes expressed in breast tissue. *Mol Pharmacol* **69:**908-920.

Ciotti M, Cho JW, George J and Owens IS (1998) Required buried alpha-helical structure in the bilirubin UDP-glucuronosyltransferase, UGT1A1, contains a nonreplaceable phenylalanine. *Biochemistry* **37:**11018-11025.

Ciotti M and Owens IS (1996) Evidence for overlapping active sites for 17 alpha-ethynlestradiol and bilirubin in the human major bilirubin UDPglucuronosyltransferase. *Biochemistry* **35:**10119-10124.

Collom SL, Laddusaw RM, Burch AM, Kuzmic P, Perry MD, Jr. and Miller GP (2008) CYP2E1 substrate inhibition. Mechanistic interpretation through an effector site for monocyclic compounds. *J Biol Chem* **283:**3487-3496.

Court MH (2005) Isoform-selective probe substrates for in vitro studies of human UDP-glucuronosyltransferases. *Methods Enzymol* **400:**104-116.

Crawford JM, Ransil BJ, Narciso JP and Gollan JL (1992) Hepatic microsomal bilirubin UDP-glucuronosyltransferase. The kinetics of bilirubin mono- and diglucuronide synthesis. *J Biol Chem* **267:**16943-16950.

De Ewenson IW, Gianturco FA and Gramaccioni P (1966) On the stability of bilirubin. *Experientia* **22:**14-15.

Domanski TL, He YA, Harlow GR and Halpert JR (2000) Dual role of human cytochrome P450 3A4 residue Phe-304 in substrate specificity and cooperativity. *J Pharmacol Exp Ther* **293:**585-591.

Doumas BT, Perry BW, Sasse EA and Straumfjord JV, Jr. (1973) Standardization in bilirubin assays: evaluation of selected methods and stability of bilirubin solutions. *Clin Chem* **19:**984-993.

Ehmer U, Vogel A, Schutte JK, Krone B, Manns MP and Strassburg CP (2004) Variation of hepatic glucuronidation: Novel functional polymorphisms of the UDP-glucuronosyltransferase UGT1A4. *Hepatology* **39:**970-977.

Fallon JK, Harbourt DE, Maleki SH, Kessler FK, Ritter JK and Smith PC (2008) Absolute quantification of human uridine-diphosphate glucuronosyl transferase (UGT) enzyme isoforms 1A1 and 1A6 by tandem LC-MS. *Drug Metab Lett* **2:**210-222.

Fisher B, Costantino JP, Wickerham DL, Redmond CK, Kavanah M, Cronin WM, Vogel V, Robidoux A, Dimitrov N, Atkins J, Daly M, Wieand S, Tan-Chiu E, Ford L and Wolmark N (1998) Tamoxifen for prevention of breast cancer: report of the National Surgical Adjuvant Breast and Bowel Project P-1 Study. *J Natl Cancer Inst* **90:**1371-1388.

Fisher MB, Paine MF, Strelevitz TJ and Wrighton SA (2001) The role of hepatic and extrahepatic UDP-glucuronosyltransferases in human drug metabolism. *Drug Metab Rev* **33:**273-297.

Flockhart D (2008) CYP2D6 genotyping and the pharmacogenetics of tamoxifen. *Clin Adv Hematol Oncol* **6:**493-494.

Fujiwara R, Nakajima M, Yamanaka H, Katoh M and Yokoi T (2007) Interactions between human UGT1A1, UGT1A4, and UGT1A6 affect their enzymatic activities. *Drug Metab Dispos* **35:**1781-1787.

Fujiwara R, Nakajima M, Yamanaka H, Katoh M and Yokoi T (2008) Product inhibition of UDP-glucuronosyltransferase (UGT) enzymes by UDP

obfuscates the inhibitory effects of UGT substrates. *Drug Metab Dispos* **36:**361-367.

Galetin A, Clarke SE and Houston JB (2002) Quinidine and haloperidol as modifiers of CYP3A4 activity: multisite kinetic model approach. *Drug Metab Dispos* **30:**1512-1522.

Gallicano KD, Sahai J, Shukla VK, Seguin I, Pakuts A, Kwok D, Foster BC and Cameron DW (1999) Induction of zidovudine glucuronidation and amination pathways by rifampicin in HIV-infected patients. *Br J Clin Pharmacol* **48:**168-179.

Ghosh SS, Sappal BS, Kalpana GV, Lee SW, Chowdhury JR and Chowdhury NR (2001) Homodimerization of human bilirubin-uridine-diphosphoglucuronate glucuronosyltransferase-1 (UGT1A1) and its functional implications. *J Biol Chem* **276:**42108-42115.

Gong QH, Cho JW, Huang T, Potter C, Gholami N, Basu NK, Kubota S, Carvalho S, Pennington MW, Owens IS and Popescu NC (2001) Thirteen UDPglucuronosyltransferase genes are encoded at the human UGT1 gene complex locus. *Pharmacogenetics* **11:**357-368.

Gordon ER and Goresky CA (1980) The formation of bilirubin diglucuronide by rat liver microsomal preparations. *Can J Biochem* **58:**1302-1310.

Gordon ER, Sommerer U and Goresky CA (1983) The hepatic microsomal formation of bilirubin diglucuronide. *J Biol Chem* **258:**15028-15036.

Green MD and Tephly TR (1996) Glucuronidation of amines and hydroxylated xenobiotics and endobiotics catalyzed by expressed human UGT1.4 protein. *Drug Metab Dispos* **24:**356-363.

Gregory PA and Mackenzie PI (2002) The homeodomain Pbx2-Prep1 complex modulates hepatocyte nuclear factor 1alpha-mediated activation of the UDP-glucuronosyltransferase 2B17 gene. *Mol Pharmacol* **62:**154-161.

Guillemette C (2003) Pharmacogenomics of human UDP-glucuronosyltransferase enzymes. *Pharmacogenomics J* **3:**136-158.

Gupta B, LeVea C, Litwin A and Fakih MG (2007) Reversible grade 4 hyperbilirubinemia in a patient with UGT1A1 7/7 genotype treated with irinotecan and cetuximab. *Clin Colorectal Cancer* **6:**447-449.

Hallifax D and Houston JB (2006) Binding of drugs to hepatic microsomes: comment and assessment of current prediction methodology with recommendation for improvement. *Drug Metab Dispos* **34:**724-726; author reply 727.

Hanioka N, Ozawa S, Jinno H, Ando M, Saito Y and Sawada J (2001) Human liver UDP-glucuronosyltransferase isoforms involved in the glucuronidation of 7-ethyl-10-hydroxycamptothecin. *Xenobiotica* **31:**687-699.

Harlow GR and Halpert JR (1997) Alanine-scanning mutagenesis of a putative substrate recognition site in human cytochrome P450 3A4. Role of residues 210 and 211 in flavonoid activation and substrate specificity. *J Biol Chem* **272:**5396-5402.

Harlow GR and Halpert JR (1998) Analysis of human cytochrome P450 3A4 cooperativity: construction and characterization of a site-directed mutant that displays hyperbolic steroid hydroxylation kinetics. *Proc Natl Acad Sci U S A* **95:**6636-6641.

Hashizume T, Xu Y, Mohutsky MA, Alberts J, Hadden C, Kalhorn TF, Isoherranen N, Shuhart MC and Thummel KE (2008) Identification of human UDP-glucuronosyltransferases catalyzing hepatic 1alpha,25-dihydroxyvitamin D3 conjugation. *Biochem Pharmacol* **75:**1240-1250.

He YA, Roussel F and Halpert JR (2003) Analysis of homotropic and heterotropic cooperativity of diazepam oxidation by CYP3A4 using site-directed mutagenesis and kinetic modeling. *Arch Biochem Biophys* **409:**92-101.

Heirwegh KP, Van de Vijver M and Fevery J (1972) Assay and properties of dititonin-activated bilirubin uridine diphosphate glucuronyltransferase from rat liver. *Biochem J* **129:**605-618.

Houston JB and Galetin A (2005) Modelling atypical CYP3A4 kinetics: principles and pragmatism. *Arch Biochem Biophys* **433:**351-360.

Houston JB and Kenworthy KE (2000) In vitro-in vivo scaling of CYP kinetic data not consistent with the classical Michaelis-Menten model. *Drug Metab Dispos* **28:**246-254.

Huber W and Koella JC (1993) A comparison of three methods of estimating EC50 in studies of drug resistance of malaria parasites. *Acta Trop* **55:**257-261.

Hutzler JM, Hauer MJ and Tracy TS (2001) Dapsone activation of CYP2C9-mediated metabolism: evidence for activation of multiple substrates and a two-site model. *Drug Metab Dispos* **29:**1029-1034.

Hutzler JM, Kolwankar D, Hummel MA and Tracy TS (2002) Activation of CYP2C9-mediated metabolism by a series of dapsone analogs: kinetics and structural requirements. *Drug Metab Dispos* **30:**1194-1200.

Hutzler JM, Wienkers LC, Wahlstrom JL, Carlson TJ and Tracy TS (2003) Activation of cytochrome P450 2C9-mediated metabolism: mechanistic evidence in support of kinetic observations. *Arch Biochem Biophys* **410:**16-24.

Hyland R, Osborne T, Payne A, Kempshall S, Logan YR, Ezzeddine K and Jones B (2009) In vitro and in vivo glucuronidation of midazolam in humans. *Br J Clin Pharmacol* **67:**445-454.

Ikushiro S, Emi Y and Iyanagi T (1997) Protein-protein interactions between UDP-glucuronosyltransferase isozymes in rat hepatic microsomes. *Biochemistry* **36:**7154-7161.

Ishii Y, Hansen AJ and Mackenzie PI (2000) Octamer transcription factor-1 enhances hepatic nuclear factor-1alpha-mediated activation of the human UDP glucuronosyltransferase 2B7 promoter. *Mol Pharmacol* **57:**940-947.

Iwuchukwu OF and Nagar S (2008) Resveratrol (trans-resveratrol, 3,5,4'-trihydroxy-trans-stilbene) glucuronidation exhibits atypical enzyme kinetics in various protein sources. *Drug Metab Dispos* **36:**322-330.

Jackson MR, Fournel-Gigleux S, Harding D and Burchell B (1988) Examination of the substrate specificity of cloned rat kidney phenol UDP-glucuronyltransferase expressed in COS-7 cells. *Mol Pharmacol* **34:**638-642.

Jansen PL (1973) The isomerisation of bilirubin monoglucuronide. *Clin Chim Acta* **49:**233-240.

Johnson EF, Schwab GE and Vickery LE (1988) Positive effectors of the binding of an active site-directed amino steroid to rabbit cytochrome P-450 3c. *J Biol Chem* **263:**17672-17677.

Kadakol A, Ghosh SS, Sappal BS, Sharma G, Chowdhury JR and Chowdhury NR (2000) Genetic lesions of bilirubin uridine-diphosphoglucuronate glucuronosyltransferase (UGT1A1) causing Crigler-Najjar and Gilbert syndromes: correlation of genotype to phenotype. *Hum Mutat* **16:**297-306.

Kaku T, Ogura K, Nishiyama T, Ohnuma T, Muro K and Hiratsuka A (2004) Quaternary ammonium-linked glucuronidation of tamoxifen by human liver microsomes and UDP-glucuronosyltransferase 1A4. *Biochem Pharmacol* **67:**2093-2102.

Kamisako T (2004) What is Gilbert's syndrome? Lesson from genetic polymorphisms of UGT1A1 in Gilbert's syndrome from Asia. *J Gastroenterol Hepatol* **19:**955-957.

Kamisako T, Kobayashi Y, Takeuchi K, Ishihara T, Higuchi K, Tanaka Y, Gabazza EC and Adachi Y (2000) Recent advances in bilirubin

metabolism research: the molecular mechanism of hepatocyte bilirubin transport and its clinical relevance. *J Gastroenterol* **35:**659-664.

Kenworthy KE, Bloomer JC, Clarke SE and Houston JB (1999) CYP3A4 drug interactions: correlation of 10 in vitro probe substrates. *Br J Clin Pharmacol* **48:**716-727.

Kenworthy KE, Clarke SE, Andrews J and Houston JB (2001) Multisite kinetic models for CYP3A4: simultaneous activation and inhibition of diazepam and testosterone metabolism. *Drug Metab Dispos* **29:**1644-1651.

Khan KK, He YQ, Domanski TL and Halpert JR (2002) Midazolam oxidation by cytochrome P450 3A4 and active-site mutants: an evaluation of multiple binding sites and of the metabolic pathway that leads to enzyme inactivation. *Mol Pharmacol* **61:**495-506.

Kiang TK, Ensom MH and Chang TK (2005) UDP-glucuronosyltransferases and clinical drug-drug interactions. *Pharmacol Ther* **106:**97-132.

King CD, Rios GR, Green MD and Tephly TR (2000) UDP-glucuronosyltransferases. *Curr Drug Metab* **1:**143-161.

Koley AP, Buters JT, Robinson RC, Markowitz A and Friedman FK (1995a) CO binding kinetics of human cytochrome P450 3A4. Specific interaction of substrates with kinetically distinguishable conformers. *J Biol Chem* **270:**5014-5018.

Koley AP, Buters JT, Robinson RC, Markowitz A and Friedman FK (1997a) Differential mechanisms of cytochrome P450 inhibition and activation by alpha-naphthoflavone. *J Biol Chem* **272:**3149-3152.

Koley AP, Robinson RC, Markowitz A and Friedman FK (1995b) Interaction of polycyclic aromatic hydrocarbons and flavones with cytochromes P450 in the endoplasmic reticulum: effect on CO binding kinetics. *Biochemistry* **34:**1942-1947.

Koley AP, Robinson RC, Markowitz A and Friedman FK (1997b) Drug-drug interactions: effect of quinidine on nifedipine binding to human cytochrome P450 3A4. *Biochem Pharmacol* **53:**455-460.

Korzekwa KR, Krishnamachary N, Shou M, Ogai A, Parise RA, Rettie AE, Gonzalez FJ and Tracy TS (1998) Evaluation of atypical cytochrome P450 kinetics with two-substrate models: evidence that multiple substrates can simultaneously bind to cytochrome P450 active sites. *Biochemistry* **37:**4137-4147.

Kumar V, Wahlstrom JL, Rock DA, Warren CJ, Gorman LA and Tracy TS (2006) CYP2C9 inhibition: impact of probe selection and pharmacogenetics on in vitro inhibition profiles. *Drug Metab Dispos* **34:**1966-1975.

Kurkela M, Garcia-Horsman JA, Luukkanen L, Morsky S, Taskinen J, Baumann M, Kostiainen R, Hirvonen J and Finel M (2003) Expression and characterization of recombinant human UDP-glucuronosyltransferases (UGTs). UGT1A9 is more resistant to detergent inhibition than other UGTs and was purified as an active dimeric enzyme. *J Biol Chem* **278:**3536-3544.

Lankisch TO, Moebius U, Wehmeier M, Behrens G, Manns MP, Schmidt RE and Strassburg CP (2006) Gilbert's disease and atazanavir: from phenotype to UDP-glucuronosyltransferase haplotype. *Hepatology* **44:**1324-1332.

Lepine J, Bernard O, Plante M, Tetu B, Pelletier G, Labrie F, Belanger A and Guillemette C (2004) Specificity and regioselectivity of the conjugation of estradiol, estrone, and their catecholestrogen and methoxyestrogen metabolites by human uridine diphospho-glucuronosyltransferases expressed in endometrium. *J Clin Endocrinol Metab* **89:**5222-5232.

Levesque E, Beaulieu M, Hum DW and Belanger A (1999) Characterization and substrate specificity of UGT2B4 (E458): a UDP-glucuronosyltransferase encoded by a polymorphic gene. *Pharmacogenetics* **9:**207-216.

Lichtsteiner S, Wuarin J and Schibler U (1987) The interplay of DNA-binding proteins on the promoter of the mouse albumin gene. *Cell* **51:**963-973.

Lin JH and Wong BK (2002) Complexities of glucuronidation affecting in vitro in vivo extrapolation. *Curr Drug Metab* **3:**623-646.

Lin Y, Lu P, Tang C, Mei Q, Sandig G, Rodrigues AD, Rushmore TH and Shou M (2001) Substrate inhibition kinetics for cytochrome P450-catalyzed reactions. *Drug Metab Dispos* **29:**368-374.

Lotsch J and Geisslinger G (2001) Morphine-6-glucuronide: an analgesic of the future? *Clin Pharmacokinet* **40:**485-499.

Luukkanen L, Taskinen J, Kurkela M, Kostiainen R, Hirvonen J and Finel M (2005) Kinetic characterization of the 1A subfamily of recombinant human UDP-glucuronosyltransferases. *Drug Metab Dispos* **33:**1017-1026.

Mackenzie P, Little JM and Radominska-Pandya A (2003a) Glucosidation of hyodeoxycholic acid by UDP-glucuronosyltransferase 2B7. *Biochem Pharmacol* **65:**417-421.

Mackenzie PI, Bock KW, Burchell B, Guillemette C, Ikushiro S, Iyanagi T, Miners JO, Owens IS and Nebert DW (2005) Nomenclature update for the mammalian UDP glycosyltransferase (UGT) gene superfamily. *Pharmacogenet Genomics* **15:**677-685.

Mackenzie PI, Gregory PA, Gardner-Stephen DA, Lewinsky RH, Jorgensen BR, Nishiyama T, Xie W and Radominska-Pandya A (2003b) Regulation of UDP glucuronosyltransferase genes. *Curr Drug Metab* **4:**249-257.

Malik S, Arif H and Hirsch LJ (2006) Lamotrigine and its applications in the treatment of epilepsy and other neurological and psychiatric disorders. *Expert Rev Neurother* **6:**1609-1627.

Mano Y, Usui T and Kamimura H (2004) Effects of beta-estradiol and propofol on the 4-methylumbelliferone glucuronidation in recombinant human UGT isozymes 1A1, 1A8 and 1A9. *Biopharm Drug Dispos* **25:**339-344.

Mano Y, Usui T and Kamimura H (2007) Substrate-dependent modulation of UDP-glucuronosyltransferase 1A1 (UGT1A1) by propofol in recombinant human UGT1A1 and human liver microsomes. *Basic Clin Pharmacol Toxicol* **101:**211-214.

Marcuello E, Altes A, Menoyo A, Del Rio E, Gomez-Pardo M and Baiget M (2004) UGT1A1 gene variations and irinotecan treatment in patients with metastatic colorectal cancer. *Br J Cancer* **91:**678-682.

Mathijssen RH, van Alphen RJ, Verweij J, Loos WJ, Nooter K, Stoter G and Sparreboom A (2001) Clinical pharmacokinetics and metabolism of irinotecan (CPT-11). *Clin Cancer Res* **7:**2182-2194.

Miley MJ, Zielinska AK, Keenan JE, Bratton SM, Radominska-Pandya A and Redinbo MR (2007) Crystal structure of the cofactor-binding domain of the human phase II drug-metabolism enzyme UDP-glucuronosyltransferase 2B7. *J Mol Biol* **369:**498-511.

Miners JO, Knights KM, Houston JB and Mackenzie PI (2006) In vitro-in vivo correlation for drugs and other compounds eliminated by glucuronidation in humans: pitfalls and promises. *Biochem Pharmacol* **71:**1531-1539.

Miners JO, Mackenzie PI and Knights KM (2010) The prediction of drug-glucuronidation parameters in humans: UDP-glucuronosyltransferase enzyme-selective substrate and inhibitor probes for reaction phenotyping and in vitro-in vivo extrapolation of drug clearance and drug-drug interaction potential. *Drug Metab Rev* **42:**189-201.

Miners JO, Smith PA, Sorich MJ, McKinnon RA and Mackenzie PI (2004) Predicting human drug glucuronidation parameters: application of in vitro and in silico modeling approaches. *Annu Rev Pharmacol Toxicol* **44:**1-25.

Mori A, Maruo Y, Iwai M, Sato H and Takeuchi Y (2005) UDP-glucuronosyltransferase 1A4 polymorphisms in a Japanese population and kinetics of clozapine glucuronidation. *Drug Metab Dispos* **33:**672-675.

Morrell MJ, Isojarvi J, Taylor AE, Dam M, Ayala R, Gomez G, O'Neill F, Tennis P and Messenheimer J (2003) Higher androgens and weight gain with

valproate compared with lamotrigine for epilepsy. *Epilepsy Res* **54:**189-199.

Nakamura A, Nakajima M, Yamanaka H, Fujiwara R and Yokoi T (2008) Expression of UGT1A and UGT2B mRNA in human normal tissues and various cell lines. *Drug Metab Dispos* **36:**1461-1464.

Nielsen IL and Williamson G (2007) Review of the factors affecting bioavailability of soy isoflavones in humans. *Nutr Cancer* **57:**1-10.

Oelberg DG, Chari MV, Little JM, Adcock EW and Lester R (1984) Lithocholate glucuronide is a cholestatic agent. *J Clin Invest* **73:**1507-1514.

Ohman I, Luef G and Tomson T (2008) Effects of pregnancy and contraception on lamotrigine disposition: new insights through analysis of lamotrigine metabolites. *Seizure* **17:**199-202.

Ohno S, Kawana K and Nakajin S (2008) Contribution of UDP-glucuronosyltransferase 1A1 and 1A8 to morphine-6-glucuronidation and its kinetic properties. *Drug Metab Dispos* **36:**688-694.

Ohno S and Nakajin S (2009) Determination of mRNA expression of human UDP-glucuronosyltransferases and application for localization in various human tissues by real-time reverse transcriptase-polymerase chain reaction. *Drug Metab Dispos* **37:**32-40.

Onoue M, Terada T, Kobayashi M, Katsura T, Matsumoto S, Yanagihara K, Nishimura T, Kanai M, Teramukai S, Shimizu A, Fukushima M and Inui K (2009) UGT1A1*6 polymorphism is most predictive of severe neutropenia

induced by irinotecan in Japanese cancer patients. *Int J Clin Oncol* **14:**136-142.

Operana TN and Tukey RH (2007) Oligomerization of the UDP-glucuronosyltransferase 1A proteins: homo- and heterodimerization analysis by fluorescence resonance energy transfer and co-immunoprecipitation. *J Biol Chem* **282:**4821-4829.

Osborne CK (1998) Tamoxifen in the treatment of breast cancer. *N Engl J Med* **339:**1609-1618.

Pasqualini JR, Gelly C, Nguyen BL and Vella C (1989) Importance of estrogen sulfates in breast cancer. *J Steroid Biochem* **34:**155-163.

Pennell PB, Newport DJ, Stowe ZN, Helmers SL, Montgomery JQ and Henry TR (2004) The impact of pregnancy and childbirth on the metabolism of lamotrigine. *Neurology* **62:**292-295.

Peters WH and Jansen PL (1986) Microsomal UDP-glucuronyltransferase-catalyzed bilirubin diglucuronide formation in human liver. *J Hepatol* **2:**182-194.

Peters WH, Jansen PL and Nauta H (1984) The molecular weights of UDP-glucuronyltransferase determined with radiation-inactivation analysis. A molecular model of bilirubin UDP-glucuronyltransferase. *J Biol Chem* **259:**11701-11705.

Pfeiffer E, Treiling CR, Hoehle SI and Metzler M (2005) Isoflavones modulate the glucuronidation of estradiol in human liver microsomes. *Carcinogenesis* **26:**2172-2178.

Radominska-Pandya A, Bratton S and Little JM (2005) A historical overview of the heterologous expression of mammalian UDP-glucuronosyltransferase isoforms over the past twenty years. *Curr Drug Metab* **6:**141-160.

Radominska-Pandya A, Czernik PJ, Little JM, Battaglia E and Mackenzie PI (1999) Structural and functional studies of UDP-glucuronosyltransferases. *Drug Metab Rev* **31:**817-899.

Reimers A, Helde G and Brodtkorb E (2005) Ethinyl estradiol, not progestogens, reduces lamotrigine serum concentrations. *Epilepsia* **46:**1414-1417.

Remmel RP, Zhou J and Upendra AA (2008) UDP-Glucuronosyltransferases, in: *Drug-Drug Interactions (2nd Edition)* (Rodrigues D ed), pp 87-133, Informa Healthcare USA, Inc., New York.

Rios GR and Tephly TR (2002) Inhibition and active sites of UDP-glucuronosyltransferases 2B7 and 1A1. *Drug Metab Dispos* **30:**1364-1367.

Rock DA, Perkins BN, Wahlstrom J and Jones JP (2003) A method for determining two substrates binding in the same active site of cytochrome P450BM3: an explanation of high energy omega product formation. *Arch Biochem Biophys* **416:**9-16.

Rotger M, Taffe P, Bleiber G, Gunthard HF, Furrer H, Vernazza P, Drechsler H, Bernasconi E, Rickenbach M and Telenti A (2005) Gilbert syndrome and the development of antiretroviral therapy-associated hyperbilirubinemia. *J Infect Dis* **192:**1381-1386.

Rowland A, Elliot DJ, Knights KM, Mackenzie PI and Miners JO (2008) The "albumin effect" and in vitro-in vivo extrapolation: sequestration of long-chain unsaturated fatty acids enhances phenytoin hydroxylation by human liver microsomal and recombinant cytochrome P450 2C9. *Drug Metab Dispos* **36:**870-877.

Rowland A, Elliot DJ, Williams JA, Mackenzie PI, Dickinson RG and Miners JO (2006) In vitro characterization of lamotrigine N2-glucuronidation and the lamotrigine-valproic acid interaction. *Drug Metab Dispos* **34:**1055-1062.

Rowland A, Knights KM, Mackenzie PI and Miners JO (2009) Characterization of the binding of drugs to human intestinal fatty acid binding protein (IFABP): potential role of IFABP as an alternative to albumin for in vitro-in vivo extrapolation of drug kinetic parameters. *Drug Metab Dispos* **37:**1395-1403.

Saeki M, Saito Y, Jinno H, Sai K, Hachisuka A, Kaniwa N, Ozawa S, Kawamoto M, Kamatani N, Shirao K, Minami H, Ohtsu A, Yoshida T, Saijo N, Komamura K, Kotake T, Morishita H, Kamakura S, Kitakaze M, Tomoike H and Sawada J (2005) Genetic variations and haplotypes of UGT1A4 in a Japanese population. *Drug Metab Pharmacokinet* **20:**144-151.

Schrag ML and Wienkers LC (2001) Triazolam substrate inhibition: evidence of competition for heme-bound reactive oxygen within the CYP3A4 active site. *Adv Exp Med Biol* **500:**347-350.

Schwab GE, Raucy JL and Johnson EF (1988) Modulation of rabbit and human hepatic cytochrome P-450-catalyzed steroid hydroxylations by alpha-naphthoflavone. *Mol Pharmacol* **33:**493-499.

Segel I (1993) *Enzyme Kinetics: Behavior and Analysis of Rapid Equilibrium and Steady-State Enzyme Systems*. Wiley Classics Library, Ney Jersey.

Segel IH (1975) *Enzyme Kinetics: Behavior and Analysis of Rapid Equilibrium and Steady-State Enzyme Systems*. John Wiley & Sons, Inc. .

Senafi SB, Clarke DJ and Burchell B (1994) Investigation of the substrate specificity of a cloned expressed human bilirubin UDP-glucuronosyltransferase: UDP-sugar specificity and involvement in steroid and xenobiotic glucuronidation. *Biochem J* **303 (Pt 1):**233-240.

Senay C, Battaglia E, Chen G, Breton R, Fournel-Gigleux S, Magdalou J and Radominska-Pandya A (1999) Photoaffinity labeling of the aglycon binding site of the recombinant human liver UDP-glucuronosyltransferase UGT1A6 with 7-azido-4-methylcoumarin. *Arch Biochem Biophys* **368:**75-84.

Senay C, Ouzzine M, Battaglia E, Pless D, Cano V, Burchell B, Radominska A, Magdalou J and Fournel-Gigleux S (1997) Arginine 52 and histidine 54 located in a conserved amino-terminal hydrophobic region (LX2-R52-G-H54-X3-V-L) are important amino acids for the functional and structural integrity of the human liver UDP-glucuronosyltransferase UGT1*6. *Mol Pharmacol* **51:**406-413.

Seppen J, Bosma PJ, Goldhoorn BG, Bakker CT, Chowdhury JR, Chowdhury NR, Jansen PL and Oude Elferink RP (1994) Discrimination between Crigler-Najjar type I and II by expression of mutant bilirubin uridine diphosphate-glucuronosyltransferase. *J Clin Invest* **94:**2385-2391.

Shou M, Grogan J, Mancewicz JA, Krausz KW, Gonzalez FJ, Gelboin HV and Korzekwa KR (1994) Activation of CYP3A4: evidence for the simultaneous binding of two substrates in a cytochrome P450 active site. *Biochemistry* **33:**6450-6455.

Shou M, Lin Y, Lu P, Tang C, Mei Q, Cui D, Tang W, Ngui JS, Lin CC, Singh R, Wong BK, Yergey JA, Lin JH, Pearson PG, Baillie TA, Rodrigues AD and Rushmore TH (2001) Enzyme kinetics of cytochrome P450-mediated reactions. *Curr Drug Metab* **2:**17-36.

Shou M, Mei Q, Ettore MW, Jr., Dai R, Baillie TA and Rushmore TH (1999) Sigmoidal kinetic model for two co-operative substrate-binding sites in a cytochrome P450 3A4 active site: an example of the metabolism of diazepam and its derivatives. *Biochem J* **340 (Pt 3):**845-853.

Sidhu J, Job S, Singh S and Philipson R (2006) The pharmacokinetic and pharmacodynamic consequences of the co-administration of lamotrigine and a combined oral contraceptive in healthy female subjects. *Br J Clin Pharmacol* **61:**191-199.

Soars MG, Ring BJ and Wrighton SA (2003) The effect of incubation conditions on the enzyme kinetics of udp-glucuronosyltransferases. *Drug Metab Dispos* **31:**762-767.

Stone AN, Mackenzie PI, Galetin A, Houston JB and Miners JO (2003) Isoform selectivity and kinetics of morphine 3- and 6-glucuronidation by human udp-glucuronosyltransferases: evidence for atypical glucuronidation kinetics by UGT2B7. *Drug Metab Dispos* **31:**1086-1089.

Strassburg CP (2008) Pharmacogenetics of Gilbert's syndrome. *Pharmacogenomics* **9:**703-715.

Strassburg CP, Kneip S, Topp J, Obermayer-Straub P, Barut A, Tukey RH and Manns MP (2000) Polymorphic gene regulation and interindividual variation of UDP-glucuronosyltransferase activity in human small intestine. *J Biol Chem* **275:**36164-36171.

Strassburg CP, Manns MP and Tukey RH (1998) Expression of the UDP-glucuronosyltransferase 1A locus in human colon. Identification and characterization of the novel extrahepatic UGT1A8. *J Biol Chem* **273:**8719-8726.

Strassburg CP, Oldhafer K, Manns MP and Tukey RH (1997) Differential expression of the UGT1A locus in human liver, biliary, and gastric tissue: identification of UGT1A7 and UGT1A10 transcripts in extrahepatic tissue. *Mol Pharmacol* **52:**212-220.

Sun D, Chen G, Dellinger RW, Duncan K, Fang JL and Lazarus P (2006) Characterization of tamoxifen and 4-hydroxytamoxifen glucuronidation by human UGT1A4 variants. *Breast Cancer Res* **8:**R50.

Takeuchi K, Kobayashi Y, Tamaki S, Ishihara T, Maruo Y, Araki J, Mifuji R, Itani T, Kuroda M, Sato H, Kaito M and Adachi Y (2004) Genetic

polymorphisms of bilirubin uridine diphosphate-glucuronosyltransferase gene in Japanese patients with Crigler-Najjar syndrome or Gilbert's syndrome as well as in healthy Japanese subjects. *J Gastroenterol Hepatol* **19:**1023-1028.

Tang C, Hochman JH, Ma B, Subramanian R and Vyas KP (2003) Acyl glucuronidation and glucosidation of a new and selective endothelin ET(A) receptor antagonist in human liver microsomes. *Drug Metab Dispos* **31:**37-45.

Toide K, Takahashi Y, Yamazaki H, Terauchi Y, Fujii T, Parkinson A and Kamataki T (2002) Hepatocyte nuclear factor-1alpha is a causal factor responsible for interindividual differences in the expression of UDP-glucuronosyltransferase 2B7 mRNA in human livers. *Drug Metab Dispos* **30:**613-615.

Tracy TS (2006) Atypical cytochrome p450 kinetics: implications for drug discovery. *Drugs R D* **7:**349-363.

Tracy TS and Hummel MA (2004) Modeling kinetic data from in vitro drug metabolism enzyme experiments. *Drug Metab Rev* **36:**231-242.

Tran TA, Leppik IE, Blesi K, Sathanandan ST and Remmel R (2002) Lamotrigine clearance during pregnancy. *Neurology* **59:**251-255.

Trubetskoy O, Finel M and Trubetskoy V (2008) High-throughput screening technologies for drug glucuronidation profiling. *J Pharm Pharmacol* **60:**1061-1067.

Tukey RH and Strassburg CP (2001) Genetic multiplicity of the human UDP-glucuronosyltransferases and regulation in the gastrointestinal tract. *Mol Pharmacol* **59:**405-414.

Turgeon D, Carrier JS, Levesque E, Hum DW and Belanger A (2001) Relative enzymatic activity, protein stability, and tissue distribution of human steroid-metabolizing UGT2B subfamily members. *Endocrinology* **142:**778-787.

Uchaipichat V, Galetin A, Houston JB, Mackenzie PI, Williams JA and Miners JO (2008) Kinetic modeling of the interactions between 4-methylumbelliferone, 1-naphthol, and zidovudine glucuronidation by udp-glucuronosyltransferase 2B7 (UGT2B7) provides evidence for multiple substrate binding and effector sites. *Mol Pharmacol* **74:**1152-1162.

Udomuksorn W, Elliot DJ, Lewis BC, Mackenzie PI, Yoovathaworn K and Miners JO (2007) Influence of mutations associated with Gilbert and Crigler-Najjar type II syndromes on the glucuronidation kinetics of bilirubin and other UDP-glucuronosyltransferase 1A substrates. *Pharmacogenet Genomics* **17:**1017-1029.

Veal GJ and Back DJ (1995) Metabolism of Zidovudine. *Gen Pharmacol* **26:**1469-1475.

Wiener D, Doerge DR, Fang JL, Upadhyaya P and Lazarus P (2004a) Characterization of N-glucuronidation of the lung carcinogen 4-(methylnitrosamino)-1-(3-pyridyl)-1-butanol (NNAL) in human liver:

importance of UDP-glucuronosyltransferase 1A4. *Drug Metab Dispos* **32:**72-79.

Wiener D, Fang JL, Dossett N and Lazarus P (2004b) Correlation between UDP-glucuronosyltransferase genotypes and 4-(methylnitrosamino)-1-(3-pyridyl)-1-butanone glucuronidation phenotype in human liver microsomes. *Cancer Res* **64:**1190-1196.

Williams JA, Hyland R, Jones BC, Smith DA, Hurst S, Goosen TC, Peterkin V, Koup JR and Ball SE (2004) Drug-drug interactions for UDP-glucuronosyltransferase substrates: a pharmacokinetic explanation for typically observed low exposure (AUCi/AUC) ratios. *Drug Metab Dispos* **32:**1201-1208.

Williams JA, Ring BJ, Cantrell VE, Campanale K, Jones DR, Hall SD and Wrighton SA (2002) Differential modulation of UDP-glucuronosyltransferase 1A1 (UGT1A1)-catalyzed estradiol-3-glucuronidation by the addition of UGT1A1 substrates and other compounds to human liver microsomes. *Drug Metab Dispos* **30:**1266-1273.

Yin H, Bennett G and Jones JP (1994) Mechanistic studies of uridine diphosphate glucuronosyltransferase. *Chem Biol Interact* **90:**47-58.

Zhang D, Chando TJ, Everett DW, Patten CJ, Dehal SS and Humphreys WG (2005) In vitro inhibition of UDP glucuronosyltransferases by atazanavir and other HIV protease inhibitors and the relationship of this property to in vivo bilirubin glucuronidation. *Drug Metab Dispos* **33:**1729-1739.

Zhang D, Zhang D, Cui D, Gambardella J, Ma L, Barros A, Wang L, Fu Y, Rahematpura S, Nielsen J, Donegan M, Zhang H and Humphreys WG (2007) Characterization of the UDP glucuronosyltransferase activity of human liver microsomes genotyped for the UGT1A1*28 polymorphism. *Drug Metab Dispos* **35:**2270-2280.

Zhou D, Guo J, Linnenbach AJ, Booth-Genthe CL and Grimm SW (2010a) Role of Human UGT2B10 in N-Glucuronidation of Tricyclic Antidepressants, Amitriptyline, Imipramine, Clomipramine and Trimipramine. *Drug Metab Dispos*.

Zhou D, Guo J, Linnenbach AJ, Booth-Genthe CL and Grimm SW (2010b) Role of human UGT2B10 in N-glucuronidation of tricyclic antidepressants, amitriptyline, imipramine, clomipramine, and trimipramine. *Drug Metab Dispos* **38:**863-870.

Zhou J, Tracy TS and Remmel RP (2010c) Glucuronidation of Dihydrotestosterone and trans-Androsterone by Recombinant UDP-Glucuronosyltransferase (UGT) 1A4: Evidence for Multiple UGT1A4 Aglycone Binding Sites. *Drug Metab Dispos* **38:**431-440.

Zhou J, Zhang J and Xie W (2005) Xenobiotic nuclear receptor-mediated regulation of UDP-glucuronosyl-transferases. *Curr Drug Metab* **6:**289-298.

Appendix 1: Equations

Equation 1.1: $$V_0 = \frac{V_{max} \times [S]^n}{S_{50}{}^n + [S]^n}$$

Equation 1.2: $$V_0 = \frac{V_{max} \times [S]}{K_m + [S] \times (1 + \frac{[S]}{K_{si}})}$$

Equation 2.1: $$f_u = \frac{1}{1 + C \bullet 10^{0.072 \bullet \log P^2 + 0.067 \bullet \log P - 1.126}}$$

Equation 2.2: $$V_0 = \frac{V_{max} \times [S]}{K_m + [S]}$$

Equation 2.3: $$V_0 = \frac{V_{max}}{1 + \frac{K_m}{[S]} + \frac{[S]}{K_{si}}}$$

Equation 2.4: $$V_0 = \frac{V_{max} \times [S]}{K_m \times (1 + \frac{[I]}{K_i}) + [S]}$$

Equation 2.5: $$V_0 = \frac{V_{max} \times [S]}{K_m \times (1 + \frac{[I]}{K_i}) + [S] \times (1 + \frac{[I]}{K_i})}$$

Equation 2.6: $$V_0 = \frac{V_{max} \times [S]}{K_m \times (1 + \frac{[I]}{K_i}) + [S] \times (1 + \frac{[I]}{\alpha K_i})}$$

Equation 2.7: $$V_0 = \frac{V_{max} \bullet (\frac{[S]}{K_s} + \frac{b \bullet [S]^2}{K_s{}^2})}{1 + \frac{[S]}{K_s} + \frac{[S]^2}{K_s{}^2}}$$

Equation 2.8: $$V_0 = \frac{V_{max} \bullet (\frac{[DHT]}{K_{DHT}} + \frac{c \bullet [TAM] \bullet [DHT]}{d \bullet K_{TAM} \bullet K_{DHT}})}{1 + \frac{[DHT]}{K_{DHT}} + \frac{[TAM]}{K_{TAM}} + \frac{[TAM]^2}{K_{TAM}{}^2} + \frac{[TAM] \bullet [DHT]}{d \bullet K_{TAM} \bullet K_{DHT}}}$$

Equation 2.9: $$V_0 = \frac{V_{max} \bullet \left(\frac{[TAM]}{K_{TAM}} + \frac{b \bullet [TAM]^2}{K_{TAM^2}} + \frac{c \bullet [TAM] \bullet [DHT]}{d \bullet K_{TAM} \bullet K_{DHT}}\right)}{1 + \frac{[DHT]}{K_{DHT}} + \frac{[TAM]}{K_{TAM}} + \frac{[TAM]^2}{K_{TAM^2}} + \frac{[TAM] \bullet [DHT]}{d \bullet K_{TAM} \bullet K_{DHT}}}$$

Equation 2.10:

$$V_0 = \frac{V_{max} \bullet \left(\frac{[TAM]}{K_{TAM}} + \frac{b \bullet [TAM]^2}{K_{TAM^2}} + \frac{c \bullet [TAM] \bullet [t-AND]}{d \bullet K_{TAM} \bullet K_{t-AND}}\right)}{1 + \frac{[t-AND]}{K_{t-AND}} + \frac{[t-AND]^2}{K_{t-AND^2}} + \frac{[TAM]}{K_{TAM}} + \frac{[TAM]^2}{K_{TAM^2}} + \frac{2 \bullet [TAM] \bullet [DHT]}{d \bullet K_{TAM} \bullet K_{t-AND}}}$$

Equation2.11:

$$V_0 = \frac{V_{max} \bullet \left(\frac{[TAM]}{K_{TAM}} + \frac{b \bullet [TAM]^2}{K_{TAM^2}} + \frac{c \bullet [TAM] \bullet [t-AND]}{d \bullet K_{TAM} \bullet K_{t-AND}}\right)}{1 + \frac{[t-AND]}{K_{t-AND}} + \frac{[t-AND]^2}{K_{t-AND^2}} + \frac{[TAM]}{K_{TAM}} + \frac{[TAM]^2}{K_{TAM^2}} + \frac{[TAM] \bullet [DHT]}{d \bullet K_{TAM} \bullet K_{t-AND}}}$$

Equation 2.12: $$V_0 = \frac{V\max \bullet \left(1 + \frac{\beta[I]}{\alpha \bullet Ki}\right) \Big/ \left(1 + \frac{[I\}}{\alpha \bullet Ki}\right)}{1 + \frac{Km}{[S]} \bullet \left(1 + \frac{[I]}{Ki}\right) \Big/ \left(1 + \frac{[I]}{\alpha \bullet Ki}\right)}$$

Equation 3.1: $$V_0 = \frac{V_{max} \times [S]}{K_m + [S]}$$

Equation 3.2: $$V_0 = \frac{V_{max} \times [S]^n}{S_{50}{}^n + [S]^n}$$

Equation 3.3: $$V_0 = \frac{V_{max} \bullet \left(\frac{[S]}{K_s} + \frac{[S]^2}{a \bullet K_{s^2}} + \frac{c \bullet [S] \bullet [A]}{a \bullet K_s \bullet K_a}\right)}{1 + \frac{2[S]}{K_s} + \frac{2[A]}{K_a} + \frac{[S]^2}{a \bullet K_{s^2}} + \frac{2 \bullet [S] \bullet [A]}{a \bullet K_s \bullet K_a} + \frac{[A]^2}{K_a{}^2}}$$

Equation 3.4: $$V_0 = \frac{V_{max} \bullet \left(\frac{[S]}{K_s} + \frac{[S]^2}{a \bullet K_{s^2}} + \frac{c \bullet [S] \bullet [I]}{d \bullet K_s \bullet K_i} + \frac{c \bullet [S]^2 \bullet [I]}{a \bullet d \bullet K_s{}^2 \bullet K_i}\right)}{1 + \frac{2[S]}{K_s} + \frac{[I]}{K_i} + \frac{[S]^2}{a \bullet K_{s^2}} + \frac{2 \bullet [S] \bullet [I]}{d \bullet K_s \bullet K_i} + \frac{[S]^2 \bullet [I]}{a \bullet d \bullet K_s{}^2 \bullet K_i}}$$

Appendix 2: Derivation of rate equations for formation of BMG, BDG and total glucuronide based on a sequential reaction model in Figure 3-7

Rate for BMG formation = $\frac{d[BMG]}{dt} = k_{-4}[BMG-E] - k_4[BMG]\bullet[E]$

Rate for BMD formation = $\frac{d[BDG]}{dt} = k_{-5}[BDG-E] - k_4[BDG]\bullet[E]$

At initial rate conditions, [BMG] and [BDG] are equal to zero

Therefore, rate for BMG formation = $\frac{d[BMG]}{dt} = k_{-4}[BMG-E]$ and rate for BMD formation = $\frac{d[BDG]}{dt} = k_{-5}[BDG-E]$

At steady state,

$$\frac{d[BMG-E]}{dt} = k_2\bullet[B-E] + k_4\bullet[BMG]\bullet[E] - k_{-4}\bullet[BMG-E] - k_3\bullet[BMG-E]$$
$$= k_2\bullet[B-E] - k_{-4}\bullet[BMG-E] - k_3\bullet[BMG-E] = 0$$

Therefore, $[BMG-E] = \frac{k_2}{k_{-4}+k_3}\bullet[B-E]$

Also at steady state,

$$\frac{d[BDG-E]}{dt} = k_3\bullet[BMG-E] + k_5\bullet[BDG]\bullet[E] - k_{-5}\bullet[BDG-E]$$
$$= k_3\bullet[BMG-E] - k_{-5}\bullet[BDG-E] = 0$$

Therefore, $[BDG-E] = \frac{k_3}{k_{-5}}\bullet[BMG-E] = \frac{k_3}{k_{-5}}\bullet\frac{k_2}{k_{-4}+k_3}\bullet[B-E]$

In addition,
$$[E]_{total} = [E] + [B-E] + [BMG-E] + [BDG-E]$$
$$= [E] + [BE] + \frac{k_2}{k_{-4}+k_3}\bullet[B-E] + \frac{k_3}{k_{-5}}\bullet\frac{k_2}{k_{-4}+k_3}\bullet[B-E]$$

Therefore, $[E] = [E]_{total} - [B-E] - \frac{k_2}{k_{-4}+k_3}\bullet[B-E] - \frac{k_3}{k_{-5}}\bullet\frac{k_2}{k_{-4}+k_3}\bullet[B-E]$

Again with steady state assumption:

$$\frac{d[B-E]}{dt} = k_1 \bullet [B] \bullet [E] - k_{-1} \bullet [B-E] - k_2 \bullet [B-E] = 0$$

$$k_1 \bullet [B] \bullet (([E]_{total} - [B-E] - \frac{k_2}{k_{-4}+k_3} \bullet [B-E] - \frac{k_3}{k_{-5}} \bullet \frac{k_2}{k_{-4}+k_3} \bullet [B-E]) - k_{-1} \bullet [B-E] - k_2 \bullet [B-E] =$$

Therefore, $$[B-E] = \frac{k_1 \bullet [B] \bullet [E]_{total}}{k_{-1} + k_2 + (1 + \frac{k_2}{k_{-4}+k_3} + \frac{k_3}{k_{-5}} \bullet \frac{k_2}{k_{-4}+k_3}) \bullet k_1 \bullet [B]}$$

Therefore, rate for BMG formation =

$$\frac{d[BMG]}{dt} = k_{-4}[BMG-E] = k_{-4} \bullet \frac{k_2}{k_{-4}+k_3} \bullet [B-E]$$
$$= \frac{k_{-4} \bullet k_2 \bullet k_1 \bullet [B] \bullet [E]_{total}}{(k_{-1}+k_2) \bullet (k_{-4}+k_3) + (k_{-4}+k_3+k_2+\frac{k_3 \bullet k_2}{k_{-5}}) \bullet k_1 \bullet [B]}$$

Therefore, $$\boxed{V_{0,BMG} = \frac{\frac{k_{-4} \bullet k_2}{(k_{-4}+k_3+k_2+\frac{k_3 \bullet k_2}{k_{-5}})} \bullet [B] \bullet [E]_{total}}{\frac{(k_{-1}+k_2) \bullet (k_{-4}+k_3)}{(k_{-4}+k_3+k_2+\frac{k_3 \bullet k_2}{k_{-5}}) \bullet k_1} + [B]}}$$

Rate for BDG formation =

$$\frac{d[BDG]}{dt} = k_{-5}[BDG-E] = k_{-5} \bullet \frac{k_3}{k_{-5}} \bullet [BMG-E] = k_3 \bullet [BMG-E]$$

Therefore, (rate for BMG formation)/(rate for BDG formation)= k_{-4}/k_3

Therefore, $$V_{0,\,BDG} = \frac{\frac{k_3 \bullet k_2}{(k_{-4} + k_3 + k_2 + \frac{k_3 \bullet k_2}{k_{-5}})} \bullet [B] \bullet [E]_{total}}{\frac{(k_{-1} + k_2) \bullet (k_{-4} + k_3)}{(k_{-4} + k_3 + k_2 + \frac{k_3 \bullet k_2}{k_{-5}}) \bullet k_1} + [B]}$$

Rate for total glucuronide formation =rate for BDG formation + rate for BMG

$$\text{formation} = \frac{\frac{k_3 \bullet k_2}{(k_{-4} + k_3 + k_2 + \frac{k_3 \bullet k_2}{k_{-5}})} \bullet [B] \bullet [E]_{total}}{\frac{(k_{-1} + k_2) \bullet (k_{-4} + k_3)}{(k_{-4} + k_3 + k_2 + \frac{k_3 \bullet k_2}{k_{-5}}) \bullet k_1} + [B]} + \frac{\frac{k_{-4} \bullet k_2}{(k_{-4} + k_3 + k_2 + \frac{k_3 \bullet k_2}{k_{-5}})} \bullet [B] \bullet [E]_{total}}{\frac{(k_{-1} + k_2) \bullet (k_{-4} + k_3)}{(k_{-4} + k_3 + k_2 + \frac{k_3 \bullet k_2}{k_{-5}}) \bullet k_1} + [B]}$$

Therefore , $$V_{o,\,total} = \frac{\frac{(k_{-4} + k_3) \bullet k_2}{(k_{-4} + k_3 + k_2 + \frac{k_3 \bullet k_2}{k_{-5}})} \bullet [B] \bullet [E]_{total}}{\frac{(k_{-1} + k_2) \bullet (k_{-4} + k_3)}{(k_{-4} + k_3 + k_2 + \frac{k_3 \bullet k_2}{k_{-5}}) \bullet k_1} + [B]}$$

Therefore, rate equations for formation of BDG, BMG or total glucuronide can all be written in the format of Michaelis-Menten equation and K_ms for BDG, BMG, and total glucuronidation formation are the same, which are equal to

$$\frac{(k_{-1} + k_2) \bullet (k_{-4} + k_3)}{(k_{-4} + k_3 + k_2 + \frac{k_3 \bullet k_2}{k_{-5}}) \bullet k_1}$$